Prefabrication of Vascularized Large Bone Grafts

Inauguraldissertation

zur

Erlangung der Würde eines Doktors der Philosophie vorgelegt der

Philosophisch-Naturwissenschaftlichen Fakultät

der Universität Basel

von

Alexander Haumer

Aus Italien und Österreich

Basel, 2018

Genehmigt von der Philosophisch-Naturwissenschaftlichen Fakultät

auf Antrag von

Prof. Markus Affolter, PhD

Prof. Ivan Martin, PhD

Dr. Martin Ehrbar, PhD

Basel, den 27.3.2018

Prof. Dr. Martin Spiess

ABSTRACT

Infection, trauma or neoplasia can lead to extensive bone tissue loss. Current reconstructive approaches for large, complex bone defects, especially in the maxillo-facial region, rely on autologous bone grafting. However, reconstruction by autologous tissue transfer can encounter major difficulties. Not only is tissue transfer restricted by donor site morbidity and limited availability, the three-dimensional suitability of donor and recipient tissue can represent a major hurdle. To avoid these shortcomings, it would be of high interest to generate a prefabricated, vascularized, custom-shapeable bone graft. The envisioned bone graft surrogate relies on the concept of combining an efficient vascularization strategy with an engineered material, providing robust bone formation.

In this thesis I investigate whether an arteriovenous (AV) bundle is suitable as an efficient vascularization method, able to fully revitalize a critically sized bone graft. In combination with an osteoconductive ceramic material and a living cell source, the stromal vascular fraction (SVF) from adipose tissue, the AV bundle is able to induce and support bone formation. A newly developed, contrast-enhanced, microtomographic imaging technique made it possible to critically assess vascularization and bone formation within such a graft in its entirety. Eventually, implementation of an engineered matrix, useable as an off-the-shelf material, in the above mentioned graft allowed to generate a germ of osteoinduction and vascularization.

The developed concept of a prefabricated, pedicled, large bone graft, customizable to the patients' needs, offers a vast variety of clinical applications.

INDEX

- Introduction
- Materials and methods
- Results
- Discussion
- References

Chapter V: Prefabrication of vascularized bone grafts

- Abstract
- Introduction
- Materials and methods
- Results
- Discussion
- References

Chapter VI: Delivery of cellular factors to regulate bone healing

- Introduction
- Key regulators of bone healing
- Cell-free strategies to delivery MSC-produced regenerative factors
- Conclusions
- References

5. Conclusion and perspective
6. Curriculum Vitae

CHAPTER I:

Introduction

1. Bone:

The human skeleton is composed by bones, which, on the one hand give structural stability and protection to the vulnerable viscera through their rigid and on the other hand allow movement of extremities and thus locomotion. Bone is a highly dynamic system which takes active part in a variety of aspects of the human metabolism: it regulates mineral storage and supply (e.g. calcium and phosphorus), it balances pH fluctuations by buffering excesses and exerts detoxifying effects by storing heavy metals or other toxic elements [1]. Importantly, bone produces white and red blood cells within its bone marrow.

Bone consists majorly of two components, collagen and calcium phosphate, albeit it is not uniformly solid. One can distinguish a more solid bone structure, the so-called cortical (compact) bone and a less dense one, termed cancellous (trabecular, spongy). Based on their properties the two types are found in different locations and fulfil different functions. Whereas compact bone is principally located in the diaphysis (shaft) of long bones and constitutes the outer lining thereof, the cancellous type is a porous trabecular network majorly present in the end of long bones (metaphysis and epiphysis). While the compact bone facilitates functions such as structural support and lever for musculoskeletal interaction, the cancellous bone hosts the bone marrow and gives bone flexibility through its inferior density.

The difference in structure and function of the two bone types derives from their different microscopic composition. Cortical bone is highly organized: Mineralized collagen fibers form into sheets (lamellae) which wind around a central canal to form a so-called osteon or Haversian system (Fig. 1)[2]. The cylindrical osteons, with a diameter of about 200-250 µm, are piled one next to another, parallel to the long axis of the bone. Cancellous bone's primary units are the so-called trabeculae, which are

arranged in an interconnecting framework aligned towards the mechanical load dispersion the bone experiences. Bone is home to three major active bone cell types all residing within the bone matrix: Osteoblasts, which create and mineralize bone, osteocytes, responsible for bone maintenance and osteoclasts, which resorb bone.

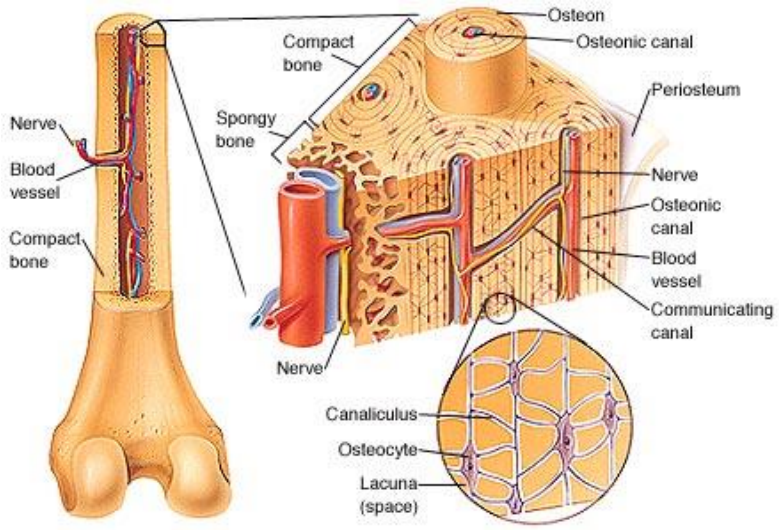

Figure 1: Schematic image of bone structure. (http://www.mhhe.com/biosci/esp/2001_gbio/folder_structure/an/m5/s2/index.htm)

1.1. Bone development:

The process of bone formation, or ossification, occurs by two main mechanisms in human embryogenesis, termed intramembranous (i.e. direct) and endochondral (indirect) ossification (Fig. 2). While intramembranous ossification involves deposition of bone matrix in the mesenchyme by mesenchymal progenitor cells directly differentiated into osteoblasts, endochondral bone formation occurs through a cartilaginous precursor. Progenitor cells are recruited, condensate, proliferate and primarily differentiate into chondrocytes [3]. This cartilaginous matrix, called perichondrium at its borders and rich in Collagen II and aggrecan expresses high levels of SOX-9 [4–6]. Within the growing cartilaginous primordium chondrocytes stop

proliferating, begin to hypertrophy and synthesize primarily collagen X. Hypertrophic chondrocytes instruct mineralization of the matrix, secern factors supporting vascularization and promote both chondroclasts for degradation of cartilage and perichondral cells to become osteoblasts [7,8]. Eventually, the hypertrophic chondrocytes undergo apoptosis leaving behind a cartilaginous scaffold whereto osteoblasts migrate, fully remodeling the cartilage template to bone. (Fig. 3)

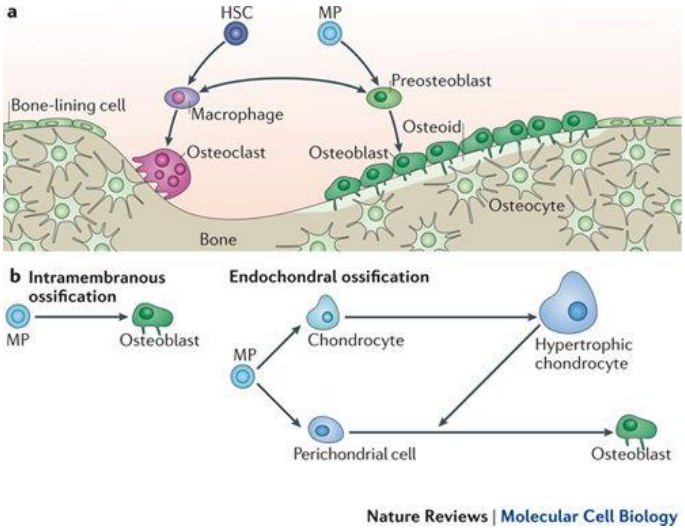

Figure 2: The intramembranous and endochondral ossification processes. Adapted from Long et al. 2012 [7]

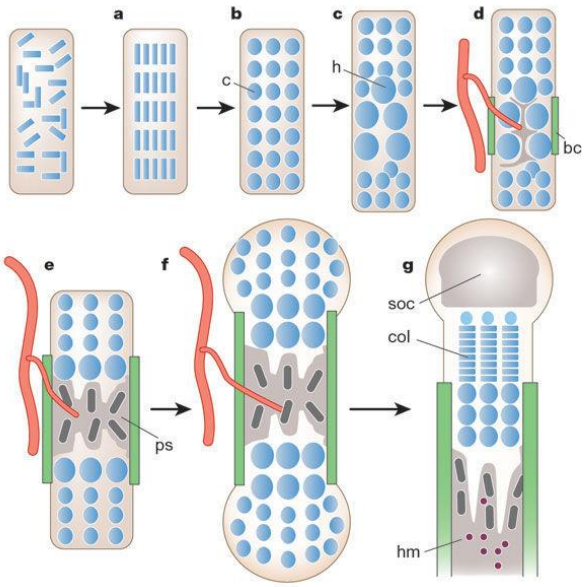

Figure 3: Endochondral ossification from mesenchymal cell condensation (**a**), chondrogenic differentiation thereof (**b**), transformation of perichondral cells to osteoblasts, which is defined as the bone collar (bc). Successive apoptosis of hypertrophic chondrocytes is accompanied by osteoblastic and vascular invasion (**d&e**). Proliferating chondrocytes elongate the bone (**f**) and persist (col) below the secondary ossification centers (soc) (**g**). Adapted from Kronenberg et al .2003 [9]

1.2. Bone vascularization:

Ever since early embryogenesis, when blood vessels are directed towards the newly forming bone by secretion of proangiogenic factors released in the matrix, bone tissue is a highly vascularized tissue [8,10]. The vasculature retains an important role in bone throughout life, not only due to its function in growth and homeostasis of the tissue but also during fracture healing [11]. As in other organs, vessels control the nutrient, oxygen and cytokine delivery to bone tissue and thus are a major limiting factor regarding its physiological function. Approximately 10 % of the cardiac output is directed to bone, which does not only reflect the high need of bone-related cells (osteoblasts, osteocytes and osteoclasts) and the bone marrow but also allows a high degree of remodeling and repair [12]. Hereby the precise anatomy of bone related vessels ensure steady perfusion of the bone organ:

In long bones the cortex is pierced by arteries in the three anatomical subdivisions: epiphyseal, metaphyseal and diaphyseal arteries warrant blood supply to each area (Fig. 4 A). Perfusion of the periosteum is ensured by periosteal vessels, arranged circumferentially and connected by numerous vertical anastomoses. Once the vessels penetrate the bone, arteries branch into arterioles and finally capillaries which allow metabolite exchange as it is common in the rest of the human organism [13–15]. However, the vasculature within bone is unique because the blood flows within a rather rigid cavity where pressure must be kept constant and at the same time minerals, hormones, blood cells and other products of the bone marrow have to be carried to the entire organism [15]. Venous blood is collected in a large central sinus (Fig. 4 B), which can alter its volume drastically (up to five times) upon stimulation [16]. Veins, parallel to the bone related arteries, drain the sinusoidal blood back into the large venous vessels of the limbs and into systemic circulation [17].

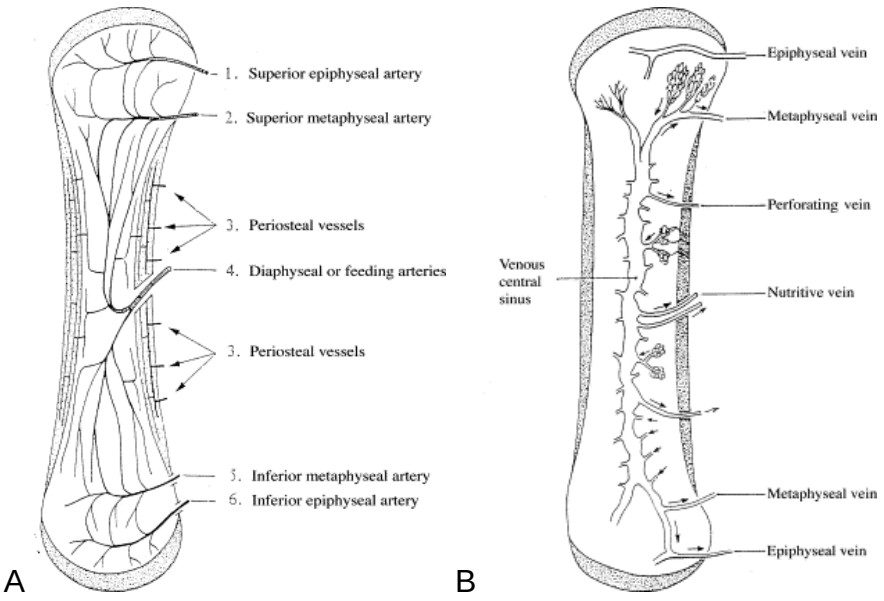

Figure 4: Anatomical subdivision of arterial (**A**) and venous (**B**) systems suppling bone. Adapted from Laroche et al. 2002 [15].

It seems reasonable that impairment of blood supply to bone compromises both its development (and growth) and repair, because it deprives the tissue of essential nutrients and cyto- and chemokines [11,12,18–21]. Besides these metabolites, oxygen and hypoxia have been recognized to have a special role in bone function [12]. The oxygen tension within healthy bone marrow lies within the range of median interstitial pO_2 levels of other tissues [22,23]. Since the physiological variation capability of this system is rather narrow, cells respond promptly to fluctuations above or below the range with hypoxia inducible transcription factors (HIFs) [24]. When oxygen tension decreases, oxygen is not available to induce degradation of HIF-a. HIF-a heterodimerizes with HIF-β, which initiates transcription of hypoxia-related genes responsible for proangiogenic processes, involving crucial mediators such as VEGF and PDGF [25,26]. In addition to the effect of oxygen on the molecular cascade affecting the transcription of proangiogenic, proliferative and metabolic factors, it also directly affects cells of bone tissue, i.e. osteoblasts and osteoclasts. Studies have shown that when pO_2 levels drop below 2% bone formation nearly ceases due to a strong inhibitory effect of hypoxia on osteoblasts [27,28]. This restraint is due to a direct inhibitory effect on the proliferation and differentiation of the osteoblasts as well as to a reduction of collagen production elicited by decreased activity of enzymes required for post-translational modification of the protein. The inhibitory activity of hypoxia on osteoblasts is accentuated by an enhancing effect on their counterpart – the osteoclasts, which thrive under hypoxic conditions. In contrast to osteoblasts, osteoclasts derive from the mononuclear phagocytic system. This cell lineage is geared to operate in environments with low oxygen and pH content, circumstances normally found in inflammatory areas [23]. Thus, when oxygen tension and pH drop, these cells have enhanced proliferation and activity. This was shown in cultures of mononuclear cells of mice and humans, where number and size of osteoclasts were

stimulated when kept in hypoxic conditions also yielding higher resorption pits [12,29–31].

1.3. Bone Tissue repair:

Bone has a strong intrinsic capacity for regeneration. Beginning during skeletal development in embryogenesis, this property is maintained in the continuous remodeling throughout adult life or as part of the repair process in response to injury [32,33]. Bone healing occurs through the classical healing cascade characterized by the inflammatory, repair and remodeling phases (Fig. 5). At the same time the injury site is progressively revascularized, which represents a crucial part of the regenerative process as stated above. The well-orchestrated interplay of biological events of bone induction and conduction that happen during bone regeneration involves many different cell types and molecular signaling pathways, happening in a well-defined temporal and spatial sequence. Fracture healing, as the most common form of bone regeneration, recapitulates both the direct and the indirect ossification routes [34]. This finely tuned balance influenced by fracture and location type, allows injuries and fractures of bone to heal without any scar formation, unlike many other organs.

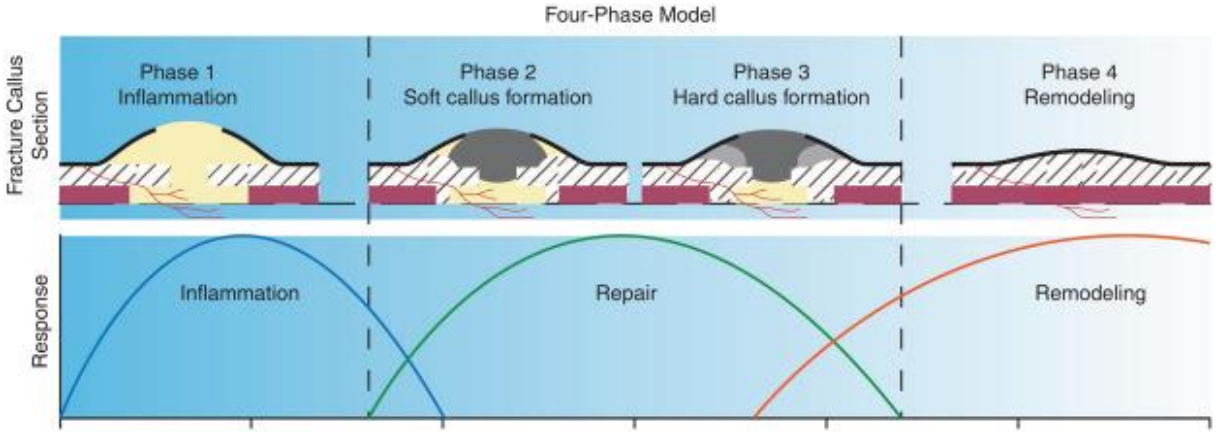

Figure 5: The fracture healing model consisting of the three response phases of inflammatory, repair and remodeling phase, accompanied by an increasing vascularization of the fracture site. Adapted from Pivonka et al. 2012 [35].

1.3.1. The phases of bone healing:

After bone fracture, ruptured blood vessels and vasoconstriction considerably lower blood flow to the injury site [36]. The molecular mechanisms activated by the hypoxic, post-traumatic environment trigger the release of pro-angiogenic factors such as vascular endothelial growth factor (VEGF) and other factors such as angiopoetin-1 and platelet-derived growth factor (PDGF). These factors lead to formation of new capillaries invading the fibrin clot and the developing newly-formed bone [37,38]. However, the role of these factors can be multifunctional: VEGF for example, whose primary function is related to vascularization, is also implicated in the recruitment and differentiation of osteoprogenitor cells. Additionally, VEGF can regulate various osteoinductive factors (e.g. TGF-β1, insulin-like growth factors (IGF), fibroblast growth factor (FGF-2)), which in turn regulate its expression pattern. Degranulating platelets release PDGF at the injury site, which represents another crucial factor for fracture healing involved in both angiogenic and osteogenic processes. PDGF is chemotactic for progenitor cells, such as osteoblasts and is directly and indirectly pro-angiogenic (e.g. through upregulation of VEGF expression) [39].

Progressive healing and concomitant changes in the mechanical forces within the newly formed bone entail secretion of matrix metalloproteinases (MMPs), which further stimulate vessel ingrowth and vascularization of the tissue [40]. As vascularization of the area further advances, normoxic conditions are restored and invading fibroblasts can start with remodeling the fracture hematoma , replacing it with highly vascularized granulation tissue [41,42].

The anatomical location and mechanical factors influence the subsequent repair phase: when the two fractured fragments are compressed and thus interfragmentary movement is minimal, primary healing allows for direct deposition of mineralized matrix. In contrast, mechanically instable fractures heal through indirect healing

[32,41,43,44]. When the two surfaces are mechanically stable and compressed Haversian systems can bridge and later be infiltrated by osteoclasts, initiating the physiological process of bone remodeling [41,43,45]. Tunneling of the two segments by osteoclasts creates void space promptly colonized by blood vessels. Innate immune cells (e.g. Monocytes, macrophages) invading the area secern cytokines and chemotactic factors which further recruit local and systemic osteoprogenitors, fibroblasts and MSCs [46,47]. In contrast to direct deposition of mineralized matrix, indirect bone healing involves both intramembranous and endochondral ossification. The latter mechanism, also occurring during long bone development, involves bony transformation of a cartilaginous callus (described in previous chapters) and represents the central part of indirect bone healing.

After the initial inflammatory phase, about 3 to 7 days after bone injury osteoblasts derived from the unharmed periosteum initiate intramembranous bone formation [48,49]. Once mineralized matrix has been directly deposited by periosteal progenitors, cartilaginous tissue formation begins 7-10 days after injury [32,50]. Cartilage tissue is formed as a result of low oxygen content in the injury area, which drives balance towards chondrogenic differentiation of progenitor cells [41,51,52]. Mechanical strain on the tissue hampers new vessel formation and the distance to the intact periosteal vascular network leads to insufficient blood supply to the area [53,54]. In the subsequent steps long bone development is resembled, comprising progenitor cell recruitment and condensation, proliferation, chondrogenic differentiation, mineralization, vascularization and remodeling. Initially in this process stromal cell-derived factor-1α (SDF-1 α) plays a major role in progenitor cell recruitment [55,56]. SDF-1α is highly released during the acute phase of bone healing and efficiently mobilizes osteoprogenitor cells from the bone marrow which express CD44 and CXCR4, receptors of osteopontin and SDF-1, respectively [55]. FGF, Wnt, and BMP

pathways are other factors that drive the precisely orchestrated processes of endochondral ossification during bone healing. FGF and Wnt signaling synergistically control limb growth and inhibit chondrogenesis by maintaining progenitors in a proliferative and potential osteogenic state [4,5]. On the other hand BMP and TGFβ signaling are responsible for chondrogenic differentiation of cartilage progenitors [6]. Following the endochondral ossification route, BMP triggers hypertrophy of chondrocytes through expression of Runt-related transcription factor 2 (Runx2), which together with the negative regulatory feedback loop between Indian Hedgehog (IHH) and Parathyroid Hormone-related Protein (PTHrP) represents the necessary steps of cartilage development towards bone [8,57,58]. These mechanisms are observed in the repair phase and the ensuing remodeling phase which can last years in the adult human and eventually bear a fully loadable bone [32,33,59]. The hypertrophic chondrocytes undergo apoptosis and release calcium, which increases the mechanical stability of the fracture site [53,60,61]. Low tissue strain favors blood vessel ingrowth in the injury area which supply the site with MSCs and monocytes [32]. While the former differentiate into osteoblasts, osteoclasts derived from the latter ones promote remodeling of deposited woven bone into lamellar bone. These two cell types tightly regulate each other by secretion of the cytokines MCSF, involved in osteoclast differentiation, and RANKL, responsible for osteoclast differentiation and the coordination of bone formation and bone resorption [62]. The diminishing strain on tissue in the injury site not only enhances vascularization but also allows intramembranous bone formation [44,63]. Together with a decrease of most inflammatory cytokines, except IL-1, TNF-α and BMP-2, this phase occurs 4-6 weeks after fracture [51].

1.4. Large, complex bone defects and current treatment options:

In the clinical routine the bone healing process can be aided by several interventional or conservative treatments. When treating bone fractures, surgeons can adapt and compress the two fragments to facilitate a rapid direct bone healing process. To stabilize the fracture, another key element for good bone healing as outlined in the section above, the treatment can foresee interventional procedures such as internal or external fixation or conservative application of a cast (or splint). Age, health condition of the patient, location and complexity of the fracture and concomitant injuries and diseases are determining factors for selecting the correct treatment strategy. If the bone fragments are well-aligned and stable, conservative treatment with a cast or a splint can be sufficient to allow good bone healing. However more complex or instable fractures can be treated by internal fixation, a long-established procedure which dates back to the mid nineteenth century [64]. The fixation can be performed with an intramedullary nail, which is inserted in the medullary cavity or by orthopedic plates and screws applied on the surface of the bone. During external fixation screws are fixed in the bone, pierced through the skin and combined by plates outside the body [65,66].

However, in large or highly complex bone defects the natural healing process often fails. This can be due to insufficient blood supply, extensive soft tissue injury around the bone, infection, neoplasm, radiotherapy, systemic disease or congenital disorders resulting in delayed union or non-union of bone.

1.4.1. Treatment options in reconstructive surgery:

For large defects which are unlikely to heal within a reasonable amount of time, plastic surgery has developed various reconstructive strategies: autologous grafts, including so called local flaps, regional flaps and free tissue transfer and procedures involving

allogeneic substitutes or synthetic materials count among the different options surgeons have [67]. The individual clinical scenario dictates the treatment algorithm to use, but vascular supply strongly influences successful accomplishment of every approach. Blood vessels guarantee survival of the transferred tissue by supplying required oxygen and nutrients, removing toxic waste products and by ensuring immunological protection of the tissue. Vascularization of tissue can occur spontaneously from the recipient site when the graft is not too large and the environmental quality of the defect site allows for it. Split thickness skin grafts in burn patients or cancellous bone grafts for bone reconstruction are examples where vascular ingrowth from the donor site is sufficient. In the first 48 hours simple oxygen diffusion and fluid imbibition enable graft survival of non-vascularized tissue after which neovascularization and/or inosculation take over. In neovascularization, new vessels sprout and invade the transferred tissue, while inosculation requires a preexisting vascular network of the graft, which connects to the recipient site and thus enables an almost instantaneous reperfusion [68,69]. Rapid perfusion is essential for large tissue transfers which cannot rely on vascularization from the injured site only. Vascular ingrowth would take too long to provide adequate perfusion to the entire graft, leading to complications such as necrosis and infection or even to loss of the graft. Circumventing this drawback by transferring the corresponding vessels together with the graft and microsurgically connecting them at the recipient site is the principle of the so-called “flap surgery”. In flap surgery the original blood vessel network of a tissue remains intact, thus, once connected to the recipient vessels, the graft does not depend on revascularization form the underlying recipient vascular bed. This makes it possible to transfer a significantly greater tissue volume than when non-vascularized grafts are transferred. Besides the great quantity of transferrable tissue, the great multiplicity of

tissue types in flaps make them an attractive solution: in one graft skin, muscle, nerve, fascia, and bone can be used to fill both large and multifactorial defects.

With preserved original vascularization, the flap is immediately perfused after the inset into the defect. As a result, graft-survival and -engraftment as well as tolerance to infection and mechanical stress are improved compared to non-vascularized grafts. [70] The great versatility of flaps has allowed developing a large arsenal of grafting possibilities, which the treating surgeon can apply depending on several factors, such as viability of the surrounding tissue, size, shape and volume of the defect, desired biomechanical and biological characteristics of the graft, possible complications at the donor site, costs and ethical considerations. Together with these grafts, substitute materials are used, which can be either synthetic, biologically based, tissue-engineered or a combination thereof [67,71].

2. Enhancement of bone regeneration

2.1. Engineered, vascularized bone grafts

As elaborate as aforementioned reconstructive techniques are, they all bear their bottlenecks. As many of them rely on autologous tissue, limited availability and donor site morbidity represent major hurdles, together with the fact that often they are not easily moldable to exactly fit in the defect site. In order to overcome these shortcomings tissue engineering has tried to develop alternative strategies for bone defects. Long-term survival and function of a bone graft highly depends on its vascularization, supplying the indispensable oxygen and glucose when transplanted [72]. Given the fact that new vessels grow at approx. 5 µm/h and oxygen has a limited diffusion distance, a vascular network is mandatory to avoid necrosis of large grafts [73,74]. This vascular network can either be reestablished from scratch by rapidly ingrowing vessels from the recipient site, as it happens in angiogenesis, or by inosculation, where

a pre-existing microvascular tree in the donor tissue connects with the recipient vessels [75,76]. Many approaches aimed at enhancing angiogenesis by altering the chemistry of the biomaterial or bioactivating their scaffold by incorporation of proteins [69,77–84] Others have tried to exploit the process of inosculation due to the almost instantaneous perfusion of the tissue after connection of the vessels. This upcoming concept in engineering bone grafts is intriguing because it allows high engraftment rates in large defects and in cases where the recipient environment has been damaged (e.g. infection, metabolic diseases, radiation etc.) [69,85–87]. In order to be endowed with a microvascular network available for inosculation, the to-be graft needs to be prefabricated, a procedure initially established in plastic and reconstructive surgery. Prefabrication consists in implementing an axial vascular pedicle in a formerly not axially perfused tissue. Neovascularization, driven by the inserted pedicle, generates a complete vascular network which supplies the flap. Eventually, the well revascularized tissue can be freely transplanted with a pedicle [88–90]. This concept has led to several strategies to prevascularize tissue in vitro or in vivo. In vitro cultures and co-cultures apply distinct cell types alone or together to achieve prevascularization [91–96]. Together with the cells, tissue engineering has tried to recreate the highly sensitive balance of available nutrients, cytokines, oxygen concentration, pH, ionic and electrical potential and mechanical stimulation in artificial settings [97]. Inability to resemble these extremely complex interactions has urged tissue engineers to avail themselves of the organism as a natural bioreactor, exploiting the body’s own regenerative capacity to generate vascularized bone grafts [97–101]. The basic elements of bone, namely osteogenic cells, an osteoconductive scaffold and osteoinductive proteins were combined within the organism to recapitulate skeletogenesis [101]. Cells, biomaterials and growth factors, representing the classical triad of tissue engineering, were tested in many different combinations and locations

applying the same underlying principle of the in vivo bioreactor. Developments in this field have led to the most notorious case which gave the engineering community a strong momentum. In the clinical case described by Warnke in 2004 a bone graft was prefabricated ectopically by prevascularization of a titanium cage filled with bovine bone ECM, BMP-7 and the patients BMSC [100]. After the bone graft was successfully transplanted to the patient's mandibular defect as a composite muscle-bone graft, the patient died one year and three months later due to unrelated circumstances. However, besides the great surgical success and research breakthrough, the concept was never broadly applied in surgical practice due to unmet requirements to the graft, such as an non-resorbable titanium cage and heterogeneous distribution of mineralized tissue within the graft [102]. Nevertheless this study has demonstrated the great potential of translating tissue engineered concepts to the clinical practice, by ectopically engineering prefabricated composite grafts.

2.2. Strategies of vascularization

Using the body as an in vivo bioreactor by implanting a scaffolding material in an easily accessible area of the body represents a highly effective prevascularization strategy [103]. The strong angiogenic response drives random ingrowth of newly developing vessels in the tissue and generates a fully functional microvascular tree which allows the graft to be transplanted and the connect to vessels at the defect site by inosculation [75,104]. To generate a prevascularized tissue, several techniques have been developed. They can be categorized mainly in the arteriovenous (AV) loop - and the arteriovenous (AV) bundle technique (Fig. 6).

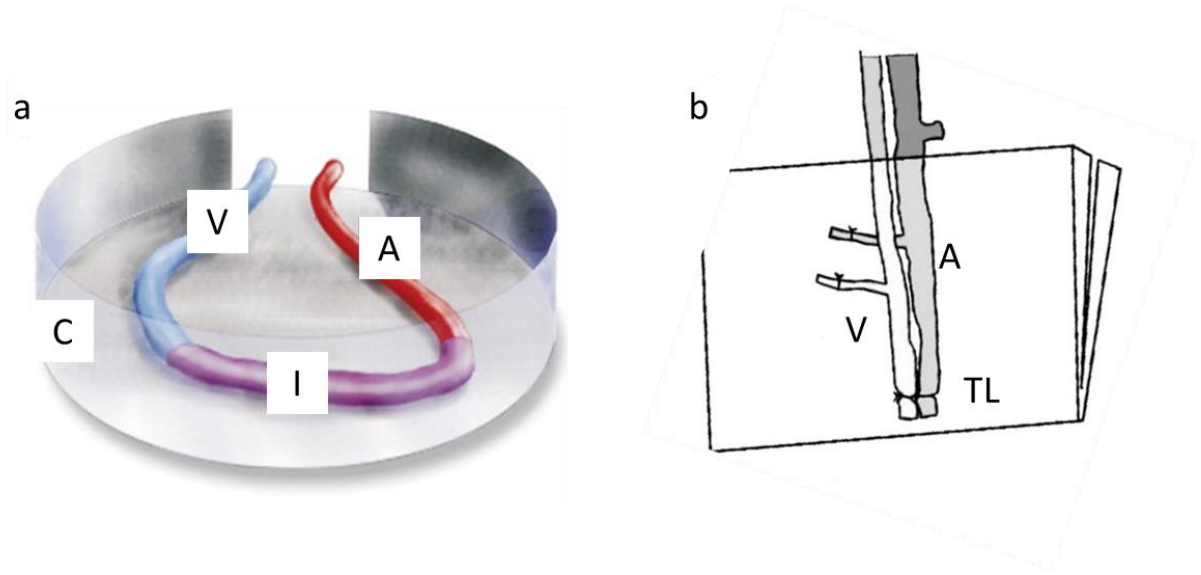

Figure 6: The arteriovenous loop (a) and the arteriovenous bundle (b) represent the most prominent strategies to vascularize tissue. In the AV loop an artery (A) is microsurgically anastomosed to a vein (V) by an interpositional graft (I). C represents the chamber in which the loop is studied. In the AV bundle an artery (A) and a vein (V) are ligated terminally (TL) to form a vessel bundle, without microsurgical anastomosis of the lumen. The bundle is then inserted into the desired tissue structure, e.g. in bone segments, where capillaries and fibroblasts proliferate and provided osteoclasts and osteoblasts take part in bone remodeling. Adapted from Polykandriotis et al. 2012 [105] and from Tanaka et al. 2003 [106].

2.2.1. The arteriovenous loop:

Erol and Sira demonstrated already in 1980 that by inserting an arteriovenous loop, namely an artery connected to a vein by an interpositional vein graft (Fig. 6a), between two dermal layers a vascular bed was created by spontaneous sprouting of vessels [107]. Inserting such a arteriovenous fistula proved to be a potent method of vascularization which did not only allowed upscaling of the graft but also generating a composite graft made up of multiple tissue types. Further proof for the high potency of the AV loop was provided twenty years later, when it was shown that an AV loop was able to revascularize a hollow plastic chamber devoid of a specific extracellular matrix. In a staged manner, the plastic chamber was initially filled with coagulated inflammatory exudate and granulation tissue, later with scar tissue which remodeled into mature dense connective tissue after 12 weeks [108]. This property of de-novo

tissue formation opened interesting opportunities, since tissue could be transferred without having the major drawback of tissue loss at harvesting site. Contingent on the tissue requirements at the defect site, donor site morbidity could be avoided completely [109]. Over time, different materials and extracellular matrices have been investigated in the context of AV loops, such as fibrin gel or matrigel [110]. These studies evidenced that a limiting factor for vascularization was the integration capability of the newly forming vessels with the supporting material. The better the integration could take place, the higher the vascularization was.

2.2.2. The arteriovenous bundle:

In contrast to the loop technique described in the paragraph above, the arteriovenous bundle consists in ligation of an artery and a vein at their ends (Fig. 6b). The AV bundle plays a major clinical role, e.g. when muscle flaps are harvested together with their vessels, which are terminally ligated [88,111]. The high efficiency of this technique in terms of tissue regeneration and vascularization was recognized already 4 decades ago, almost simultaneously to the studies performed on the AV loop [112]. This allowed its application in challenging clinical scenarios, such as osteonecrosis of the bone, by inducing bon regeneration in isolated bone segments, necrotized bone, and bone allografts. When comparing the bundle to singularly transplanted vessels or arteriovenous shunts, such as the loop, it was demonstrated that both techniques were comparable in revascularizing tissues [106]. New vessels, sprouting from the vein, were able to efficiently revascularize tissue in the same manner. However, the tissue generated by the AV bundle had already undergone extensive remodeling and reorganization after one month, whereas the tissue of the AV loop was still primordially organized. This increased regenerative capacity of the AV bundle is attributable to an underlying mechanism originating in the close surrounding of the vessels. The

sheathing tissue transplanted together with the bundle itself not only contains connecting capillaries and proliferating fibroblasts, but importantly also progenitors of any kind. In the case of bone, progenitors of osteoblasts and osteoclasts, residing therein, can initiate new bone formation and enhance resorption of necrotic bone. Eventually this means that the recipient bone, transplanted together with the bundle actively takes part of the remodeling bone. This knowledge, showing that the AV bundle is able to both effectively vascularize large tissues and to enhance bone tissue remodeling opened the possibilities apply this method to challenging clinical scenarios such as large and complex bone defects [112].

3. **Aims of the Thesis:**

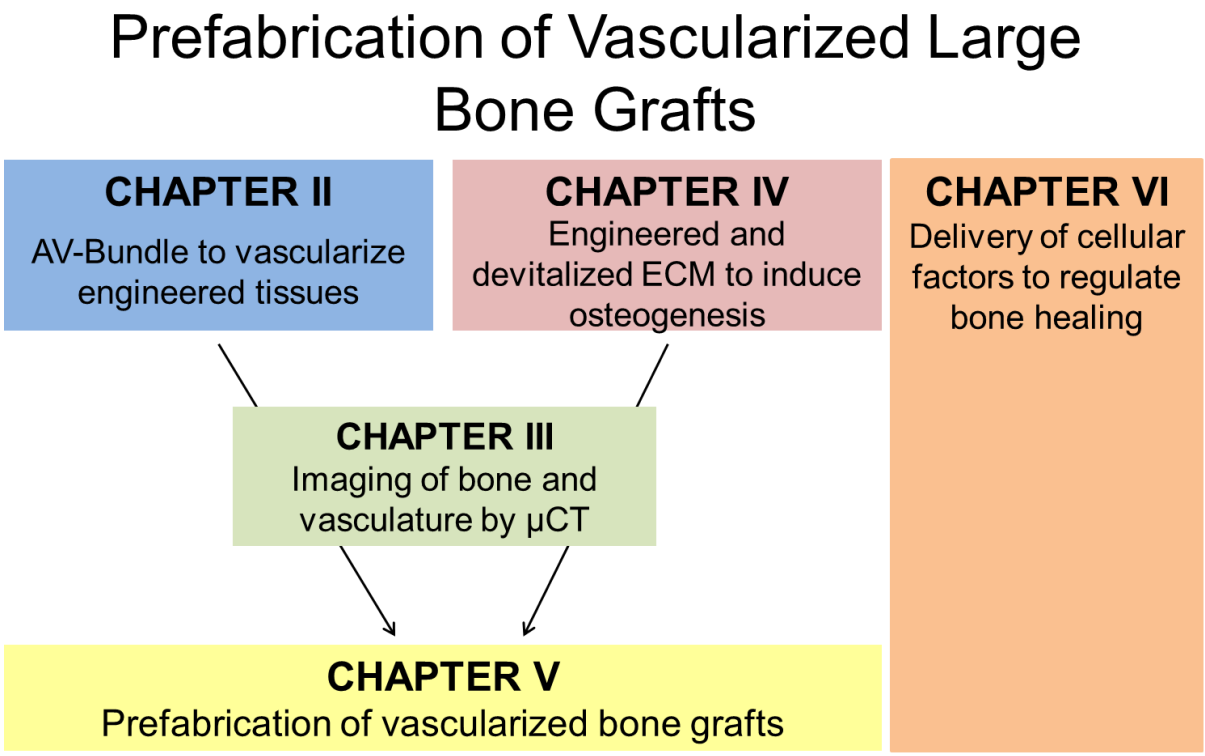

3.1. General aims of the thesis:

Based on the concepts described in the introductive chapter, the goal of my thesis is to generate a vascularized bone graft surrogate for large and complex bone defects. Stepwise, the challenges of such a bone graft were addressed: I aimed at developing an animal model to study large, complex bone defects and engineering an axially vascularized bone graft substitute, able to revascularize and induce efficient bone formation in this model (Chapter II). Secondly, I wanted to develop an appropriate imaging strategy thereof (Chapter III). Extensive review of the literature in chapter VI, led to development of a strategy to improve osteogenicity of the graft. Materials that in vivo can undergo robust bone formation processes, i.e. endochondral ossification, can be applied as off-the-shelf materials (Chapter IV) and finally integrating these concepts in the initially developed model (Chapter V).

3.2. Specific Aims of the thesis:

Chapter II “Engineered, axially-vascularized osteogenic grafts from human adipose-derived cells to treat avascular necrosis of bone in a rat model.”

This chapter aims to develop an animal model suitable to study large bone defects and to generate an osteogenic vascularized graft. The hypothesis is that such a graft would be potent enough to revascularize and revitalize the entire devitalized bone block and generate new bone. Specifically, we assessed whether addition of SVF cells to the vascularized graft could create a favorable immunological response, enhance vasculogenesis in the area of simulated AVN, and improve bone deposition and resorption in the graft.

Chapter III “Contrast-Enhanced Microtomographic Characterization of Vessels in Native Bone and Engineered Vascularized Grafts Using Ink-Gelatin Perfusion and Phosphotungstic Acid.”

In this chapter the aim was to develop an imaging technique for vascularized bones (e.g., rat femur and tibia). In particular, we investigated the reliability of the μCT-based analysis of vessels contrasted with ink-gelatin/PTA and compared it to the standard histological assessment. Finally, we aimed to demonstrate the application of this method on

simple engineered grafts consisting of vascularized porous hydroxyapatite, adapted from an avascular necrosis model used in rats.

Chapter IV “Fat-derived stromal vascular fraction cells enhance the bone forming capacity of devitalized engineered hypertrophic cartilage matrix.”

This chapter investigates the applicability of hypertrophic cartilage as off-the-shelf material for bone tissue replacement. To address the limitations of devitalized hypertrophic cartilage chips (HCC), which forfeits efficacy of bone formation by the

devitalization process, we tested the possibility to reactivate HCC with stromal vascular fraction (SVF) cells. We hypothesize that the mesenchymal, endothelial and osteoclastic progenitors, present in the SVF, can reactivate the HCC and thus lead to better bone formation.

Chapter V “Prefabrication of a large pedicled bone graft by engineering the germ for de novo vascularization and osteoinduction”

The aim of this study was to engineer an axially vascularized bone graft based on a developmentally inspired extracellular matrix. The hypothesis is that an engineered and devitalized cartilage matrix, combined with an AV bundle, is able to provide a germ for osteoinduction and vascularization.

Chapter VI “Delivery of cellular factors to regulate bone healing”

Bone tissue has a strong intrinsic regenerative capacity, thanks to a delicate and complex interplay of cellular and molecular processes, which tightly involve the immune system. In this chapter I review different approaches based on the delivery of regenerative cues produced by cells but in cell-free, possibly off-the-shelf configurations which could enhance bone replacement strategies.

4. Bibliography

[1] M. Jaishankar, T. Tseten, N. Anbalagan, B.B. Mathew, K.N. Beeregowda, Toxicity, mechanism and health effects of some heavy metals, Interdiscip. Toxicol. 7 (2014) 60–72. doi:10.2478/intox-2014-0009.

[2] J.Y. Rho, L. Kuhn-Spearing, P. Zioupos, Mechanical properties and the hierarchical structure of bone, Med. Eng. Phys. 20 (1998) 92–102. doi:10.1016/S1350-4533(98)00007-1.

[3] B.K. Hall, T. Miyake, All for one and one for all: Condensations and the initiation of skeletal development, BioEssays. 22 (2000) 138–147. doi:10.1002/(SICI)1521-1878(200002)22:2<138::AID-BIES5>3.0.CO;2-4.

[4] D. ten Berge, S.A. Brugmann, J.A. Helms, R. Nusse, Wnt and FGF signals interact to coordinate growth with cell fate specification during limb development, Development. 135 (2008) 3247–3257.

[5] N. Quarto, M.T. Longaker, FGF-2 inhibits osteogenesis in mouse adipose tissue-derived stromal cells and sustains their proliferative and osteogenic potential state, Tissue Eng. 12 (2006) 1405–1418.

[6] J.-D. Bénazet, M. Bischofberger, E. Tiecke, A. Gonçalves, J.F. Martin, A. Zuniga, F. Naef, R. Zeller, A self-regulatory system of interlinked signaling feedback loops controls mouse limb patterning, Science (80-.). 323 (2009) 1050–1053.

[7] F. Long, Building strong bones: Molecular regulation of the osteoblast lineage, Nat. Rev. Mol. Cell Biol. 13 (2012) 27–38. doi:10.1038/nrm3254.

[8] H.M. Kronenberg, Developmental regulation of the growth plate, Nature. 423 (2003) 332–336.

[9] H.M. Kronenberg, Developmental regulation of the growth plate, Nature. 423 (2003) 332–336. doi:10.1038/nature01657.

[10] C. Carulli, M. Innocenti, M.L. Brandi, Bone vascularization in normal and disease conditions, Front. Endocrinol. (Lausanne). 4 (2013). doi:10.3389/fendo.2013.00106.

[11] M.L. Brandi, P. Collin-Osdoby, Vascular biology and the skeleton, J. Bone Miner. Res. 21 (2006) 183–192. doi:10.1359/JBMR.050917.

[12] M. Marenzana, T.R. Arnett, The Key Role of the Blood Supply to Bone, Bone Res. 1 (2013) 203–215. doi:10.4248/BR201303001.

[13] M. Brookes, A.C. Elkin, R.G. Harrison, C.B. Heald, A NEW CONCEPT OF CAPILLARY CIRCULATION IN BONE CORTEX, Lancet. 277 (2018) 1078–1081. doi:10.1016/S0140-6736(61)92309-1.

[14] G.L. Mulfinger, J. Trueta, The blood supply of the talus., J. Bone Joint Surg. Br. 52 (1970) 160–167. doi:10.1017/S0022215100054803.

[15] M. Laroche, Intraosseous circulation from physiology to disease, Jt. Bone Spine. 69 (2002) 262–269. doi:10.1016/S1297-319X(02)00391-3.

[16] J. Pooley, J.E. Pooley, R.J. Montgomery, The Central Venous Sinus of Long Bones - Its Role in Relation to Exercise, in: J. Arlet, B. Mazières (Eds.), Bone Circ. Bone Necrosis, Springer Berlin Heidelberg, Berlin, Heidelberg, 1990: pp. 35–39.

[17] O.O.A. Oni, P.J. Gregg, The Routes of Venous Escape from the Marrow of the Diaphysis of Long Bones, in: J. Arlet, B. Mazières (Eds.), Bone Circ. Bone Necrosis, Springer Berlin Heidelberg, Berlin, Heidelberg, 1990: pp. 7–10.

[18] J. TRUETA, J.D. MORGAN, The vascular contribution to osteogenesis. I. Studies by the injection method., J. Bone Joint Surg. Br. 42-B (1960) 97–109.

[19] J. Trueta, Blood supply and the rate of healing of tibial fractures., Clin. Orthop. Relat. Res. (1974) 11–26.

[20] G. Bridgeman, M. Brookes, Blood supply to the human femoral diaphysis in youth and senescence., J. Anat. 188 (Pt 3 (1996) 611–621.

[21] O. Enjolras, R. Chapot, J.J. Merland, Vascular anomalies and the growth of limbs: a review., J. Pediatr. Orthop. Part B / Eur. Paediatr. Orthop. Soc. Pediatr. Orthop. Soc. North Am. 13 (2004) 349–357. doi:10.1097/01202412-200411000-00001.

[22] J.S. Harrison, P. Rameshwar, V. Chang, P. Bandari, Oxygen saturation in the bone

marrow of healthy volunteers., Blood. 99 (2002) 394. doi:10.1182/blood.v99.1.394.
[23] T.R. Arnett, Acidosis, hypoxia and bone, Arch. Biochem. Biophys. 503 (2010) 103–109. doi:10.1016/j.abb.2010.07.021.
[24] H.M. Sowter, R.R. Raval, J.W. Moore, P.J. Ratcliffe, A.L. Harris, Predominant role of hypoxia-inducible transcription factor (Hif)-1alpha versus Hif-2alpha in regulation of the transcriptional response to hypoxia., Cancer Res. 63 (2003) 6130–6134.
[25] K.E. Johnson, T.A. Wilgus, Vascular Endothelial Growth Factor and Angiogenesis in the Regulation of Cutaneous Wound Repair, Adv. Wound Care. 3 (2014) 647–661. doi:10.1089/wound.2013.0517.
[26] E. Schipani, C. Maes, G. Carmeliet, G.L. Semenza, Regulation of osteogenesis-angiogenesis coupling by HIFs and VEGF, J. Bone Miner. Res. 24 (2009) 1347–1353. doi:10.1359/jbmr.090602.
[27] J. Chang, S.G. Jackson, J. Wardale, S.W. Jones, Hypoxia modulates the phenotype of osteoblasts isolated from knee osteoarthritis patients, leading to undermineralized bone nodule formation, Arthritis Rheumatol. 66 (2014) 1789–1799. doi:10.1002/art.38403.
[28] J.C. Utting, S.P. Robins, A. Brandao-Burch, I.R. Orriss, J. Behar, T.R. Arnett, Hypoxia inhibits the growth, differentiation and bone-forming capacity of rat osteoblasts, Exp. Cell Res. 312 (2006) 1693–1702. doi:10.1016/j.yexcr.2006.02.007.
[29] T.C. Dandajena, M.A. Ihnat, B. Disch, J. Thorpe, G.F. Currier, Hypoxia triggers a HIF-mediated differentiation of peripheral blood mononuclear cells into osteoclasts, Orthod. Craniofacial Res. 15 (2012) 1–9. doi:10.1111/j.1601-6343.2011.01530.x.
[30] J.C. Utting, A.M. Flanagan, A. Brandao-Burch, I.R. Orriss, T.R. Arnett, Hypoxia stimulates osteoclast formation from human peripheral blood, Cell Biochem. Funct. 28 (2010) 374–380. doi:10.1002/cbf.1660.
[31] C. Salomon, J. Ryan, L. Sobrevia, M. Kobayashi, K. Ashman, M. Mitchell, G.E. Rice, Exosomal Signaling during Hypoxia Mediates Microvascular Endothelial Cell Migration and Vasculogenesis, PLoS One. 8 (2013). doi:10.1371/journal.pone.0068451.
[32] T. a Einhorn, The cell and molecular biology of fracture healing., Clin. Orthop. Relat. Res. (1998) S7–S21. doi:10.1097/00003086-199810001-00003.
[33] T. a Einhorn, The science of fracture healing., J. Orthop. Trauma. 19 (2005) S4–S6. doi:10.1097/00005131-200511101-00002.
[34] P. Lenas, M. Moos, F.P. Luyten, Developmental engineering: a new paradigm for the design and manufacturing of cell-based products. Part I: from three-dimensional cell growth to biomimetics of in vivo development., Tissue Eng. Part B. Rev. 15 (2009) 381–94. doi:10.1089/ten.TEB.2008.0575.
[35] P. Pivonka, C.R. Dunstan, Role of mathematical modeling in bone fracture healing, Bonekey Rep. 1 (2012). doi:10.1038/bonekey.2012.221.
[36] O. Grundnes, O. Reikeras, Blood flow and mechanical properties of healing bone, Femoral osteotomies studied in rats, Acta OrthoD Scand. 63 (1992) 487–491. doi:10.3109/17453679209154720.
[37] U. Mayr-Wohlfart, J. Waltenberger, H. Hausser, S. Kessler, K.-P. Günther, C. Dehio, W. Puhl, R.E. Brenner, Vascular endothelial growth factor stimulates chemotactic migration of primary human osteoblasts, Bone. 30 (2002) 472–477.
[38] K. Hu, B.R. Olsen, The roles of vascular endothelial growth factor in bone repair and regeneration, Bone. 91 (2016) 30–38. doi:http://dx.doi.org/10.1016/j.bone.2016.06.013.
[39] K.D. Hankenson, M. Dishowitz, C. Gray, M. Schenker, Angiogenesis in bone regeneration, Injury. 42 (2011) 556–561. doi:http://dx.doi.org/10.1016/j.injury.2011.03.035.
[40] A. Groothuis, G.N. Duda, C.J. Wilson, M.S. Thompson, M.R. Hunter, P. Simon, H.J. Bail, K.M. van Scherpenzeel, G. Kasper, Mechanical stimulation of the pro-angiogenic capacity of human fracture haematoma: involvement of VEGF mechano-regulation, Bone. 47 (2010) 438–444.
[41] B. McKibbin, The biology of fracture healing in long bones., J. Bone Joint Surg. Br. 60-B (1978) 150–162.

[42] G. Kumar, B. Narayan, The biology of fracture healing in long bones, in: Class. Pap. Orthop., 2014: pp. 531–533. doi:10.1007/978-1-4471-5451-8_139.
[43] S.M. Perren, Evolution of the internal fixation of long bone fractures. The scientific basis of biological internal fixation: choosing a new balance between stability and biology., J. Bone Joint Surg. Br. 84 (2002) 1093–1110. doi:10.1115/1.4026364.
[44] L. Cleas, N. Maurer-Klein, T. Henke, H. Gerngross, M. McInyk, P. Augat, Moderate Soft Tissue Trauma Delays New Bone Formation Only in the Early Phase of Fracture Healing, J. Orthop. Res. 24 (2006) 1178–1185. doi:10.1002/jor.
[45] H. Willenegger, S.M. Perren, R. Schenk, [Primary and secondary healing of bone fractures]., Chirurg. 42 (1971) 241–252.
[46] T. Kon, T. Cho, T. Aizawa, M. Yamazaki, N. Nooh, D. Graves, L.C. Gerstenfeld, T.A. Einhorn, Expression of Osteoprotegerin, Receptor Activator of NF- κB Ligand (Osteoprotegerin Ligand) and Related Proinflammatory Cytokines During Fracture Healing, J. Bone Miner. Res. 16 (2001) 1004–1014.
[47] R. Bielby, E. Jones, D. McGonagle, The role of mesenchymal stem cells in maintenance and repair of bone, Injury. 38 (2007) S26–S32.
[48] L.E. Claes, C.A. Heigele, Magnitudes of local stress and strain along bony surfaces predict the course and type of fracture healing, J. Biomech. 32 (1999) 255–266. doi:10.1016/S0021-9290(98)00153-5.
[49] H. Nakahara, S.P. Bruder, S.E. Haynesworth, J.J. Holecek, M.A. Baber, V.M. Goldberg, A.I. Caplan, Bone and cartilage formation in diffusion chambers by subcultured cells derived from the periosteum, Bone. 11 (1990) 181–188. doi:10.1016/8756-3282(90)90212-H.
[50] R. Marsell, T.A. Einhorn, The biology of fracture healing, Injury. 42 (2011) 551–555. doi:10.1016/j.injury.2011.03.031.
[51] L. Claes, S. Recknagel, A. Ignatius, Fracture healing under healthy and inflammatory conditions, Nat. Rev. Rheumatol. 8 (2012) 133–143. doi:10.1038/nrrheum.2012.1.
[52] C.A. Bassett, I. Herrmann, Influence of oxygen concentration and mechanical factors on differentiation of connective tissues in vitro., Nature. 190 (1961) 460–461.
[53] L. Claes, K. Eckert-Hübner, P. Augat, The effect of mechanical stability on local vasularization and tissue differentiation in callus healing, J. Orthop. Res. 20 (2002) 1099–1105.
[54] F.W. Rhinelander, Tibial blood supply in relation to fracture healing, Clin.Orthop. No. 105 (1974) 34–81. doi:10.1097/00003086-197411000-00005.
[55] S. Otsuru, K. Tamai, T. Yamazaki, H. Yoshikawa, Y. Kaneda, Circulating Bone Marrow-Derived Osteoblast Progenitor Cells Are Recruited to the Bone-Forming Site by the CXCR4/Stromal Cell-Derived Factor-1 Pathway, Stem Cells. 26 (2008) 223–234. doi:10.1634/stemcells.2007-0515.
[56] T. Kitaori, H. Ito, E.M. Schwarz, R. Tsutsumi, H. Yoshitomi, S. Oishi, M. Nakano, N. Fujii, T. Nagasawa, T. Nakamura, Stromal cell–derived factor 1/CXCR4 signaling is critical for the recruitment of mesenchymal stem cells to the fracture site during skeletal repair in a mouse model, Arthritis Rheum. 60 (2009) 813–823. doi:10.1002/art.24330.
[57] K.K. Mak, H.M. Kronenberg, P.-T. Chuang, S. Mackem, Y. Yang, Indian hedgehog signals independently of PTHrP to promote chondrocyte hypertrophy, Development. 135 (2008) 1947–1956.
[58] E.J. Mackie, Y.A. Ahmed, L. Tatarczuch, K.S. Chen, M. Mirams, Endochondral ossification: How cartilage is converted into bone in the developing skeleton, Int. J. Biochem. Cell Biol. 40 (2008) 46–62. doi:10.1016/j.biocel.2007.06.009.
[59] E.M. Thompson, A. Matsiko, E. Farrell, D.J. Kelly, F.J. O'Brien, Recapitulating endochondral ossification: A promising route to in vivo bone regeneration, J. Tissue Eng. Regen. Med. 9 (2015) 889–902. doi:10.1002/term.1918.
[60] M. Melnyk, T. Henke, L. Claes, P. Augat, Revascularisation during fracture healing with soft tissue injury, Arch. Orthop. Trauma Surg. 128 (2008) 1159–1165. doi:10.1007/s00402-007-0543-0.
[61] F.W. Rhinelander, Tibial blood supply in relation to fracture healing, Clin.Orthop. No.

105 (1974) 34–81. doi:10.1097/00003086-197411000-00005.
[62] A. Schindeler, M.M. McDonald, P. Bokko, D.G. Little, Bone remodeling during fracture repair: The cellular picture, Semin. Cell Dev. Biol. 19 (2008) 459–466. doi:10.1016/j.semcdb.2008.07.004.
[63] L. Claes, Biomechanical principles and mechanobiologic aspects of flexible and locked plating., J. Orthop. Trauma. 25 Suppl 1 (2011) S4–7. doi:10.1097/BOT.0b013e318207093e.
[64] S. Thomas, Surgery, Science and Industry, Springer International Publishing, 2002. doi:10.1057/9780230513280.
[65] D.L. Helfet, N.P. Haas, J. Schatzker, P. Matter, R. Moser, B. Hanson, AO Philosophy and Principles of Fracture Management-Its Evolution and Evaluation*, J. Bone Jt. Surg. 85 (2003) 1156–1160. doi:10.2106/00004623-200306000-00029.
[66] T.P. Rüedi, C. Sommer, A. Leutenegger, New techniques in indirect reduction of long bone fractures., Clin. Orthop. Relat. Res. (1998) 27–34. http://www.ncbi.nlm.nih.gov/pubmed/9520872.
[67] A. Haumer, T. Ismail, A. Lunger, R. Osinga, A. Scherberich, D.J. Schaefer, I. Martin, From Autologous Flaps to Engineered Vascularized Grafts for Bone Regeneration, in: W. Holnthoner, A. Banfi, J. Kirkpatrick, H. Redl (Eds.), Vasc. Tissue Eng. Regen. Med., Springer International Publishing, Cham, 2017: pp. 1–34. doi:10.1007/978-3-319-21056-8_16-1.
[68] M.W. Laschke, M.D. Menger, Vascularization in tissue engineering: Angiogenesis versus inosculation, Eur. Surg. Res. 48 (2012) 85–92. doi:10.1159/000336876.
[69] M.W. Laschke, B. Vollmar, M.D. Menger, Inosculation: connecting the life-sustaining pipelines., Tissue Eng. Part B. Rev. 15 (2009) 455–65. doi:10.1089/ten.TEB.2009.0252.
[70] J. Rouwkema, N.C. Rivron, C.A. van Blitterswijk, Vascularization in tissue engineering, Trends Biotechnol. 26 (2008) 434–441. doi:10.1016/j.tibtech.2008.04.009.
[71] A. Oryan, S. Alidadi, A. Moshiri, N. Maffulli, Bone regenerative medicine: classic options, novel strategies, and future directions., J. Orthop. Surg. Res. 9 (2014) 18. doi:10.1186/1749-799X-9-18.
[72] M. Deschepper, M. Manassero, K. Oudina, J. Paquet, L.E. Monfoulet, M. Bensidhoum, D. Logeart-Avramoglou, H. Petite, Proangiogenic and prosurvival functions of glucose in human mesenchymal stem cells upon transplantation, Stem Cells. 31 (2013) 526–535. doi:10.1002/stem.1299.
[73] a W. Orr, C. a Elzie, D.F. Kucik, J.E. Murphy-Ullrich, Thrombospondin signaling through the calreticulin/LDL receptor-related protein co-complex stimulates random and directed cell migration., J. Cell Sci. 116 (2003) 2917–27. doi:10.1242/jcs.00600.
[74] M.I. Santos, R.L. Reis, Vascularization in bone tissue engineering: Physiology, current strategies, major hurdles and future challenges, Macromol. Biosci. 10 (2010) 12–27. doi:10.1002/mabi.200900107.
[75] M.W. Laschke, B. Vollmar, M.D. Menger, Inosculation: connecting the life-sustaining pipelines., Tissue Eng. Part B. Rev. 15 (2009) 455–65. doi:10.1089/ten.TEB.2009.0252.
[76] M.W. Laschke, Y. Harder, M. Amon, I. Martin, J. Farhadi, A. Ring, N. Torio-Padron, R. Schramm, M. Rücker, D. Junker, J.M. Häufel, C. Carvalho, M. Heberer, G. Germann, B. Vollmar, M.D. Menger, Angiogenesis in tissue engineering: breathing life into constructed tissue substitutes., Tissue Eng. 12 (2006) 2093–2104. doi:10.1089/ten.2006.12.ft-130.
[77] P.K.D. V Yarlagadda, M. Chandrasekharan, J.Y.M. Shyan, Recent advances and current developments in tissue scaffolding., Biomed. Mater. Eng. 15 (2005) 159–177.
[78] M. R??cker, M.W. Laschke, D. Junker, C. Carvalho, A. Schramm, R. M??lhaupt, N.C. Gellrich, M.D. Menger, Angiogenic and inflammatory response to biodegradable scaffolds in dorsal skinfold chambers of mice, Biomaterials. 27 (2006) 5027–5038. doi:10.1016/j.biomaterials.2006.05.033.
[79] M. R??cker, M.W. Laschke, D. Junker, C. Carvalho, F. Tavassol, R. M??lhaupt, N.C. Gellrich, M.D. Menger, Vascularization and biocompatibility of scaffolds consisting of

different calcium phosphate compounds, J. Biomed. Mater. Res. - Part A. 86 (2008) 1002–1011. doi:10.1002/jbm.a.31722.
[80] T.P. Richardson, M.C. Peters, a B. Ennett, D.J. Mooney, Polymeric system for dual growth factor delivery., Nat. Biotechnol. 19 (2001) 1029–1034. doi:10.1038/nbt1101-1029.
[81] S.T.M. Nillesen, P.J. Geutjes, R. Wismans, J. Schalkwijk, W.F. Daamen, T.H. van Kuppevelt, Increased angiogenesis and blood vessel maturation in acellular collagen-heparin scaffolds containing both FGF2 and VEGF, Biomaterials. 28 (2007) 1123–1131. doi:10.1016/j.biomaterials.2006.10.029.
[82] M.W. Laschke, M. R??cker, G. Jensen, C. Carvalho, R. M??lhaupt, N.C. Gellrich, M.D. Menger, Incorporation of growth factor containing Matrigel promotes vascularization of porous PLGA scaffolds, J. Biomed. Mater. Res. - Part A. 85 (2008) 397–407. doi:10.1002/jbm.a.31503.
[83] F.G. Rocha, C.A. Sundback, N.J. Krebs, J.K. Leach, D.J. Mooney, S.W. Ashley, J.P. Vacanti, E.E. Whang, The effect of sustained delivery of vascular endothelial growth factor on angiogenesis in tissue-engineered intestine, Biomaterials. 29 (2008) 2884–2890. doi:10.1016/j.biomaterials.2008.03.026.
[84] M. Ehrbar, S.M. Zeisberger, G.P. Raeber, J.A. Hubbell, C. Schnell, A.H. Zisch, The role of actively released fibrin-conjugated VEGF for VEGF receptor 2 gene activation and the enhancement of angiogenesis, Biomaterials. 29 (2008) 1720–1729. doi:10.1016/j.biomaterials.2007.12.002.
[85] Z. Lokmic, G.M. Mitchell, Engineering the microcirculation., Tissue Eng. Part B. Rev. 14 (2008) 87–103. doi:10.1089/teb.2007.0299.
[86] M.A. Pogrel, S. Podlesh, J.P. Anthony, J. Alexander, A comparison of vascularized and nonvascularized bone grafts for reconstruction of mandibular continuity defects, J. Oral Maxillofac. Surg. 55 (1997) 1200–1206. doi:10.1016/S0278-2391(97)90165-8.
[87] R.D. Foster, J.P. Anthony, A. Sharma, M.A. Pogrel, Vascularized bone flaps versus nonvascularized bone grafts for mandibular reconstruction: An outcome analysis of primary bony union and endosseous implant success, Head Neck. 21 (1999) 66–71. doi:10.1002/(SICI)1097-0347(199901)21:1<66::AID-HED9>3.0.CO;2-Z.
[88] J.J. Pribaz, N. Fine, D.P. Orgill, Flap prefabrication in the head and neck: a 10-year experience, Plast Reconstr Surg. 103 (1999) 808–820. http://www.ncbi.nlm.nih.gov/pubmed/10077069.
[89] N.T. Hoang, M. Kloeppel, R. Staudenmaier, S. Schweinbeck, E. Biemer, Neovascularization in prefabricated flaps using a tissue expander and an implanted arteriovenous pedicle, Microsurgery. 25 (2005) 213–219. doi:10.1002/micr.20098.
[90] A. von Bomhard, J. Veit, C. Bermueller, N. Rotter, R. Staudenmaier, K. Storck, H.N. The, Prefabrication of 3D Cartilage Contructs: Towards a Tissue Engineered Auricle - A Model Tested in Rabbits, PLoS One. 8 (2013). doi:10.1371/journal.pone.0071667.
[91] a F. Black, F. Berthod, N. L'heureux, L. Germain, F. a Auger, In vitro reconstruction of a human capillary-like network in a tissue-engineered skin equivalent., FASEB J. 12 (1998) 1331–1340. doi:0892-6638/98/0012-1331.
[92] N. Koike, D. Fukumura, O. Gralla, P. Au, J.S. Schechner, R.K. Jain, Tissue engineering: creation of long-lasting blood vessels., Nature. 428 (2004) 138–139. doi:10.1038/428138a.
[93] S. Levenberg, J. Rouwkema, M. Macdonald, E.S. Garfein, D.S. Kohane, D.C. Darland, R. Marini, C.A. van Blitterswijk, R.C. Mulligan, P.A. D'Amore, R. Langer, Engineering vascularized skeletal muscle tissue, Nat Biotechnol. 23 (2005) 879–884. doi:10.1038/nbt1109.
[94] B.R. Shepherd, D.R. Enis, F. Wang, Y. Suarez, J.S. Pober, J.S. Schechner, Vascularization and engraftment of a human skin substitute using circulating progenitor cell-derived endothelial cells., FASEB J. 20 (2006) 1739–1741. doi:10.1096/fj.05-5682fje.
[95] Z.Z. Wang, P. Au, T. Chen, Y. Shao, L.M. Daheron, H. Bai, M. Arzigian, D. Fukumura, R.K. Jain, D.T. Scadden, Endothelial cells derived from human embryonic stem cells form durable blood vessels in vivo., Nat. Biotechnol. 25 (2007) 317–8.

doi:10.1038/nbt1287.
[96] A. Arkudas, J.P. Beier, K. Heidner, J. Tjiawi, E. Polykandriotis, S. Srour, M. Sturzl, R.E. Horch, U. Kneser, Axial prevascularization of porous matrices using an arteriovenous loop promotes survival and differentiation of transplanted autologous osteoblasts., Tissue Eng. 13 (2007) 1549–1560. doi:10.1089/ten.2006.0387.
[97] S.D. McCullen, A.G.Y. Chow, M.M. Stevens, In vivo tissue engineering of musculoskeletal tissues, Curr. Opin. Biotechnol. 22 (2011) 715–720. doi:10.1016/j.copbio.2011.05.001.
[98] S.F. Badylak, R.M. Nerem, Progress in tissue engineering and regenerative medicine., Proc. Natl. Acad. Sci. U. S. A. 107 (2010) 3285–3286. doi:10.1073/pnas.1000256107.
[99] M.M. Stevens, R.P. Marini, D. Schaefer, J. Aronson, R. Langer, V.P. Shastri, In vivo engineering of organs: the bone bioreactor., Proc. Natl. Acad. Sci. U. S. A. 102 (2005) 11450–5. doi:10.1073/pnas.0504705102.
[100] P. Warnke, I. Springer, P.J. Wiltfang, P.Y. Acil, P.H. Eufinger, M. Wehmöller, P. Russo, H. Bolte, E. Sherry, E. Behrens, P.H. Terheyden, Growth and transplantation of a custom vascularised bone graft in a man, Lancet. 364 (2004) 766–770. doi:10.1016/S0140-6736(04)16935-3.
[101] G.E. Holt, J.L. Halpern, T.T. Dovan, D. Hamming, H.S. Schwartz, Evolution of an in vivo bioreactor, J. Orthop. Res. 23 (2005) 916–923. doi:10.1016/j.orthres.2004.10.005.
[102] I.N. Springer, P.F. Nocini, K. a Schlegel, D. De Santis, J. Park, P.H. Warnke, H. Terheyden, R. Zimmermann, L. Chiarini, K. Gardner, F. Ferrari, J. Wiltfang, Two techniques for the preparation of cell-scaffold constructs suitable for sinus augmentation: steps into clinical application., Tissue Eng. 12 (2006) 2649–2656. doi:10.1089/ten.2006.12.ft-206.
[103] M.W. Laschke, M. Rücker, G. Jensen, C. Carvalho, R. Mülhaupt, N.C. Gellrich, M.D. Menger, Improvement of vascularization of PLGA scaffolds by inosculation of in situ-preformed functional blood vessels with the host microvasculature, Ann. Surg. 248 (2008) 939–947. doi:10.1097/SLA.0b013e31818fa52f.
[104] M.W. Laschke, M.D. Menger, Prevascularization in tissue engineering: Current concepts and future directions, Biotechnol. Adv. 34 (2015) 112–121. doi:10.1016/j.biotechadv.2015.12.004.
[105] E. Polykandriotis, J. Tjiawi, S. Euler, A. Arkudas, A. Hess, K. Brune, P. Greil, A. Lametschwandtner, R.E. Horch, U. Kneser, The venous graft as an effector of early angiogenesis in a fibrin matrix, Microvasc. Res. 75 (2008) 25–33. doi:10.1016/j.mvr.2007.04.003.
[106] Y. Tanaka, K.-C. Sung, A. Tsutsumi, S. Ohba, K. Ueda, W. a Morrison, Tissue engineering skin flaps: which vascular carrier, arteriovenous shunt loop or arteriovenous bundle, has more potential for angiogenesis and tissue generation?, Plast. Reconstr. Surg. 112 (2003) 1636–44. doi:10.1097/01.PRS.0000086140.49022.AB.
[107] O.O. Erol, M. Sira, New capillary bed formation with a surgically constructed arteriovenous fistula., Plast. Reconstr. Surg. 66 (1980) 109–15. doi:10.1097/00006534-198208000-00093.
[108] R. Mian, W. a Morrison, J. V Hurley, a J. Penington, R. Romeo, Y. Tanaka, K.R. Knight, Formation of new tissue from an arteriovenous loop in the absence of added extracellular matrix., Tissue Eng. 6 (2000) 595–603. doi:10.1089/10763270050199541.
[109] A.M. Eweida, A.S. Nabawi, M. Abouarab, M. Kayed, H. Elhammady, A. Etaby, M.R. Khalil, M.S. Shawky, U. Kneser, R.E. Horch, N. Nagy, M.K. Marei, Enhancing mandibular bone regeneration and perfusion via axial vascularization of scaffolds, Clin. Oral Investig. 18 (2014) 1671–1678. doi:10.1007/s00784-013-1143-8.
[110] O.C. Cassell, W.A. Morrison, A. Messina, A.J. Penington, E.W. Thompson, G.W. Stevens, J.M. Perera, H.K. Kleinman, J. V Hurley, R. Romeo, K.R. Kinght, The influence of extracellular matrix on the generation of vascularized, engineered, transplantable tissue., Ann. N. Y. Acad. Sci. 944 (2001) 429–42. doi:10.1111/j.1749-6632.2001.tb03853.x.

[111] Y. Shintomi, T. Ohura, The use of muscle vascularized pedicle flaps., Plast. Reconstr. Surg. 70 (1982) 725–735.
[112] Y. Hori, S. Tamai, H. Okuda, H. Sakamoto, T. Takita, K. Masuhara, Blood vessel transplantation to bone, J. Hand Surg. Am. 4 (1979) 23–33. doi:10.1016/S0363-5023(79)80101-X.
[113] C. Di Bella, E. Lucarelli, D. Donati, Historical review of bone prefabrication, Chir. Organi Mov. 92 (2008) 73–78. doi:10.1007/s12306-008-0052-5.
[114] A.M. Muller, A. Mehrkens, D.J. Schafer, C. Jaquiery, S. Guven, M. Lehmicke, R. Martinetti, I. Farhadi, M. Jakob, A. Scherberich, I. Martin, Towards an intraoperative engineering of osteogenic and vasculogenic grafts from the stromal vascular fraction of human adipose tissue., Eur. Cell. Mater. 19 (2010) 127–135.
[115] A. Mehrkens, F. Saxer, S. Güven, W. Hoffmann, A.M. Müller, M. Jakob, F.E. Weber, I. Martin, A. Scherberich, Intraoperative engineering of osteogenic grafts combining freshly harvested, human adipose-derived cells and physiological doses of bone morphogenetic protein-2, Eur. Cells Mater. 24 (2012) 308–319.
[116] R.J. Pignolo, M. Kassem, Circulating osteogenic cells: Implications for injury, repair, and regeneration., J. Bone Miner. Res. 26 (2011) 1685–1693. doi:10.1002/jbmr.370.
[117] G.Z. Eghbali-Fatourechi, J. Lamsam, D. Fraser, D. Nagel, B.L. Riggs, S. Khosla, Circulating Osteoblast-Lineage Cells in Humans, N. Engl. J. Med. 352 (2005) 1959–1966. doi:10.1056/NEJMoa044264.
[118] T. Ismail, R. Osinga, A.J. Todorov, A. Haumer, L.A. Tchang, C. Epple, N. Allafi, N. Menzi, R.D. Largo, A. Kaempfen, I. Martin, D.J. Schaefer, A. Scherberich, Engineered, axially-vascularized osteogenic grafts from human adipose-derived cells to treat avascular necrosis of bone in a rat model., Acta Biomater. (2017). doi:10.1016/j.actbio.2017.09.003.
[119] H. Kaneko, T. Arakawa, H. Mano, T. Kaneda, A. Ogasawara, M. Nakagawa, Y. Toyama, Y. Yabe, M. Kumegawa, Y. Hakeda, Direct stimulation of osteoclastic bone resorption by bone morphogenetic protein (BMP)-2 and expression of BMP receptors in mature osteoclasts., Bone. 27 (2000) 479–486.
[120] P. Bourgine, C. Le Magnen, S. Pigeot, J. Geurts, A. Scherberich, I. Martin, Combination of immortalization and inducible death strategies to generate a human mesenchymal stromal cell line with controlled survival, Stem Cell Res. 12 (2014) 584. doi:10.1016/j.scr.2013.12.006.

Chapter II:

AV-bundle to vascularize engineered tissues

Acta Biomaterialia 63 (2017) 236–245

Contents lists available at ScienceDirect

Acta Biomaterialia

journal homepage: www.elsevier.com/locate/actabiomat

Engineered, axially-vascularized osteogenic grafts from human adipose-derived cells to treat avascular necrosis of bone in a rat model

Tarek Ismail [a,b,1], Rik Osinga [a,b,1], Atanas Todorov Jr. [a], Alexander Haumer [a], Laurent A. Tchang [a,b], Christian Epple [a], Nima Allafi [a], Nadia Menzi [a], René D. Largo [a,b], Alexandre Kaempfen [a,b], Ivan Martin [a,c,*], Dirk J. Schaefer [b], Arnaud Scherberich [a,b,c]

[a] Department of Biomedicine, University Hospital Basel, University of Basel, Switzerland
[b] Department of Plastic, Reconstructive, Aesthetic and Hand Surgery, University Hospital Basel, Switzerland
[c] Department of Biomedical Engineering, University of Basel, Switzerland

ARTICLE INFO

Article history:
Received 17 May 2017
Received in revised form 4 September 2017
Accepted 5 September 2017
Available online 8 September 2017

Keywords:
Avascular necrosis
Treatment
Axial vascularization
Osteogenic graft
Tissue engineering

ABSTRACT

Background: Avascular necrosis of bone (AVN) leads to sclerosis and collapse of bone and joints. The standard of care, vascularized bone grafts, is limited by donor site morbidity and restricted availability. The aim of this study was to generate and test engineered, axially vascularized SVF cells-based bone substitutes in a rat model of AVN.
Methods: SVF cells were isolated from lipoaspirates and cultured onto porous hydroxyapatite scaffolds within a perfusion-based bioreactor system for 5 days. The resulting constructs were inserted into devitalized bone cylinders mimicking AVN-affected bone. A ligated vascular bundle was inserted upon subcutaneous implantation of constructs in nude rats. After 1 and 8 weeks in vivo, bone formation and vascularization were analyzed.
Results: Newly-formed bone was found in 80% of SVF-seeded scaffolds after 8 weeks but not in unseeded controls. Human ALU + cells in the bone structures evidenced a direct contribution of SVF cells to bone formation. A higher density of regenerative, M2 macrophages was observed in SVF-seeded constructs. In both experimental groups, devitalized bone was revitalized by vascularized tissue after 8 weeks.
Conclusion: SVF cells-based osteogenic constructs revitalized fully necrotic bone in a challenging AVN rat model of clinically-relevant size. SVF cells contributed to accelerated initial vascularization, to bone formation and to recruitment of pro-regenerative endogenous cells.

Statement of significance

Avascular necrosis (AVN) of bone often requires surgical treatment with autologous bone grafts, which is surgically demanding and restricted by significant donor site morbidity and limited availability. This paper describes a *de novo* engineered axially-vascularized bone graft substitute and tests the potential to revitalize dead bone and provide efficient new bone formation in a rat model.
The engineering of an osteogenic/vasculogenic construct of clinically-relevant size with stromal vascular fraction of human adipose, combined to an arteriovenous bundle is described. This construct revitalized and generated new bone tissue. This successful approach proposes a novel paradigm in the treatment of AVN, in which an engineered, vascularized osteogenic graft would be used as a germ to revitalize large volumes of necrotic bone.

1. Introduction

Avascular necrosis of bone (AVN) often affects joints and can have a very destructive course. It is not a specific disease entity, but rather the final common pathway of a number of conditions leading to bone death due to impaired blood supply. The specific etiopathogenesis is not known in detail, but the last steps include ischemia of bone and osteocyte death. This is believed to be the

* Corresponding author at: Department of Biomedicine, University Hospital Basel, Hebelstrasse 20, Basel 4031, Switzerland.
E-mail addresses: tarek.ismail@usb.ch (T. Ismail), rik.osinga@usb.ch (R. Osinga), atanastodo@gmail.com (A. Todorov Jr.), alexander.haumer@usb.ch (A. Haumer), laurenttchang@hotmail.com (L.A. Tchang), christian.epple.ce@gmail.com (C. Epple), n.allafi@icloud.com (N. Allafi), nadia.menzi@hotmail.com (N. Menzi), rene.largo@yahoo.com (R.D. Largo), alexandre.kaempfen@usb.ch (A. Kaempfen), ivan.martin@usb.ch (I. Martin), dirk.schaefer@usb.ch (D.J. Schaefer), arnaud.scherberich@usb.ch (A. Scherberich).
[1] Contributed equally to this study.

http://dx.doi.org/10.1016/j.actbio.2017.09.003
1742-7061/

result of a combined effect of genetic predisposition, metabolic factors, and local factors affecting blood supply, such as vascular damage/increased intraosseous pressure, and mechanical stresses [1–4]. Known risk factors are the use of corticosteroids, alcohol, bisphosphonates, previous trauma, malignancies or metabolic disorders, but often the underlying mechanisms remain unclear [5]. Reactive hyperemia and fibrous repair occur in the adjacent bony tissue and revascularization of the dead bone begins. Repair of the damage is attempted through bone resorption by osteoclasts and new bone deposition by osteoblasts. In many cases, the integrity of the bony mass is damaged and stress fractures occur over time, resulting in a collapse of the osteochondral area in articulating bones [6,7], causing painful osteoarthritis. In addition, immunological reaction with an imbalance between pro-inflammatory M1 macrophages and pro-regenerative M2 macrophages further inhibits physiological tissue remodeling [8]. Treatment of AVN remains very controversial but the goal of therapy is clear: preserving the native joint for as long as possible to avoid total joint replacement. Nonoperative management is reported to provide adequate clinical results in only 20% of patients approximately [9–11]. Osteotomy, core decompression, cell based therapies, non vascularized bone grafts and vascularized fibular grafts are current operative procedures. Most consistent successful results are seen after free vascularized fibula grafting [12]. However, this procedure is surgically demanding, has limited availability, is associated with significant donor site morbidity [13] and complex three-dimensional grafts cannot be generated.

We have previously demonstrated that freshly isolated stromal vascular fraction (SVF) cells from human adipose tissue, seeded and cultured within a large porous hydroxyapatite scaffold in a perfusion bioreactor system, can generate osteogenic grafts with intrinsic vascularization and rapid engraftment capacity in vivo [14,15]. To test the effectiveness of such engineered grafts into a clinically-relevant setting of AVN, we adapted a previously described rabbit model [16], whereby devitalized bone matrix was used to simulate necrotic bone. In order to restore efficient vascularization in the model by a strategy which is clinically relevant and translatable, the ligated arteriovenous (AV) bundle was favored over a loop approach because of lower risk of thrombus formation and better surgical feasibility [17].

The aim of this study was to engineer an axially vascularized bone graft substitute to revitalize, revascularize and finally induce efficient bone formation in an in vivo model reflecting the clinical setting of AVN. For this purpose, the well-defined vascular supply of an AV bundle was combined with a SVF cell seeded hydroxyapatite scaffold and tested in a rat model of AVN, developed based on the rabbit model described earlier [16]. We hypothesized that such osteogenic vascularized graft would (i) be potent enough to generate bone in the hydroxyapatite core and (ii) revitalize the outer devitalized bone block mimicking AVN. Specifically, we tested whether addition of SVF cells to the vascularized graft could create a favorable immunological response, enhance vasculogenesis in the area of simulated AVN, and improve bone deposition and resorption in the graft.

2. Materials and methods

2.1. SVF cells isolation

Human adipose samples were collected with informed consent in accordance with the local ethical commission (EKBB; Ref. No 78/07). Stromal vascular fraction (SVF) cells were extracted from lipoaspiration or minced excision material of human adipose tissue of 5 healthy female donors (mean age 43 ± 12 years), as previously described [14]. The cellular pellet was suspended in serum free medium (α-MEM, 1% HEPES, 1% sodium pyruvate, 1% of Penicillin-Streptomycin-Glutamine, all from Gibco) and serially filtered through a tea strainer and a 100 μm nylon mesh (Sarstedt, Nümbrecht, Germany). Nucleated cells were counted in a Neubauer chamber (Marienfeld, Lauda-Königshofen, Germany) after staining with crystal violet (Sigma-Aldrich, Buchs, Switzerland).

2.2. Graft seeding and preparation

Cylinders of porous hydroxyapatite (HA) (Engipore, Finceramica-Faenza, Faenza, Italy), 1 cm diameter and 1 cm height (Fig. 1A) were seeded and cultured with SVF cells in a perfusion-based bioreactor system as described previously [14]. A suspension of 12 × 106 SVF cells in 8 ml serum free medium supplemented with 10^{-7} M dexamethasone, 25 mM ascorbic acid (Sigma-Aldrich), 5 ng/ml FGF-2 (RnD) and 10% v/v FBS (Gibco) was injected into the bioreactor system and cultured under oscillating perfusion

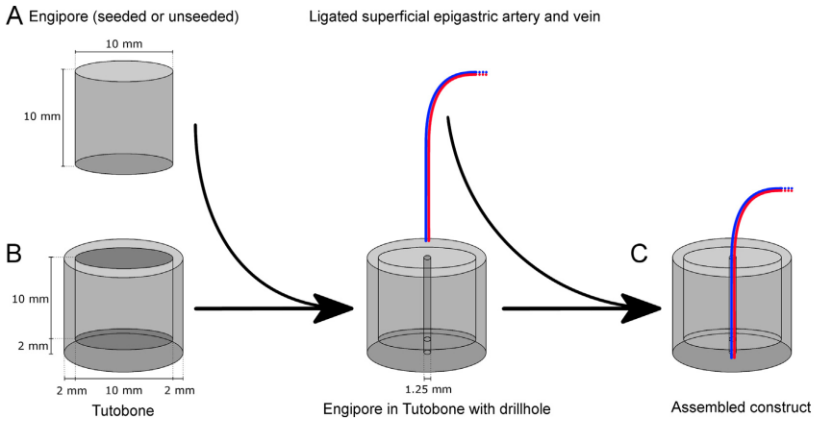

Fig. 1. Graft composition. Large cylinders of porous hydroxyapatite (HA) scaffolds (Engipore) (A) were either seeded with SVF cells in a bioreactor system or placed without seeding into a customized devitalized bovine cancellous bone construct (Tutobone) (B) mimicking AVN. After drilling a 1.25 diameter channel through the construct the graft was then vascularized by inserting the ligated superficial epigastric artery and vein (C).

at a flow rate of 1 ml / min for 5 days at 37 °C and 5% CO2. The culture medium was refreshed after 3 days. Cell-free HA cylinders were used as controls and hereafter referred to as unseeded grafts.

For 8-week implantations, grafts were inserted in a hollow tapered cylinder made of processed bovine cancellous bone (Tutobone, Tutogen Medical, Neunkirchen, Germany) (Fig. 1B) mimicking an avascular and acellular necrosis of bone.

2.3. Implantation

Animal procedures were approved by the Federal Veterinary Office (permit BS 2598). Before surgery, nude rats (Charles River, Germany) were injected subcutaneously with 0.05 mg/kg buprenorphine (Temgesic). Anaesthesia was induced and sustained with 2.5% Isofluran in 1 l/min O_2. The rats were put in a supine position, placed on an electrically heated mat to maintain body temperature, desinfected and a sterile operating field was established. Through an incision of approximately 15 mm length along the left groin the superficial inferior epigastric artery and vein were dissected free of most surrounding tissue. Upon distal ligation, the created AV bundle was inserted through a 1.25 mm axial hole drilled manually in the center of the graft (Fig. 2A). A subcutaneous pouch was created by blunt dissection and the graft was carefully inserted (Fig. 2B). In order to prevent any ingrowth of vessels from surrounding tissues, grafts were wrapped in a semipermeable anorganic-based silicone membrane (Fig. 2C) [18] (Biobrane, UDL Laboratories Inc., Rockford, IL, USA). Due to the lack of possible vascularization from the sides, an experimental group with the same materials but no AV bundle was omitted. To prevent the rats from manipulating with the suture material used, subdermal and intradermal sutures with absorbable material were applied (5-0 Monocryl thread from Ethicon, US). The rats recovered under infrared light and were transferred back to their cages with free access to food and water. Animals were monitored thereafter according to the veterinary study guidelines.

2.4. Explantation

After 1 or 8 weeks, deep anesthesia of the animals was induced by intraperitoneal injection of 100 mg/kg ketamine (Ketasol 100, Dr. E. Graeub AG, Switzerland) and 10 mg/kg xylazine (Xylasol, Dr. E. Graeub AG, Switzerland). Additional inhalation anesthesia with 2.5% Isoflurane in 1 l/min O_2 was performed. Again, the animals were placed in a supine position and the abdominal aorta of animals was exposed through median laparatomy. Distally, the aorta was cannulated with a 22-gauge butterfly cannula (BD, Heidelberg, Germany) and a heparinized saline solution (100 IU/ml, 0.9% NaCl, B.Braun AG, Switzerland) was injected until the blood vessels of the skin of the lower extremities turned pale. Subsequently a dark-blue contrasting agent was applied through the same cannula (5% w/v Gelatine-Gold, Carl Roth GmbH, Karlsruhe, Germany; 50% v/v Indian Ink, Lefranc & Bourgeois, Le Mans, France; 4% w/v D-Mannitol, Carl Roth GmbH; distilled water) until all extremities turned dark-blue. Animals were euthanized by exsanguination. Cadavers were refrigerated for at least 2 h at 4 °C to allow polymerization of the contrasting hydrogel agent. The grafts were then carefully dissected free from surrounding tissue and the semipermeable membrane surrounding the scaffold was removed. The grafts implanted for 8 weeks were additionally cut in half to generate proximal and distal constructs with respect to the entry point of the AV bundle. All samples were fixed for 1 day in 1% PFA (Formafix, Hittnau, Switzerland), and kept in PBS until further processing.

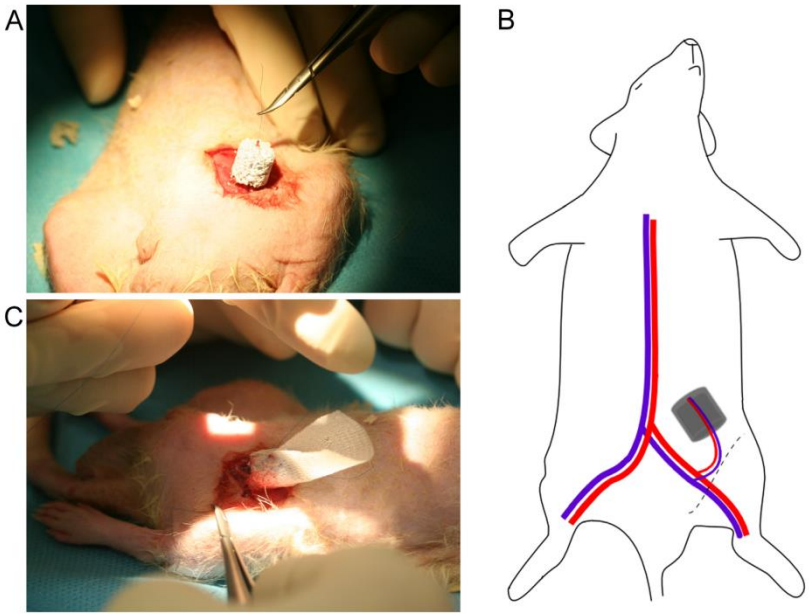

Fig. 2. Graft implantation. Intraoperative view of the hydroxyapatite scaffold with inserted ligated AV bundle (A). Tutobone is not applied for this 1 week sample. The scaffold placement is shown in this schematic depiction of the ligated superficial inferior epigastric artery and vein in the rat's groin. The dashed line represents the skin incision (B). Wrapping of a semipermeable membrane (Biobrane) around the entire construct is performed to prevent tissue ingrowth from the host (B).

2.5. Microtomography

For bone and vessel analysis, 8-week samples were scanned twice: once for bone analysis and a second time after increasing vessel-to-bone contrast as previously described [19]. For this, samples were completely decalcified with 15% w/v EDTA pH 7.0 in distilled water at 37 °C and then incubated overnight in 5% w/v phosphotungstic acid (Sigma-Aldrich) in distilled water before being scanned again. The samples were scanned for 360° using a tungsten X-ray source at 70 kV/260 μA with a 0.5 mm aluminum filter (Nanotom M, GE, USA). Volumes were reconstructed with 8 μm voxel size using the manufacturer's software and were further analyzed with VGStudio Max version 2.2 (Volume Graphics, Heidelberg, Germany). Vessel diameter was assessed within the proximal and distal halves of the constructs.

2.6. Histology

After decalcification and X-ray tomography, samples were embedded in paraffin and sectioned at different levels in 7 μm-thick sections. Standard histological Haematoxilin & Eosin (HE), Masson's trichrome (Réactifs RAL, Martillac, France), tartrate resistant acid phosphatase stainings (Sigma-Aldrich) and in situ hybridization for human specific ALU- sequences (Zytovision GmbH, Bremerhaven, Germany) was performed as previously described [20]. Immunohistochemistry was performed with primary antibodies against human CD34 (QBEND/10, Dako), human calcitonin (ab175297, Abcam, UK), matrix metalloproteinase (MMP9) (ab38898, Abcam, UK) and bone sialoprotein (BSP) (ab52128 Abcam, UK). Specific staining was visualized with the Vectastain ABC kit and the Vectastain Fast Red kit (Vector laboratories, Denmark) according to the manufacturer's protocols. Immunofluorescence was performed with labelled primary antibodies for rat CD68 (ref MCA341A488, AbD Serotec) and CD163 (ref MCA342A647, AbD Serotec) and counterstained with DAPI (Sigma-Aldrich). Images were taken with a BX61 (Olympus) microscope.

2.7. Quantifications

HE-stained midline sections covering a total depth of 210 μm per graft were used to analyze bone formation, vascularization and macrophage activity. Bone was identified by autofluorescence and manual thresholding. Areas with bone were quantified as a percentage of the selected area as described previously [21]. Bone area and distance of osteoid matrix both to the AV bundle (center) and to the scaffold edge (periphery) was measured with analysis software (Cellsens, Olympus). Vascular density and the distance of the vasculature from AV bundle were measured manually on histological slides. Structures were counted as vessels when they had endothelial cell lining, a well-defined lumen and presence of red blood cells or contrasting agent within the lumen. Human CD34 positive vessels were counted in 3 fields from the center to the periphery of the constructs under 10-fold magnification. The fraction of human vessels was multiplied with total vessel counts to yield overall number of human vessels per sample. TRAP positive multinucleated osteoclasts were manually counted per complete section under 20-fold magnification. Total and M2-polarized macrophages were here defined as CD68+ and CD68+/CD163+ cells respectively. Their number was derived by manual counting in 3 high magnification images covering the distance from the center to periphery of the constructs. Density of human cells was assessed by quantifying positive events following ALU staining of the sections.

2.8. Statistical analysis

All results are expressed as mean values with standard deviation. ANOVA analysis and t-tests were performed at a level of statistical significance $p < 0.05$ by using the GraphPad Prism software (GraphPad Software, Inc., California, USA).

3. Results

Overall, 13 SVF-seeded and 16 unseeded scaffolds were implanted (Fig. 3). One seeded scaffold was lost within the first week after implantation due to infection at the implantation site. Of the remaining 12 seeded scaffolds, 7 were explanted after one week and 5 after eight weeks. Of the unseeded scaffolds, 10 were explanted after one week and 6 after eight weeks.

3.1. Early vascularization, engraftment and host cell recruitment after 1 week

One week after in vivo implantation, thrombosis was only found within the 1 mm most distal part of the ligated AV bundle. No necrosis was observed in the central AV bundle or in newly-formed blood vessels inside the grafts, as evidenced by Indian ink

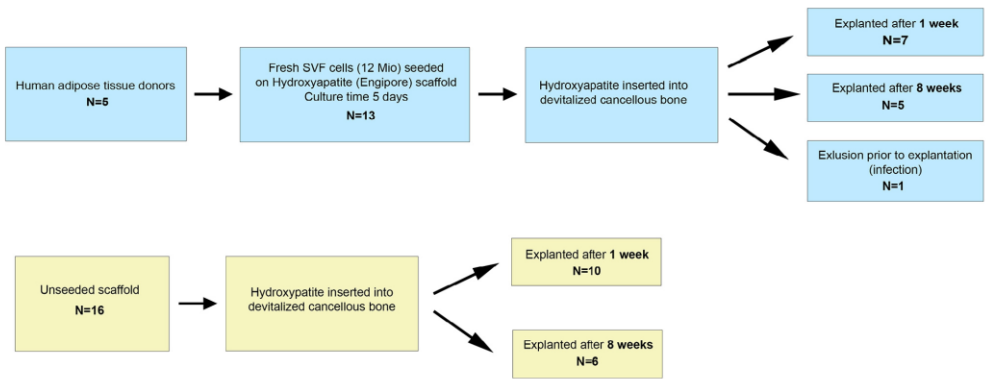

Fig. 3. Diagram showing the experimental groups tested in the study.

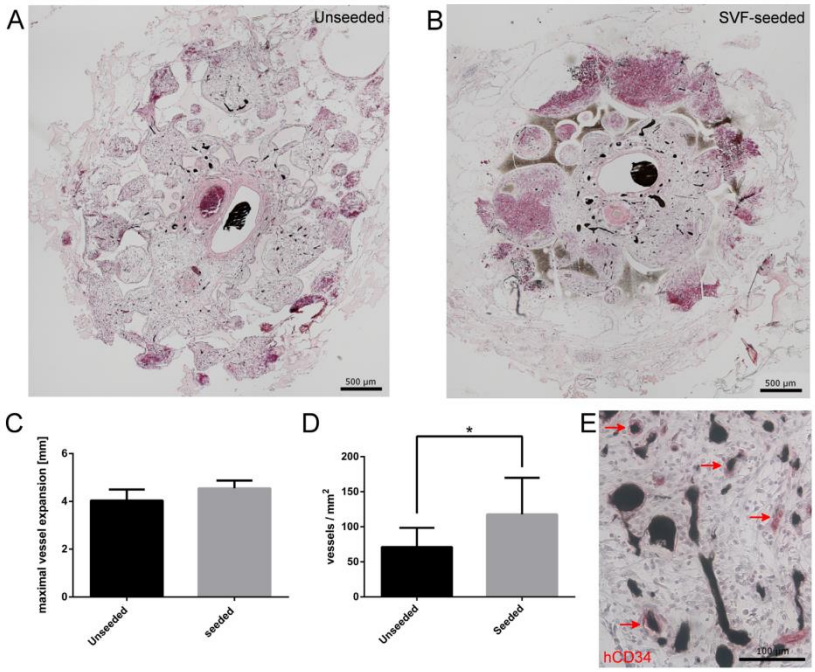

Fig. 4. Vessel analysis 1 week in vivo. Comparison of vascularization of the scaffold after 1 week: HE staining shows both in unseeded (A) and SVF cell seeded (B) scaffolds a well perfused hydroxyapatite scaffold, visualized by the black stained vessels (Indian Ink) throughout the entire construct. No signs of thrombosis or necrosis are present. Maximum vessel expansion from the bundle to the inner rim revealed no significant differences between the unseeded and seeded scaffolds (C). However, vessel density was significantly higher in the seeded scaffolds (69 ± 15 vessels/mm^2 versus 107 ± 27 vessels/mm^2, P = 0.013). The stars in the figures mark significant comparisons (D). After 1 week in vivo, almost half of the generated vascular network had derived from the seeded human SVF cells (red stained CD 34 positive cells marked with red arrows) (E).

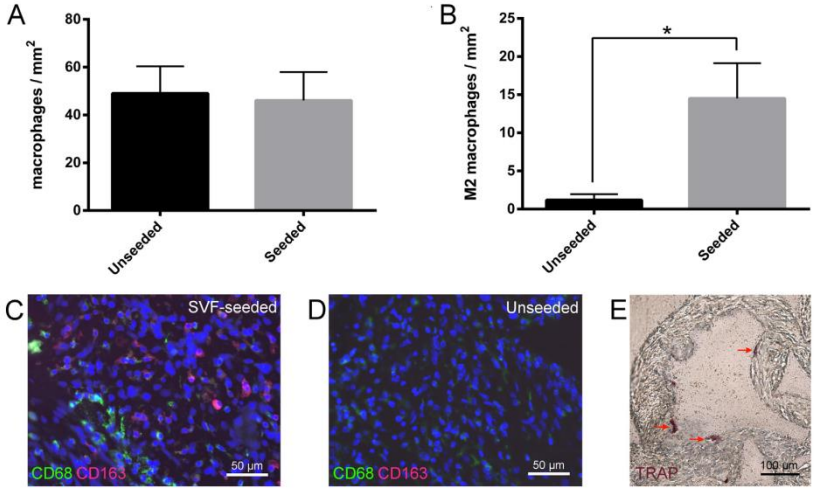

Fig. 5. Macrophage analysis. Recruitment of macrophages after 1 week in vivo was analyzed by mouse anti rat CD 68 (pan-macrophage marker, green) and CD 163 (M2 marker, purple) antibody. After 1 week macrophages were recruited in both seeded and unseeded constructs (A). Immunofluorescence analysis with DAPI (blue), CD68 (green) and CD163 (purple) of SVF cell seeded constructs shows an increased number of M2 macrophages after 1 week in vivo (B, C). Macrophages were localized mostly in the well vascularized parts, especially near the AV bundle in a collar shaped formation and only few at the periphery. In unseeded constructs, very few M2 macrophages invaded the constructs (D). TRAP positive, multinucleated cells were interpreted as osteoclasts (E). They were almost exclusively seen in seeded samples and were always of rat origin (verified by negative staining for human calcitonin receptor). Typically, osteoclasts were homogenously distributed and lining up along the hydroxyapatite edge of the scaffold. (For interpretation of the references to colour in this figure legend, the reader is referred to the web version of this article.)

staining throughout all vessels and both SVF cell seeded and unseeded grafts were completely filled with vascularized connective tissue (Fig. 4 A, B). The maximal distance between vessels and the bundle (vessel expansion) was not significantly different between seeded and unseeded grafts (Fig. 4C). However, vessel density was significantly higher in seeded grafts (Fig. 4D) ($p = 0.013$). Approximately half of the vessels (48 ± 13%) in the SVF seeded constructs were of human (graft) origin, as evidenced by staining for Indian ink and with an antibody specific for human CD34 (Fig. 4 E). CD68+ macrophages were present in the vicinity of blood vessels both in seeded and unseeded grafts at a similar density (Fig. 5 A). However, the density of CD68+/CD163+, M2 macrophages was significantly higher ($p < 0.0001$) in seeded grafts (Fig. 5B–D). M2 macrophages represented 29% of all macrophages in seeded grafts versus 4% in unseeded grafts. Another type of recruited cells, namely the TRAP-positive multinucleated osteoclasts, were present in 100% of seeded (Fig. 5E) versus 33% of unseeded samples. When present in unseeded grafts, the density of osteoclasts was not different between seeded and unseeded grafts (0.86 ± 0.47 and 0.82 ± 0.81 osteoclasts/mm^2, respectively). These osteoclasts were of host origin as demonstrated by a negative staining for human calcitonin receptor (data not shown).

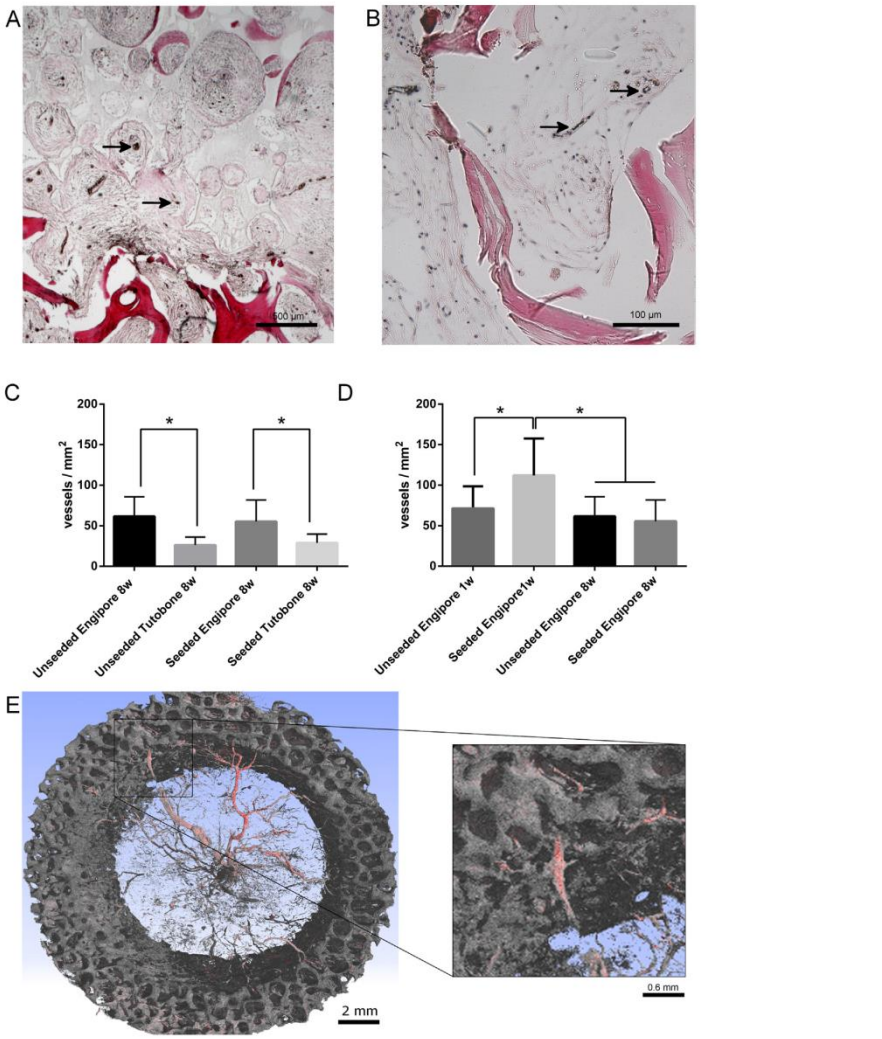

Fig. 6. Vessel analysis 8 weeks in vivo. HE staining after 8 weeks in vivo: Revitalization of initially dead area (Tutobone in red) including vessel formation (stained with Indian Ink, black arrows) and dense fibrous tissue (A: 2× magnification, B: 10× magnification). Vessel density inside the Engipore graft both in seeded and unseeded scaffolds was significantly larger compared to vessel density inside the surrounding Tutobone (C). The initial difference in vessel density after 1 week in vivo was transient. After 8 weeks in vivo no difference in vessel density was observed between seeded and unseeded grafts (D). Three dimensional reconstruction of a vessel tree originating from the bundle's vein (E).

3.2. Vascularization and bone tissue formation after 8 weeks

To assess the capacity to revitalize and revascularize, the grafts were inserted into a block of decellularized bone (Tutobone®) and the AV bundle (Fig. 1C) was inserted right before implantation in vivo. After 8 weeks, the initially avital Tutobone® contained dense and well vascularized tissue both in the seeded and unseeded experimental condition, as assessed by the vessels identified as Indian ink staining positive structures (black arrows in Fig. 6A and B). No human CD34+ vessels or human cells were found inside the Tutobone® blocks at any time. The density of blood vessels in the external Tutobone® blocks was significantly lower than in the central Engipore core, and similar for seeded and unseeded conditions (Fig. 6C). After 1 week in vivo, in the Engipore materials the vessel density was significantly higher in the seeded than in the unseeded grafts, whereas no difference was observed after 8 weeks in vivo (Fig. 6D). Micro-tomographical analysis of the vasculature showed a vessel tree originating mostly from the bundle's vein (Fig. 6E) with vessels penetrating through the engineered graft as well as through the Tutobone® material. No significant differences were found in the vascular density, quantified in the proximal and distal halves of the grafts (23 ± 8 vessels/ mm^2 in the proximal half versus 27 ± 22 vessels/mm^2 in the distal half). The vessels found in Tutobone® also exhibited a similar average diameter of vessels (0.05 ± 0.01 mm) in the proximal and distal regions.

After 8 weeks in vivo, bone formation was found in four out of five (80%) of the SVF seeded grafts (Fig. 7, with arrows indicating fibroblasts, lining osteoblasts and osteocytes), as seen by micro-computed tomography (Fig. 8A, with white arrows indicating calcified tissue inside the scaffold pores), as well as by BSP staining (Fig. 8B, red staining) and Masson Trichrome staining (Fig. 8C and D, dense green-stained lenticular structures). No bone formation was observed in any of the unseeded grafts. The highest efficiency of bone formation occurred proximally in the scaffold (Fig. 8E), at a 1.5–3 mm distance from the inserted bundle (Fig. 8C, D, F). No bone formation was observed in the neighboring Tutobone®. Graft-derived, ALU-positive human cells contributed to bone formation, as 40% of osteocytes in the newly formed bone were of human origin (Fig. 8G, black arrows). No monocyte-derived osteoclasts were found within seeded or unseeded grafts (data not shown). MMP-9 as a type IV collagenase expressed in osteoclast cells and playing an important role in bone remodelling [22] was observed both in seeded and unseeded grafts (Fig. 8H), but never inside the tissue-colonized Tutobone®.

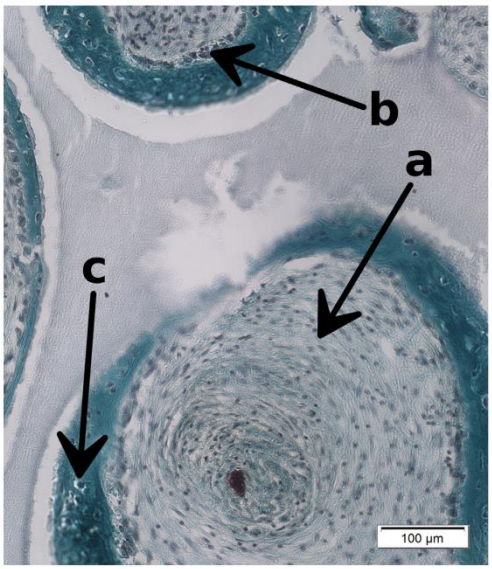

Fig. 7. Proof of bone after 8 weeks in vivo. Masson's trichrome staining reveals fibroblasts in the center of a pore of the hydroxyapatite scaffold (a), with lining osteoblasts (b) next to the new osteoid tissue and osteocytes (c).

4. Discussion

This study offers a proof of principle that grafts engineered with an AV bundle and containing human SVF cells can efficiently and entirely revitalize necrotic bone tissue of clinically relevant dimensions. In a newly developed AVN mimicking rat model, inspired from a previously described rabbit model [16], the vessels arising from the central AV pedicle efficiently revitalized the necrotic outer shell, while the SVF cells were essential to attract or polarize M2 macrophages and to induce blood vessel and bone tissue formation in the inner core of the graft. After 8 weeks in vivo, bone formation was observed in four out of five grafts which had been seeded with SVF from different human donors, but in none of the unseeded constructs. SVF cells directly contributed to bone formation, as evidenced by human osteocytes found inside the osteoid matrix, similar to previous observations in an ectopic rat model [14]. The distribution of the newly formed bone was not homogenous but rather arranged in clusters localized preferentially at a distance of 1.5–3 mm from the central AV bundle. This could be due to possible non-uniform cell seeding [23], combined with associated temporal/spatial patterns of vascularization which would need to be further investigated.

Generating pre-vascularized engineered tissues by adding vascular and endothelial progenitor cells in vitro combined with an AV bundle in vivo was already proposed to promote accelerated vascularization [16,24]. Here we describe the use of a perfusion bioreactor seeding process to generate the osteogenic constructs and SVF cells from human patients, in contrast to the use of rabbit, monolayer-expanded adipose-derived cells. Furthermore, we originally report the generation of de novo bone matrix by the implanted cells. The approach supported tissue vascularization from within the graft, in contrast to standard bone vascularization by muscular flap wrapping methods, where new vessels come from outside the graft [25]. The rationale for this choice is the clinical need for revascularization of bone in the subchondral area of joints affected by AVN, where vascularization from outside the graft is surgically not feasible and immediate blood perfusion after implantation into the osteonecrotic defect is required. Although ligated, the type of vascular bundle used in the present study showed no thrombosis and promoted vascularization of the ceramic scaffold already 1 week after implantation, resulting in vital tissue throughout the entire volume of the graft, in accordance with a previous report on engineered skin grafts [17]. Pre-vascularized osteogenic grafts using endothelial and vascular progenitor cells present in the SVF of human adipose tissue were already shown to exhibit early (1 week) anastomosis of the preformed vessels to the vasculature of the host and an improved engraftment and bone tissue formation in vivo [14]. An increased vascular density in SVF cell seeded constructs was observed in the present study 1 week after implantation, as compared to unseeded scaffolds. This should result in increased local supply of nutrients and oxygen to the developing bone tissue, as previously reported [26]. However, this increased vascularization was transient and no difference between seeded and unseeded grafts was

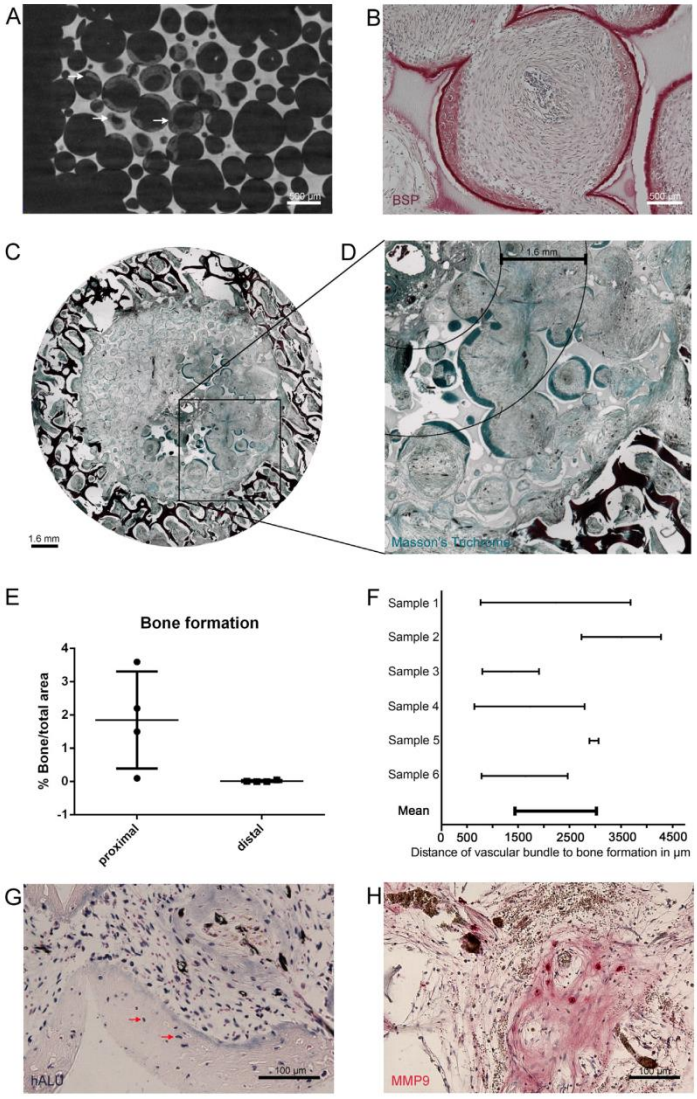

Fig. 8. Bone analysis 8 weeks in vivo. Microtomography picture after 8 weeks in vivo. White color represents bone formation in the Engipore pores (A). A similar distribution pattern of BSP stained cell can be seen in 8 weeks in vivo samples (B). Histological overview (C) and 10× magnification (D) after Masson's trichrome staining show a preferential localization of bone in the middle third of the grafts radius, approximately 1.5 mm away from the AV bundle (F). High variability of bone formation (% bone per total area) between scaffolds was recorded. The bold scale bar in (C), (D) and (F) represents the same distance of about 1.6 mm. Most bone formation occurred in the proximal half but of the four seeded scaffolds containing bone, the two with most bone formation also revealed bone in the distal part, although in significantly smaller amounts (E). ALU – staining of the seeded scaffolds displayed human cells inside the newly formed bone, illustrating the persistence and contribution of human cells to bone formation after 8 weeks. One third (36.6%) of the osteocytes were of human origin (G). MMP9 positive cells were mostly located near the bundle or other well vascularized parts of the scaffolds in proximity to dense tissue. The cells appeared in clusters and were not homogenously distributed (H). Only a few cells were found in proximity to the bone and in loose tissue. No MMP9 positive cells were found within the Tutobone. (For interpretation of the references to colour in this figure legend, the reader is referred to the web version of this article.)

observed at 8 weeks. At that time point, the bundle had generated a symmetric vessel tree with homogenous penetration into the surrounding decellularized bone, both in the seeded and unseeded grafts. Since the hydroxyapatite scaffold and the Tutobone block have a similar porosity, a comparable formation of vascularity had been expected but was constantly lower within the Tutobone.

Vascularization may have been impeded by specific environmental cues and/or signals of the Tutobone material itself. The manufacturing process to generate decellularized bone material such as Tutobone includes stringent treatments which may further explain this finding. Moreover, no human cells were found within the Tutobone. This suggests that either no signals to attract SVF cells were present in the devitalized bone, or that human cells did not have time to colonize the empty Tutobone space after 8 weeks. However, the devitalized bone was filled with host tissue and good vascularization at 8 weeks. Importantly, the fully decellularized Tutobone is a much more stringent environment compared to real-life AVN, which still contains resident osteblasts and osteoclasts, as well as close-by osteoprogenitor cells.

Recruitment of host macrophages was observed as previously described [27]. It occurred both in seeded and unseeded scaffolds, as early as 1 week after implantation. However, only SVF-seeded samples strongly recruited CD163+ macrophages, typically defined as M2. This indicates that SVF cells can directly recruit M2 macrophages and/or induce a functional switch from putative pro-inflammatory M1 to pro-regenerative M2 macrophages [28,29]. Similarly, osteoclasts were present almost exclusively in the SVF cells-seeded samples after 1 week in vivo. At 8 weeks in vivo, no osteoclasts were observed in seeded or unseeded constructs. Although SVF contains monocytes [30,31], which give rise to osteoclasts and macrophages, the macrophages and osteoclasts observed in the constructs were all of host origin. The contribution of macrophages and osteoclasts recruited by SVF cells-seeded constructs for bone formation and revitalization of the devitalized bone surrounding the graft need to be further investigated.

It is challenging to define the target range of vascular densities for an efficient treatment of an AVN defect. It likely depends on the degree of progress of the disease and the quality of the subchondral bone and vascularity in the necrotic area. It needs to be mentioned that even re-vascularized necrotic structures of AVN can still collapse and therefore new bone formation is essential to ensure mechanical stability of the initial necrotic area. In a clinical scenario, the necrotic part of a carpal bone (lunate or scaphoid) could partly be resected and replaced by the SVF-seeded HA scaffold of the size tested in this study. The intercompartmental supraretinacular vessel could then be inserted into the implanted construct. The data describing vascularization in the present study are thus relevant for translation, because the anatomical features and proportion of the vessels and the constructs have met clinical needs as seen in AVN of carpal bones. Our bundle had a length of 12–16 mm and diameter of 0.2–0.4 mm, similar to the anatomical features of the intercompartmental supraretinacular artery, which has served as a vascular pedicle for the reconstruction of lunate or scaphoid bones by a distally pedicled radius flap [32,33].

From a clinical perspective, the approach presented here could greatly reduce surgical morbidity associated with the treatment of AVN. Indeed, liposuction is much less invasive than autologous bone harvesting, especially given the low volume of adipose required. The time and cost for isolation of SVF cells from adipose and subsequent culture in the bioreactor system could be compensated by reducing the rate of re-operation and treatment of autologous bone grafting-related complications. Moreover, based on this proof-of-principle study, refined strategies could be designed to bypass SVF cell culture.

5. Conclusion

Human SVF cells accelerate vascularization of an engineered graft of clinically relevant size following insertion of an AV bundle and directly contribute to bone tissue formation in an in vivo model of AVN. Further studies are necessary to improve the amount and uniformity of the newly formed bone. The engineered constructs could bring a benefit to the patient, by minimizing donor site morbidity due to the harvesting of autologous bone, which is part of the current standard treatment.

Disclosures

No conflicts of interest were reported. This work has received funding from the People Programme (Marie Curie Actions) of the European Union's Seventh Framework Programme FP7/2007-2013/under REA grant agreement No. 607868 (iTERM, to A. Scherberich) and from the Swiss National Science Foundation (SNF Grant 310030-156291 to A. Scherberich and I. Martin). For the remaining authors, no other sources of funding were declared.

Acknowledgments

We would like to thank Susana Ibrahim from the Institute of Pathology, University of Basel, for technical assistance preparing the slides for histological analysis. Furthermore we thank Sarah Sutter, Medical School of the University of Basel, for assistance in vessel staining.

References

[1] H.J. Mankin, Nontraumatic necrosis of bone (osteonecrosis), N. Engl. J. Med. 326 (22) (1992) 1473–1479.
[2] M.A. Mont, D.S. Hungerford, Non-traumatic avascular necrosis of the femoral head, J. Bone Joint Surg. Am. 77 (3) (1995) 459–474.
[3] C.C. Chang, A. Greenspan, M.E. Gershwin, Osteonecrosis: current perspectives on pathogenesis and treatment, Semin. Arthritis Rheum. 23 (1) (1993) 47–69.
[4] M.Á. Martinez-Ferrer, P. Peris, N. Guañabens, Osteonecrosis. What is new? Reumatol. Clin. 3 (2) (2007) 78–84.
[5] K. Pavelka, Osteonecrosis, Baillieres Best Pract. Res. Clin. Rheumatol. 14 (2) (2000) 399–414.
[6] T.M. Zizic, C. Marcoux, D.S. Hungerford, M.B. Stevens, The early diagnosis of ischemic necrosis of bone, Arthritis Rheum. 29 (10) (1986) 1177–1186.
[7] D.M. LaPorte, M.A. Mont, V. Mohan, L.C. Jones, D.S. Hungerford, Multifocal osteonecrosis, J. Rheumatol. 37 (1) (1998) 1968–1974.
[8] Q. Zhang, I. Atsuta, S. Liu, C. Chen, S. Shi, S. Shi, A.D. Le, IL-17-mediated M1/M2 macrophage alteration contributes to pathogenesis of bisphosphonate-related osteonecrosis of the jaws, Clin. Cancer Res. 19 (12) (2013) 3176–3188.
[9] M.A. Mont, J.J. Carbone, A.C. Fairbank, Core decompression versus nonoperative management for osteonecrosis of the hip, Clin. Orthop. Relat. Res. 324 (1996) 169–178.
[10] M.A. Mont, K.M. Baumgarten, A. Rifai, D.A. Bluemke, L.C. Jones, D.S. Hungerford, Atraumatic osteonecrosis of the knee, J Bone Joint Surg. Am. 82 (9) (2000) 1279–1290.
[11] E.S. Musso, S.N. Mitchell, M. Schink-Ascani, M, C.A. Bassett, Results of conservative management of osteonecrosis of the femoral head. A retrosprective review, Clin. Orthop. Relat. Res. 207 (1986) 209–215.
[12] A.V. Korompilias, A.E. Beris, M.G. Lykissas, I.P. Kostas-Agnantis, P.N. Soucacos, Femoral head osteonecrosis: why choose free vascularized fibula grafting, Microsurgery 31 (3) (2011) 223–228.
[13] D. Feuvrier, Y. Jr, S. Sagawa, J. Béliard, P. Decavel Pauchot, Long-term donor-site morbidity after vascularized free fibula flap harvesting: clinical and gait analysis, J. Plast. Reconstr. Aesthet. Surg. 69 (2) (2016) 262–269.
[14] S. Güven, A. Mehrkens, F. Saxer, D.J. Schaefer, R. Martinetti, I. Martin, A. Scherberich, Engineering of large osteogenic grafts with rapid engraftment capacity using mesenchymal and endothelial progenitors from human adipose tissue, Biomaterials 32 (25) (2011) 5801–5809.
[15] A. Scherberich, R. Galli, C. Jaquiéry, J. Farhadi, I. Martin, Three-dimensional perfusion culture of human adipose tissue-derived endothelial and osteoblastic progenitors generates osteogenic constructs with intrinsic vascularization capacity, Stem Cells 25 (7) (2007) 1823–1829.
[16] O. Kloeters, I. Berger, H. Ryssel, K. Megerle, U. Leimer, G. Germann, Revitalization of cortical bone allograft by application of vascularized scaffolds seeded with osteogenic induced adipose tissue derived stem cells in a rabbit model, Arch. Orthop. Trauma Surg. 131 (10) (2011) 1459–1466.
[17] Y. Tanaka, K.C. Sung, A. Tsutsumi, S. Ohba, K. Ueda, W.A. Morrison, Tissue engineering skin flaps: which vascular carrier, arteriovenous shunt loop or arteriovenous bundle, has more potential for angiogenesis and tissue generation?, Plast Reconstr. Surg. 112 (6) (2003) 1636–1644.
[18] M. Wiedmann-Al-Ahmad, R. Gutwald, N.C. Gellrich, U. Hübner, R. Schmelzeisen, Search for ideal biomaterials to cultivate human osteoblast-like cells for reconstructive surgery, J. Mater. Sci. Mater. Med. 16 (1) (2005) 57–66.

[19] S. Sutter, A. Todorov, T. Ismail, A. Haumer, I. Fulco, G. Schulz, A. Scherberich, A. Kaempfen, I. Martin, D.J. Schaefer, Contrast-Enhanced Microtomographic Characterisation of Vessels in Native Bone and Engineered Vascularised Grafts Using Ink-Gelatin Perfusion and Phosphotungstic Acid, CMMI 2017 (2017), Article ID 4035160, 10 pages.
[20] R. Osinga, N. Di Maggio, A. Todorov, N. Allafi, A. Barbero, F. Laurent, D.J. Schaefer, I. Martin, A. Scherberich, Generation of a bone organ by human adipose-derived stromal cells through endochondral ossification, Stem Cells Transl. Med. 5 (8) (2016) 1090–1097.
[21] I. Martin, M. Mastrogiacomo, G. De Leo, A. Muraglia, F. Beltrame, R. Cancedda, R. Quarto, Fluorescence microscopy imaging of bone for automated histomorphometry, Tissue Eng. 8 (5) (2002) 847–852.
[22] K. Sundaram, R. Nishimura, J. Senn, R.F. Youssef, S.D. London, S.V. Reddy, RANK ligand signaling modulates the matrix metalloproteinase-9 gene expression during osteoclast differentiation, Exp. Cell Res. 313 (1) (2007) 168–178.
[23] A. Braccini, D. Wendt, J. Farhadi, S. Schaeren, M. Heberer, I. Martin, The osteogenicity of implanted engineered bone constructs is related to the density of clonogenic bone marrow stromal cells, J. Tissue Eng. Regen. Med. 1 (1) (2007) 60–65.
[24] P. Yang, X. Huang, J. Shen, C. Wang, X. Dang, H. Mankin, Z. Duan, K. Wang, Development of a new pre-vascularized tissue-engineered construct using pre-differentiated rADSCs, arteriovenous vascular bundle and porous nano-hydroxyapatide-polyamide 66 scaffold, BMC Musculoskelet. Disord. 14 (2013) 318.
[25] A. Kaempfen, A. Todorov, S. Güven, R.D. Largo, C. Jaquiéry, A. Scherberich, I. Martin, D.J. Schaefer, Engraftment of prevascularized, tissue engineered constructs in a novel rabbit segmental bone defect model, Int. J. Mol. Sci. 16 (6) (2015) 12616–12630.
[26] H. Yu, P.J. VandeVord, L. Mao, H.W. Matthew, P.H. Wooley, S.Y. Yang, Improved tissue-engineered bone regeneration by endothelial cell mediated vascularization, Biomaterials 30 (4) (2009) 508–517.
[27] R. Tasso, V. Ulivi, D. Reverberi, C. Lo Sicco, F. Descalzi, R. Cancedda, In vivo implanted bone marrow-derived mesenchymal stem cells trigger a cascade of cellular events leading to the formation of an ectopic bone regenerative niche, Stem Cells Dev. 22 (24) (2013) 3178–3191.
[28] T.A. Wynn, Type 2 cytokines: mechanisms and therapeutic strategies, Nat. Rev. Immunol. 15 (5) (2015) 271–282.
[29] A. Mantovani, S.K. Biswas, M.R. Galdiero, A. Sica, M. Locati, Macrophage plasticity and polarization in tissue repari and remodelling, J. Pathol. 229 (2) (2013) 176–185.
[30] P.A. Zuk, M. Zhu, P. Ashjian, D.A. De Ugarte, J.I. Huang, H. Mizuno, Z.C. Alfonso, J.K. Fraser, P. Benhaim, M.H. Hedrick, Human adipose tissue is a source of multipotent stem cells, Mol. Biol. Cell. 13 (12) (2002) 4279–4295.
[31] P. Bourin, B.A. Bunnell, L. Casteilla, M. Dominici, A.J. Katz, K.L. March, H. Redl, J. P. Rubin, K. Yoshimura, J.M. Gimble, Cytotherapy 15 (6) (2013) 641–648.
[32] Y. Saint Cast, B. Césari, G. Dagregorio, M. Le Bourg, A. Gazarian, G. Raimbeau, P. A. Fouque, F. Rabarin, J. Jeudy, F. Mallard, Simplified scaphoid reconstruction technique with Zaidemberg's vascularized radial graft, Orthop. Traumatol. Surg. Res. 98 (2012) S66–S72.
[33] A.N. Larson, A.T. Bishop, A.Y. Shin, Dorsal distal radius vascularized pedicled bone grafts for scaphoid nonunions, Tech. Hand Up Extrem. Surg. 10 (4) (2006) 212–223.

Chapter III:

Imaging of bone and vasculature by μCT

Hindawi
Contrast Media & Molecular Imaging
Volume 2017, Article ID 4035160, 10 pages
https://doi.org/10.1155/2017/4035160

WILEY | Hindawi

Research Article

Contrast-Enhanced Microtomographic Characterisation of Vessels in Native Bone and Engineered Vascularised Grafts Using Ink-Gelatin Perfusion and Phosphotungstic Acid

Sarah Sutter,[1,2] Atanas Todorov,[1,2] Tarek Ismail,[1] Alexander Haumer,[2,3] Ilario Fulco,[1] Georg Schulz,[3] Arnaud Scherberich,[1,2,3] Alexandre Kaempfen,[1] Ivan Martin,[2,3] and Dirk J. Schaefer[1]

[1]*Department of Plastic, Reconstructive, Aesthetic and Hand Surgery, University Hospital Basel, University of Basel, Spitalstrasse 21, 4031 Basel, Switzerland*
[2]*Department of Biomedicine, University Hospital Basel, University of Basel, Hebelstrasse 20, 4031 Basel, Switzerland*
[3]*Department of Biomedical Engineering, University of Basel, Gewerbestrasse 14, 4123 Allschwil, Switzerland*

Correspondence should be addressed to Ivan Martin; ivan.martin@usb.ch

Received 2 January 2017; Revised 18 March 2017; Accepted 2 April 2017; Published 23 April 2017

Academic Editor: Erik H. J. G. Aarntzen

Objectives. Bone ischemia and necrosis are challenging to treat, requiring investigation of native and engineered bone revascularisation processes through advanced imaging techniques. This study demonstrates an experimental two-step method for precise bone and vessel analysis in native bones or vascularised bone grafts using X-ray microtomography (μCT), without interfering with further histological processing. *Methods.* Distally ligated epigastric arteries or veins of 6 nude rats were inserted in central channels of porous hydroxyapatite cylinders and these pedicled grafts were implanted subcutaneously. One week later, the rats were perfused with ink-gelatin and euthanised and the femurs, tibias, and grafts were explanted. Samples were scanned using μCT, decalcified, incubated with phosphotungstic acid (PTA) for contrast enhancement, rescanned, and processed histologically. *Results.* Contrast-enhanced μCT displayed the course and branching of native bone vessels. Histologically, both central (−17%) and epiphyseal vessels (−58%) appeared smaller than in μCT scans. Hydroxyapatite cylinders were thoroughly vascularised but did not display bone formation. Grafts with a central artery had more (+58%) and smaller (−52%) vessel branches compared to grafts with a vein. *Conclusions.* We present a relatively inexpensive and easy-to-perform two-step method to analyse bone and vessels by μCT, suitable to assess a variety of bone-regenerative strategies.

1. Introduction

Bone formation and resorption depend on vessels to supply osteoblast and osteoclast progenitors, oxygen, and nutrients and guide bone formation by direct interaction with mature osteoblasts and osteoclasts [1]. Low blood supply or disturbed interaction between vessels and bone-forming cells leads to pathological conditions such as avascular bone necrosis (AVN) or fracture nonunion, in which bone does not heal after a fracture. In these cases, the required bone reconstruction is based on the use of autologous bone grafts, which generate additional morbidity and are limited by low availability [2, 3]. Bone substitute materials with enhanced osteoinductive capacity through the addition of progenitor/stem cells [4, 5] are being developed. However, these approaches have not yet proven efficient enough for a routine clinical use [6].

To test whether new therapies are able to reanimate ischemic bone, for example, by implanting engineered prevascularised bone tissue, bone vascularisation needs to be assessed. Bone vessel quantification, analysis of spatial relationships between vessels and bone trabeculae, and calculation of blood flow are nontrivial. Intravital observations such as two-photon microscopy are limited in depth and resolution and need a very thin bone cortex and sedation of animals [7]. Conversely, histological processing of explants

is destructive and artefact-prone and does not allow analysis of the full vascular tree. Developed in recent years, the 3D reconstruction of vessels in explants using contrast-enhanced X-ray microtomography (μCT) [8] has been described as a promising approach to solve this problem.

Common X-ray opaque vascular casts such as Microfill(R) [9, 10] or barium sulfate [11], used to analyse vessels between 10 μm [10] and 240 μm [12] in diameter, may compromise the analysis of bone trabeculae by displaying a similar, possibly inhomogenous signal in μCT and creating beam hardening or scattering artefacts [11]. Additionally, though standard histological processing including enzymatic, immunohistochemical, and immunofluorescent staining is possible using these methods, analysis of vessels may be compromised by cast-induced distortion of the vascular morphology [13].

To solve these issues, we propose a two-step method with separate analysis of bone (e.g., trabecular size and spacing) and the corresponding vascular tree (e.g., number and size of vessel branches, vessel length), similar to the described double scanning of bone and bone marrow using osmium tetraoxide [14]. As a first step, bones are prepared with a radiolucent soft vascular cast specifically developed for histological analysis of vessels and capillaries, consisting of Indian ink combined with gelatin (ink-gelatin) [15]. After a first scan, bones are then decalcified and incubated with a solution of phosphotungstic acid (PTA), which enhances gelatin X-ray contrast by binding to the contained collagens. PTA does not otherwise alter tissue colour or stiffness, yet it has a low penetration depth due to its ionic nature [16, 17]. Decalcification removes ions from the tissue, thus increasing PTA penetration.

In this study we tested the applicability of this method for vascularised bones (e.g., rat femur and tibia). In particular, we investigated the reliability of the μCT-based analysis of vessels contrasted with ink-gelatin/PTA and compared it to the standard histological assessment. We investigated whether enzymatic staining, immunohistochemistry, and immunofluorescence were feasible on contrast-enhanced samples. Finally, we aimed to demonstrate the application of this method on simple engineered grafts consisting of vascularised porous hydroxyapatite, adapted from an avascular necrosis model used in rats [18, 19].

2. Materials and Methods

2.1. Animals. Six male nude rats (RNU, Charles River Laboratories, Sulzfeld, Germany), 2–4 months old and weighing 300–400 g, were used in accordance with Swiss and European animal welfare regulations (permit BS 2598 by the cantonal veterinary agency, Basel, Switzerland). The methodological assessment of the reliability of ink-gelatin/PTA as a contrast agent for both μCT and histology was performed on both femurs and both tibias. Each femur and each tibia was considered a single statistical unit. To exemplify the application of ink-gelatin/PTA in a realistic setting, per animal, one hydroxyapatite scaffold with either a central vein or a central artery was implanted, as detailed below.

2.2. Implantation of Hydroxyapatite. For implantations of pedicled grafts, rats were given 0.05 mg/kg buprenorphine subcutaneously for analgesia and anaesthetised using 2.5% isoflurane in 1 l/min oxygen. They were placed supine and the left groin was disinfected using Octenisept (Schülke & Mayr GmbH, Germany). After scalpel incision, the superficial inferior epigastric artery and vein were identified and dissected free of connective tissue using an operating microscope and microsurgical tools. Vessels were ligated and cut distally but left attached proximally to ensure perfusion from the femoral vessels. Two groups of three animals each were formed and either only the artery or only the vein was pulled through the 1.25 mm central channel of a 1 × 1 cm porous hydroxyapatite cylinder (Engipore™, Finceramica Faenza, Faenza, Italy), which was wrapped in a semipermeable membrane (Biobrane, UDL Laboratories Inc., Rockford, IL, USA) to prevent additional vascularisation from outside. A subcutaneous pocket was created by blunt dissection and the vascularised graft was inserted without kinking the vessel. The wound was closed with subcutaneous and intracutaneous sutures. One rat from the artery group died after operation due to unknown causes and was not used for analysis. Rats were placed under infrared light and monitored until full recovery. They were subsequently transferred back to their cage, monitored twice daily, and given subcutaneous buprenorphine every 12 hours in the next 3 days.

2.3. Perfusion with Ink-Gelatin and Explantation of Bones and Graft. After 1 week, rats were anaesthetised using 2.5% isoflurane in 1 l/min oxygen and given 100 mg/kg ketamine (Ketasol 100, Dr. E. Graeub AG, Switzerland) and 10 mg/kg xylazine (Xylasol, Dr. E. Graeub AG) intraperitoneally. The abdominal aorta was distally cannulated with a 22-gauge needle and flushed with a heparinised saline solution (100 I.U./ml in 0.9% NaCl, B. Braun, Switzerland), before an ink-gelatin mixture was applied (5% w/v Gelatine-Gold 180 bloom, Carl Roth GmbH, Germany; 50% v/v Indian Ink, Lefranc & Bourgeois, France; 4% w/v D-Mannitol, Carl Roth GmbH; bidistilled water). After perfusion, rats were euthanised by heart explantation and exsanguination. The cadavers were cooled to 4°C for 2-3 hours for polymerisation of the ink-gelatin. Thereafter, the vascularised graft as well as both femurs and tibias was dissected free of surrounding tissue and incubated in 1.5% paraformaldehyde in phosphate-buffered solution (Sigma-Aldrich) overnight.

2.4. Microtomography without Contrast Enhancement. Femurs and tibias were scanned after fixation in paraformaldehyde. The μCT scans were performed using a nanotom® m (phoenix|x-ray, GE Sensing & Inspection Technologies GmbH, Wunstorf, Germany) equipped with a 180 kV/15 W nanofocus X-ray source. A tungsten transmission target, an accelerating voltage of 70 kV, and a beam current of 260 μA were used. To increase mean energy of the photon spectrum and consequently reduce beam hardening artefacts, a 0.5 mm aluminium filter was inserted between source and specimen. A region of air was designated in all scans as suggested by the software (GE Sensing & Inspection Technologies GmbH) to standardize the grey-scale for data interpretation. 1440

equiangular projection images were acquired over 360° with an exposure time of 1 second. The radiographs were reconstructed using a cone beam filtered back-projection algorithm with the manufacturer's software phoenix datos|x 2.0.1 RTM (GE Sensing & Inspection Technologies GmbH). Whole bones were scanned and reconstructed with a voxel size of 18.5 μm. Datasets were visualised using VG Studio MAX 2.1 (Volume Graphics GmbH, Heidelberg, Germany) and analysed using ImageJ with the BoneJ and 3D Shape plugins [20–22].

2.5. Decalcification. Bones and engineered grafts were decalcified by incubation in 15% EDTA pH 7.0 (Sigma-Aldrich) at 37°C. The decalcification solution was changed daily until samples were floating and soft when tested manually with a forceps. Engineered grafts were decalcified in 4 days, whereas bones required at least 14 days.

2.6. Contrast Enhancement Using Phosphotungstic Acid. 5% w/v phosphotungstic acid (Sigma-Aldrich) in bidistilled water was prepared freshly before each use. Decalcified samples were completely immersed in this solution and incubated at room temperature for 24 (grafts) or 48 hours (bones). A longer incubation time ensured diffusion of the contrasting agent into the bone marrow, as indicated by preliminary scans using bones incubated for 24 hours.

2.7. Microtomography with Contrast Enhancement. Whole femurs and tibias were scanned after contrast enhancement as described above. Femoral heads and tibia plateaus were then separated. Heads, plateaus, and grafts were scanned as described above and reconstructed at a resolution of 2 μm (heads, plateaus) or 7 μm (grafts) per voxel. Manual analysis of the 3D datasets was performed using VG Studio MAX 2.1. Main blood vessel diameter and length within the bone shaft, the smallest distance between cortical bone and the center of the main vessel, and the number and diameter of branches from the main vessel were measured. In femoral heads and tibia plateaus, the number and diameter of vessels and their smallest distance to bone trabeculae were analysed. In grafts, the diameter of the central vessel and the number of vessels branching from the central vessel were analysed. All measurements were performed manually in 3D and on 3 orthogonal 2D sections, in analogy to histological analysis.

2.8. Histological Processing. After scanning, the decalcified and contrast-enhanced samples were dehydrated and embedded in paraffin. Femoral heads and tibia plateaus were embedded separately. Sections of 7–10 μm thickness were stained with standard haematoxylin and eosin. Three representative midline sections were selected and vessel number, diameter, and distance to bone were analysed under a BX61 microscope (Olympus, Switzerland). For longitudinal sections of large vessels in whole bones, the largest diameter was identified along the vessel axis, the vessel center was defined as a point halfway across the diameter, and the distance from that point to the closest bone was measured. For cross-sections of small vessels, the largest and smallest diameters were identified and the center was defined as the crossing point of both diameters. The largest diameter and the distance from the center to the nearest bone were measured.

Staining for tartrate-resistant acid phosphatase (TRAP), as an exemplary enzymatic staining, was performed by incubation with a staining buffer (0.2 M sodium acetate 50 mM L+ tartaric acid, 1 mg/ml naphtol AS-MX phosphate, 1 mg/ml fast red TR salt, pH 5.0, all from Sigma-Aldrich) for 1 hour at 37°C.

For immunohistochemistry, primary antibodies against osterix (ab22552, Abcam UK, 1 : 80, no antigen retrieval) and CD31 (ab32457, Abcam UK, 1 : 50, heat enhanced antigen retrieval using a pressure cooker) were used. Appropriate biotinylated secondary antibodies were used (Abcam) and the staining was developed using the Vectastain ABC and Vectastain Fast Red kits (Vector Laboratories, UK).

For immunofluorescence, a primary Alexa488-labelled antibody against rat CD68 (ED1, AbDSerotec, 1 : 500, antigen retrieval with proteinase K) was used. Sections were counterstained with DAPI (Sigma-Aldrich) and analysed under fluorescence microscopy.

2.9. Data Analysis. Aggregation and analysis of the data with t-tests (comparisons of μCT and histology) and Mann–Whitney U tests (comparisons of grafts with artery or vein) were performed with Microsoft Excel v. 14.6.2 and GraphPad Prism v.2 (GraphPad Software Inc., California, USA). A significance level α of 0.05 was set. Averages and standard deviations are presented.

3. Results

3.1. Analysis of Bone Architecture of the Rat Femur and Tibia by Microtomography. Explanted femurs and tibias were scanned as described and reconstructed volumes did not display any artefacts, in particular no beam hardening or increased scattering (Figure 1(a)). Average bone length and mid-diaphyseal diameter were 38.8 ± 2.1 mm and 4.3 ± 0.5 mm for femurs and 36.5 ± 1.5 mm and 3.2 ± 0.4 mm for tibias. Structural analysis was performed on the reconstructed volumes by virtually extracting 1 mm^3 of the trabecular structure of the proximal metaphysis, the distal metaphysis, and the proximal epiphysis. To illustrate bone parameters unique to μCT analysis, the extracted volumes were then analysed for bone volume fraction (BV/TV), trabecular thickness (Tb.Th.), and trabecular spacing (Tb.Sp.). Results are displayed in Table 1 as averages and standard deviations of 10 samples.

3.2. Analysis of Rat Femurs and Tibias after Decalcification and Contrast Enhancement. After application of PTA for 48 hours, contrast enhancement of both the decalcified bone matrix and the central vessels inside the bone marrow cavity could be observed in reconstructed volumes (Figure 1(b)). Vessels displayed higher average grey values compared to bone matrix (184 ± 15 versus 129 ± 6, $P = 0.002$). The vessel course could be followed and branching points analysed manually by inspection of the reconstructed volumes (Figure 1(c)). An average of 16.3 ± 7.5 mm (femur) or 9.1 ± 8.1 mm (tibia) of the central vessel could be visualised, representing, respectively, 44% and 23% of the total bone

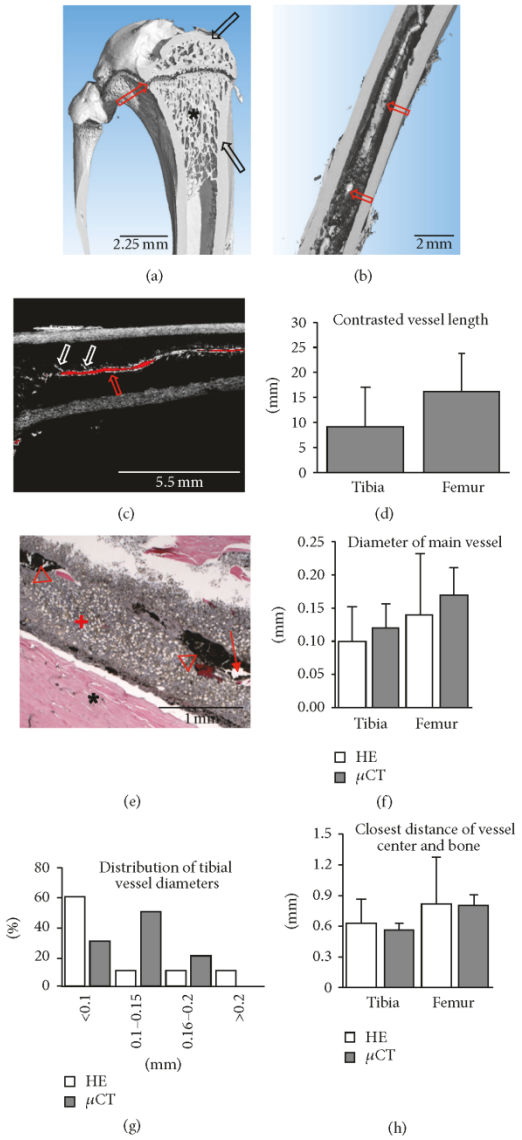

FIGURE 1: Bone architecture and contrast-enhanced vessel visualisation in rat long bones. (a) Bone architecture of rat tibia (3D rendering) with compact bone (black arrows), trabecular structure (star), and epiphyseal gap (red arrow). (b) 3D rendering of contrast-enhanced scan showing diaphysis of a rat femur with contrasted central vessel (red arrows). (c) 2D slice of the data set shown in (b). Red pixels represent grey values typical for vessels. Vessel course (red arrow) and branching (white arrows) are clearly visible. (d) Length of contrasted central vessel. (e) Haematoxylin and eosin staining of mid-diaphysis of a rat femur showing bone (star), bone marrow (plus), ink-gelatin-filled (triangles), and empty (arrow) vessels. (f) Diameter of central vessel measured in histology and microtomography. (g) Histogram of tibial vessel diameters ($n = 10$) showing a unimodal distribution, which is skewed left and wider for data from histology. Femoral vessel diameters display a similar distribution. (h) Closest distance of vessel center and bone measured in histology and microtomography.

Table 1: Bone volume fraction (BV/TV, no unit), trabecular thickness (Tb.Th., in mm), and trabecular spacing (Tb.Sp., in mm) of 1 mm^3 of the proximal metaphysis, the distal metaphysis, and the proximal epiphysis of rat femurs and tibias. Averages and standard deviations of 10 samples are shown.

			Femur	SD	Tibia	SD
BV/TV (no unit)	*Proximal*	*Epiphysis*	0.448	*0.104*	0.286	*1,000*
		Metaphysis	0.386	*0.092*	0.358	*0.12*
	Distal		0.481	*0.38*	0.127	*0.13*
Tb.Th. mm	*Proximal*	*Epiphysis*	0.026	*0.017*	0.009	*0.001*
		Metaphysis	0.159	*0.039*	0.098	*0.027*
	Distal		0.151	*0.143*	0.041	*0.048*
Tb.Sp. mm	*Proximal*	*Epiphysis*	0.064	*0.027*	0.026	*0.001*
		Metaphysis	0.309	*0.08*	0.208	*0.067*
	Distal		0.233	*0.344*	0.023	*0.178*

length (Figure 1(d)). Similar numbers of branching vessels with a similar average diameter were found in femurs (14 ± 10 branches, 0.06 ± 0.007 mm diameter) and tibias (14 ± 8 branches, 0.06 ± 0.009 mm diameter). Although histological processing of samples was straightforward, vessel analysis required selection of representative sections. It was possible to analyse vessel diameter and distance to bone. Vessels appeared mostly as longitudinal sections of large vessels or cross-sections of small vessels with an elliptical shape (Figure 1(e)). Due to the 2D nature of standard histological slides, the uncontrollable wasting of sections due to cutting errors and the disproportionate labour required to produce serial cross-sections, vessel course, or branching were not measured. Interestingly, ink-gelatin contrast was not homogenously present in central vessels, which was in line with the incomplete visualisation of vessels by μCT. The vessel diameter and closest distance of the vessel center to the corticalis were the only quantitative measurements that could be compared between histology and μCT. Both did not show any significant difference (Figures 1(f), 1(g), and 1(h)), though vessel diameter appeared smaller on average (−17%) and more variable in histology compared to μCT, possibly as a result of dehydration and shrinking during histological processing or sampling issues due to the use of longitudinal sections.

3.3. Analysis of Femoral Heads and Tibia Plateaus after Decalcification and Contrast Enhancement. High-resolution scans were performed on separated femoral heads and tibia plateaus to analyse small-calibre (approximately 10 μm to 30 μm diameter) vessels. Volume reconstructions were performed with 2 μm isometric voxels. Vessels were distinguished in reconstructed volumes both with 3D visualisation and with 2D visualisation of serial sections (Figures 2(a) and 2(b)). Manual analysis of the reconstructed volumes revealed the course and branching of vessels. Conversely, histological sections of the same samples suffered cutting artefacts and required selection of the best sections for vessel analysis (Figure 2(c)). In both femoral heads and tibia plateaus, vessels appeared on average 58% smaller in diameter in histology as compared to μCT (Figures 2(d) and 2(e)), possibly as a result of dehydration and shrinking during histological processing. However, the closest distance from the vessel center to the bone trabeculae was not significantly different (Figure 2(f)).

3.4. Enzymatic, Immunohistochemical, and Immunofluorescent Staining. Although standard haematoxylin and eosin staining was feasible, we could not exclude potential artefacts introduced by the contrast agent with more elaborate staining. Therefore we performed series of enzymatic, immunohistological, and immunofluorescent staining on sections of femurs and tibias. TRAP staining for osteoclasts (Figure 3(a)), CD31 staining for endothelial cells (Figure 3(b)), osterix staining for osteoblasts (Figure 3(c)), and CD68 immunofluorescence for macrophages (Figure 3(d)) were feasible in all samples.

3.5. Analysis of Vascularised Porous Hydroxyapatite after Decalcification and Contrast Enhancement. In order to demonstrate an exemplifying application of our method, we engineered a simple vascularised graft (Figure 4(a)). One week after implantation, we analysed tissue formation and vascularisation. μCT analysis after contrast enhancement and reconstruction with 7 μm isometric voxels clearly evidenced a perfused central vessel with branches (Figure 4(b)). Diffuse contrast enhancement at the periphery of the constructs indicated that ink-gelatin had spilled into the tissue. Indeed, upon histological examination, the perfusion of the central vessel, smaller vessels throughout the tissue, and a peripheral haemorrhage were visible (Figure 4(c)). Quantification of vessel diameter, number, and diameter of branches showed no significant difference (Figures 4(d), 4(e), and 4(f)), although constructs with central arteries tended to display larger diameter (+60%), more branches (+58%), and smaller branch diameters (−52%) compared to constructs with central veins. The parameters were not significantly different compared to vascularisation in rat femurs and tibias.

4. Discussion

In this study we demonstrated the use of ink-gelatin and PTA as contrast enhancement for μCT analysis of bone vasculature. We found that scanning after decalcification and contrast enhancement allowed for an evaluation of the

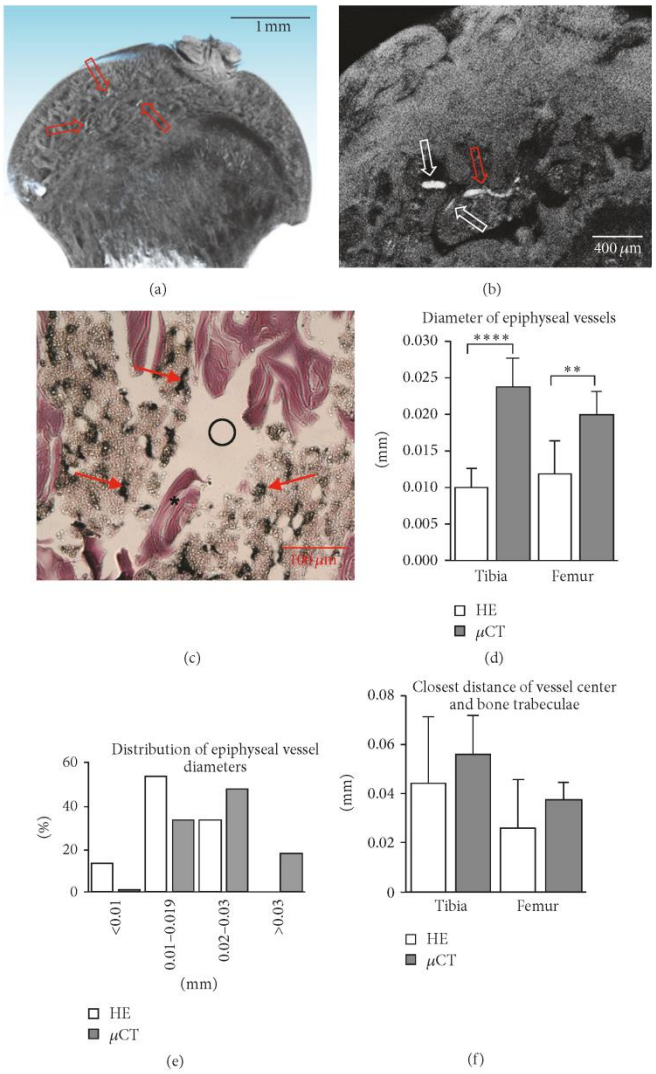

Figure 2: Analysis of small epiphyseal vessels in femoral heads and tibia plateaus. 3D rendering (a) and 2D slice (b) of contrast-enhanced scans showing contrasted vessels (red arrows) and vessel branching (white arrows). (c) H&E staining showing ink-gelatin filled vessels (arrows) and bone trabeculae (star). Large cutting artefacts are visible (circle). (d) Diameter of the epiphyseal vessels measured by histology and microtomography ($^{**}P < 0.01$, $^{****}P < 0.00001$). (e) Illustrative histogram of vessel diameters ($n = 113$) of a single femoral head showing a unimodal distribution, which is shifted left for histological data. (f) Closest distance of vessel center and bone trabeculae measured by histology and microtomography.

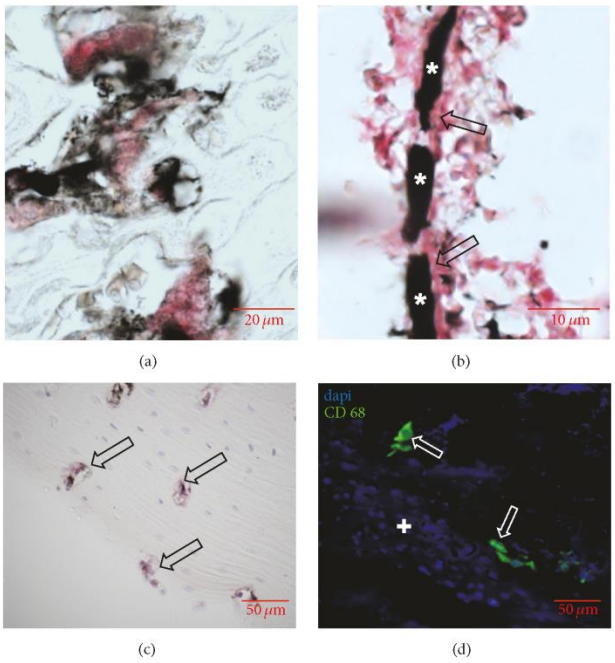

FIGURE 3: Enzymatic, immunohistochemical, and immunofluorescent staining on sections of femurs and tibias after contrast enhancement. (a) TRAP staining showing multinucleated osteoclasts (red) in the epiphyseal gap. (b) CD31 staining showing a small ink-gelatin contrasted vessel (star) with positively stained endothelial lining (arrows). (c) Immunohistochemistry for osteoblasts (arrow) in the corticalis. (d) Immunofluorescence for CD68 showing single rat macrophages (arrows) inside the bone marrow (plus).

course, branching, and average diameter of vessels, as well as the closest distance from the vessel center to adjacent bone with both large (150 μm) and small (10 μm–30 μm) vessels. Moreover, the method did not interfere with standard histological processing, enzymatic staining, immunohistochemistry, and immunofluorescence on the same samples.

Considering the significant limitations of X-ray opaque vascular casting, such as irreversible contrasting of vessels before bone scans, introduction of beam hardening and scattering artefacts, or difficulty of histological processing thereafter [8–11, 13, 23, 24], we aimed to provide an alternative method with a potentially higher precision and simplified handling. We identified a combination of two existing methods for μCT and histological contrast enhancement. On one hand, the infiltration of vessels using Indian ink and gelatin is an accepted method to analyse blood flow through vessels in histological sections [15]. The ink-gelatin is applied to the circulation and left to polymerise after euthanasia, providing a soft and coloured vascular cast. On the other hand, contrast enhancement of soft tissues in μCT has been proposed with a variety of contrasting agents [16, 17]. Interestingly, only PTA has demonstrated selectivity for collagens [25], without significantly altering the stiffness or colour of the tissue [26]. Although direct perfusion with PTA may contrast vessels in soft tissue thanks to its limited penetration in a short time [27], the resulting contrast is insufficient in bone and may be adversely affected by decalcification.

Sequential contrast enhancement ensures that bone can be analysed by standard μCT procedures [28, 29] while avoiding the generation of artefacts or difficult image segmentation commonly encountered with vascular casting. Indeed, by using this method, vessel contrasting becomes one of several optional analyses after explantation of the ink-gelatin-perfused sample.

Although many types of vessel analyses on 3D reconstructed data have been previously proposed, such as automated counting of vascular diameters, branching, or analysis of tortuosity, we chose manual measurement of diameters, number of branches from the central vessels, and distance of the vessel center to the adjacent bone trabeculae. These measurements indeed share a straightforward interpretation [11, 30] and avoid artefacts commonly generated by some automated algorithms [31–34]. Although still requiring occasional manual corrections, newer highly automated algorithms with

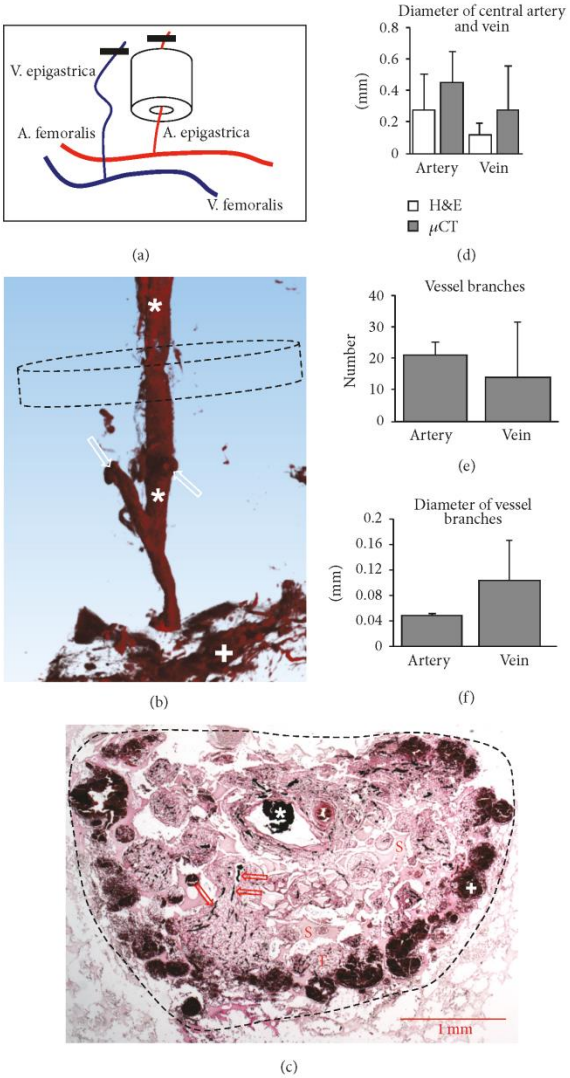

FIGURE 4: Analysis of vascularised porous hydroxyapatite. (a) Schematic of implantation. Superficial inferior epigastric vessels were identified, ligated (black bar), and cut distally. Either the artery (as shown) or the vein was pulled through the hydroxyapatite cylinder. (b) 3D rendering of contrasted central vein (star) with branches (white arrows), some diffuse contrast enhancement in the periphery (plus). After decalcification, the Engipore cylinder is no longer visible. Dashed line represents circular cross-section of Engipore cylinder. (c) H&E staining showing ink-gelatin contrasted central vein (star), small branching vessels (arrows), scaffold material (S) and pores filled with connective tissue (T), and peripheral haemorrhage with ink-gelatin (plus). Dashed line represents circular cross-section of Engipore cylinder. (d) Diameter of central artery and vein measured by histology and microtomography. (e) Number of vessels branching from central artery or vein. (f) Diameter of vessels branching from central artery or vein.

greater reliability [12, 35] should be applied when available in future applications of the herein described method to add further information and facilitate data collection.

During both μCT and histological analysis, we observed an incomplete filling of the central bone vessels with contrasting agent as well as peripheral haemorrhages from ruptured vessels, suggesting that the optimal flow properties and the optimal application of ink-gelatin still need to be characterised for future studies. Nevertheless, PTA was able to penetrate a whole rat femur/tibia and contrast the central vessel by diffusion, presenting a very useful property for the analysis of larger grafts and grafts with a closed bone marrow space.

The analysis of a simple, vascularised graft using porous hydroxyapatite with a central vein or artery exemplified an application of our method. Based on the limited data presented here, it appeared that the use of a single vein or a single artery had no impact on graft vascularisation. Although our concrete example may not be meaningful in a broader context of bone vascularisation, our method allowed a comparison of vascular branches and average branch diameter, both crucial aspects for tissue perfusion. For a more thorough evaluation of graft vascularisation, dedicated studies with greater statistical power are required, featuring previously published approaches such as vascular bundles of artery and vein [18, 36], vascular loops [15, 37], or wrapping with well-vascularised muscle tissue [38]. Though granulation tissue with rudimentary vasculature, sufficient for demonstration purposes in this study, formed after one week, longer in vivo incubation may be necessary for full maturation of the vascular tree.

In conclusion, *this study provides a relatively inexpensive and easy-to-perform two-step technique based on the use of ink-gelatin and PTA for the analysis of bone and vessels by μCT*. This technique could be applied to answer a variety of different questions in bone tissue engineering.

Additional Points

Key Points. (i) Bone vessels can be visualised using ink-gelatin and phosphotungstic acid. (ii) The size, branching, and distance from bone can be analysed. (iii) This method can be used to evaluate regenerative strategies in bone.

Conflicts of Interest

No competing financial interests exist.

Authors' Contributions

Sarah Sutter and Atanas Todorov contributed equally to this work.

Acknowledgments

The authors thank Finceramica Faenza for the provision of ceramic materials. Alexander Haumer has received funding from the People Programme (Marie Curie Actions) of the European Union's Seventh Framework Programme FP7/2007–2013/under REA Grant Agreement no. 607868 (iTERM).

References

[1] T. L. Andersen, T. E. Sondergaard, K. E. Skorzynska et al., "A physical mechanism for coupling bone resorption and formation in adult human bone," *The American Journal of Pathology*, vol. 174, no. 1, pp. 239–247, 2009.

[2] T. Al-Jabri, A. Mannan, and P. Giannoudis, "The use of the free vascularised bone graft for nonunion of the scaphoid: a systematic review," *Journal of Orthopaedic Surgery and Research*, vol. 9, article 21, 2014.

[3] N. Elmali, K. Ertem, M. Karakaplan, D. Pepele, C. Dağgez, and H. Topgül, "Vascular pedicled iliac bone grafting is effective in patients with an early stage of femoral head avascular necrosis," *Eklem Hastaliklari ve Cerrahisi*, vol. 25, no. 1, pp. 2–7, 2014.

[4] M. Jakob, F. Saxer, C. Scotti et al., "Perspective on the evolution of cell-based bone tissue engineering strategies," *European Surgical Research*, vol. 49, no. 1, pp. 1–7, 2012.

[5] P. Rosset, F. Deschaseaux, and P. Layrolle, "Cell therapy for bone repair," *Orthopaedics and Traumatology: Surgery and Research*, vol. 100, no. 1 S, pp. S107–S112, 2014.

[6] A. Papadimitropoulos, C. Scotti, P. Bourgine, A. Scherberich, and I. Martin, "Engineered decellularized matrices to instruct bone regeneration processes," *Bone*, vol. 70, pp. 66–72, 2015.

[7] M. H. Lafage-Proust, B. Roche, M. Langer et al., "Assessment of bone vascularization and its role in bone remodeling," *BoneKEy Reports*, vol. 4, article 662, 2015.

[8] S. Young, J. D. Kretlow, C. Nguyen et al., "Microcomputed tomography characterization of neovascularization in bone tissue engineering applications," *Tissue Engineering Part B: Reviews*, vol. 14, no. 3, pp. 295–306, 2008.

[9] H. Nyangoga, P. Mercier, H. Libouban, M. F. Baslé, and D. Chappard, "Three-dimensional characterization of the vascular bed in bone metastasis of the rat by microcomputed tomography (MicroCT)," *PLoS ONE*, vol. 6, no. 3, Article ID e17336, 2011.

[10] V. Alt, D. V. Kögelmaier, K. S. Lips et al., "Assessment of angiogenesis in osseointegration of a silica-collagen biomaterial using 3D-nano-CT," *Acta Biomaterialia*, vol. 7, no. 10, pp. 3773–3779, 2011.

[11] B. Roche, V. David, A. Vanden-Bossche et al., "Structure and quantification of microvascularisation within mouse long bones: what and how should we measure?" *Bone*, vol. 50, no. 1, pp. 390–399, 2012.

[12] S. Gayetskyy, O. Museyko, J. Käßer, A. Hess, G. Schett, and K. Engelke, "Characterization and quantification of angiogenesis in rheumatoid arthritis in a mouse model using μCT," *BMC Musculoskeletal Disorders*, vol. 15, article 298, 2014.

[13] H.-M. Xu, Y.-L. Wang, H.-M. Jin et al., "A novel micro-CT-based method to monitor the morphology of blood vessels in the rabbit endplate," *European Spine Journal*, vol. 26, no. 1, pp. 221–227, 2017.

[14] B. M. Khoury, E. M. R. Bigelow, L. M. Smith et al., "The use of nano-computed tomography to enhance musculoskeletal research," *Connective Tissue Research*, vol. 56, no. 2, pp. 106–119, 2015.

[15] Q.-S. Dong, H.-T. Shang, W. Wu et al., "Prefabrication of axial vascularized tissue engineering coral bone by an arteriovenous

loop: a better model," *Materials Science and Engineering: C*, vol. 32, no. 6, pp. 1536–1541, 2012.

[16] B. D. Metscher, "MicroCT for developmental biology: a versatile tool for high contrast 3D imaging at histological resolutions," *Developmental Dynamics*, vol. 238, no. 3, pp. 632–640, 2009.

[17] E. Pauwels, D. Van Loo, P. Cornillie, L. Brabant, and L. Van Hoorebeke, "An exploratory study of contrast agents for soft tissue visualization by means of high resolution X-ray computed tomography imaging," *Journal of Microscopy*, vol. 250, no. 1, pp. 21–31, 2013.

[18] O. Kloeters, I. Berger, H. Ryssel, K. Megerle, U. Leimer, and G. Germann, "Revitalization of cortical bone allograft by application of vascularized scaffolds seeded with osteogenic induced adipose tissue derived stem cells in a rabbit model," *Archives of Orthopaedic and Trauma Surgery*, vol. 131, no. 10, pp. 1459–1466, 2011.

[19] W. F. Willems, G. M. Alberton, A. T. Bishop, and T. Kremer, "Vascularized bone grafting in a canine carpal avascular necrosis model," *Clinical Orthopaedics and Related Research*, vol. 469, no. 10, pp. 2831–2837, 2011.

[20] M. Doube, M. M. Kłosowski, I. Arganda-Carreras et al., "BoneJ: free and extensible bone image analysis in ImageJ," *Bone*, vol. 47, no. 6, pp. 1076–1079, 2010.

[21] C. A. Schneider, W. S. Rasband, and K. W. Eliceiri, "NIH Image to ImageJ: 25 years of image analysis," *Nature Methods*, vol. 9, no. 7, pp. 671–675, 2012.

[22] K. G. Sheets, B. Jun, Y. Zhou et al., "Microglial ramification and redistribution concomitant with the attenuation of choroidal neovascularization by neuroprotectin D1," *Molecular Vision*, vol. 19, pp. 1747–1759, 2013.

[23] S. Grabherr, V. Djonov, K. Yen, M. I. Thali, and R. Dirnhofer, "Postmortem angiography: review of former and current methods," *American Journal of Roentgenology*, vol. 188, no. 3, pp. 832–838, 2007.

[24] T. B. Baker, R. M. McFall, and V. Shoham, "Current status and future prospects of clinical psychology: toward a scientifically principled approach to mental and behavioral health care," *Psychological Science in the Public Interest*, vol. 9, no. 2, pp. 67–103, 2008.

[25] L. Silverman and D. Glick, "The reactivity and staining of tissue proteins with phosphotungstic acid," *Journal of Cell Biology*, vol. 40, no. 3, pp. 761–767, 1969.

[26] I. Papantoniou, M. Sonnaert, L. Geris, F. P. Luyten, J. Schrooten, and G. Kerckhofs, "Three-dimensional characterization of tissue-engineered constructs by contrast-enhanced nanofocus computed tomography," *Tissue Engineering Part C: Methods*, vol. 20, no. 3, pp. 177–187, 2014.

[27] P. J. Dunmore-Buyze, E. Tate, F.-L. Xiang et al., "Three-dimensional imaging of the mouse heart and vasculature using micro-CT and whole-body perfusion of iodine or phosphotungstic acid," *Contrast Media and Molecular Imaging*, vol. 9, no. 5, pp. 383–390, 2014.

[28] M. L. Bouxsein, S. K. Boyd, B. A. Christiansen, R. E. Guldberg, K. J. Jepsen, and R. Müller, "Guidelines for assessment of bone microstructure in rodents using micro-computed tomography," *Journal of Bone and Mineral Research*, vol. 25, no. 7, pp. 1468–1486, 2010.

[29] A. Barbetta, R. Bedini, R. Pecci, and M. Dentini, "Role of X-ray microtomography in tissue engineering," *Annali dell'Istituto Superiore di Sanità*, vol. 48, no. 1, pp. 10–18, 2012.

[30] F. Jia, P. Françoise, L. Malaval, V. Laurence, and L.-P. Marie-Hélène, "Imaging and quantitative assessment of long bone vascularization in the adult rat using microcomputed tomography," *Anatomical Record*, vol. 293, no. 2, pp. 215–224, 2010.

[31] T. Boskamp, D. Rinck, F. Link, B. Kümmerlen, G. Stamm, and P. Mildenberger, "New vessel analysis tool for morphometric quantification and visualization of vessels in CT and MR imaging data sets," *Radiographics*, vol. 24, no. 1, pp. 287–297, 2004.

[32] S. Heinzer, G. Kuhn, T. Krucker et al., "Novel three-dimensional analysis tool for vascular trees indicates complete micro networks, not single capillaries, as the angiogenic endpoint in mice overexpressing human $VEGF_{165}$ in the brain," *NeuroImage*, vol. 39, no. 4, pp. 1549–1558, 2008.

[33] D.-G. Kang, D. C. Suh, and I. B. Ra, "Three-dimensional blood vessel quantification via centerline deformation," *IEEE Transactions on Medical Imaging*, vol. 28, no. 3, pp. 405–414, 2009.

[34] D. Chiller, N. Passat, M. A. J.-D. Col, and J. Baruthio, "Thickness estimation of discrete tree like tubular objects: application to vessel quantification," in *Image Analysis: 14th Scandinavian Conference, SCIA 2005, Joensuu, Finland, June 19–22 2005 Proceedings*, H. Kalviainen, J. Parkkinen, and A. Kaarna, Eds., pp. 263–271, Springer, Berlin, Germany, 2005.

[35] F. Zhao, J. Liang, D. Chen et al., "Automatic segmentation method for bone and blood vessel in murine hindlimb," *Medical Physics*, vol. 42, no. 7, pp. 4043–4054, 2015.

[36] W. F. Willems, M. Larsen, G. Giusti, P. F. Friedrich, and A. T. Bishop, "Revascularization and bone remodeling of frozen allografts stimulated by intramedullary sustained delivery of FGF-2 and VEGF," *Journal of Orthopaedic Research*, vol. 29, no. 9, pp. 1431–1436, 2011.

[37] U. Kneser, E. Polykandriotis, J. Ohnolz et al., "Engineering of vascularized transplantable bone tissues: induction of axial vascularization in an osteoconductive matrix using an arteriovenous loop," *Tissue Engineering*, vol. 12, no. 7, pp. 1721–1731, 2006.

[38] A. Kaempfen, A. Todorov, S. Güven et al., "Engraftment of prevascularized, tissue engineered constructs in a novel rabbit segmental bone defect model," *International Journal of Molecular Sciences*, vol. 16, no. 6, pp. 12616–12630, 2015.

Chapter IV:

Engineered and devitalized ECM to induce osteogenesis

STEM CELLS TRANSLATIONAL MEDICINE

TISSUE ENGINEERING AND REGENERATIVE MEDICINE

Fat-Derived Stromal Vascular Fraction Cells Enhance the Bone-Forming Capacity of Devitalized Engineered Hypertrophic Cartilage Matrix

ATANAS TODOROV,[a,b,*] MATTHIAS KREUTZ,[a,b,c,*] ALEXANDER HAUMER,[a,b] CELESTE SCOTTI,[d] ANDREA BARBERO,[a] PAUL E. BOURGINE,[a] ARNAUD SCHERBERICH,[a] CLAUDE JAQUIERY,[b,c] IVAN MARTIN[a,b]

Key Words. Bone • Bone marrow stromal cells • Adipose stromal cells • Cell transplantation • Clinical translation • Tissue regeneration

[a]Department of Biomedicine, University of Basel, Switzerland; [b]Department of Surgery and [c]Clinic for Oral and Maxillofacial Surgery, University Hospital of Basel, Basel, Switzerland; [d]Instituti di Ricovero e Cura a Carattere Scientifico, Istituto Ortopedico Galeazzi, Milano, Italy

[*]Contributed equally.

Correspondence: Ivan Martin, Ph.D., University Hospital of Basel, Hebelstrasse 20, 4031 Basel, Switzerland. Telephone: 41612652384; E-Mail: ivan.martin@usb.ch; or Claude Jaquiery, M.D., D.M.D., University Hospital of Basel, Hebelstrasse 20, 4031 Basel, Switzerland. Telephone: 41612652384; E-Mail: claude.jaquiery@usb.ch

Received January 6, 2016; accepted for publication May 13, 2016; published Online First on July 26, 2016.

1066-5099/2016/$20.00/0

http://dx.doi.org/10.5966/sctm.2016-0006

ABSTRACT

Engineered and devitalized hypertrophic cartilage (HC) has been proposed as bone substitute material, potentially combining the features of osteoinductivity, resistance to hypoxia, capacity to attract blood vessels, and customization potential for specific indications. However, in comparison with vital tissues, devitalized HC grafts have reduced efficiency of bone formation and longer remodeling times. We tested the hypothesis that freshly harvested stromal vascular fraction (SVF) cells from human adipose tissue—which include mesenchymal, endothelial, and osteoclastic progenitors—enhance devitalized HC remodeling into bone tissue. Human SVF cells isolated from abdominal lipoaspirates were characterized cytofluorimetrically. HC pellets, previously generated by human bone marrow-derived stromal cells and devitalized by freeze/thaw, were embedded in fibrin gel with or without different amounts of SVF cells and implanted either ectopically in nude mice or in 4-mm-diameter calvarial defects in nude rats. In the ectopic model, SVF cells added to devitalized HC directly contributed to endothelial, osteoblastic, and osteoclastic populations. After 12 weeks, the extent of graft vascularization and amount of bone formation increased in a cell-number-dependent fashion (up to, respectively, 2.0-fold and 2.9-fold using 12 million cells per milliliter of gel). Mineralized tissue volume correlated with the number of implanted, SVF-derived endothelial cells (CD31+ CD34+ CD146+). In the calvarial model, SVF activation of HC using 12 million cells per milliliter of gel induced efficient merging among implanted pellets and strongly enhanced (7.3-fold) de novo bone tissue formation within the defects. Our findings outline a bone augmentation strategy based on off-the-shelf devitalized allogeneic HC, intraoperatively activated with autologous SVF cells. STEM CELLS TRANSLATIONAL MEDICINE *2016;5:1684–1694*

SIGNIFICANCE

This study validates an innovative bone substitute material based on allogeneic hypertrophic cartilage that is engineered, devitalized, stored, and clinically used, together with autologous cells, intraoperatively derived from a lipoaspirate. The strategy was tested using human cells in an ectopic model and an orthotopic implantation model, in immunocompromised animals.

INTRODUCTION

Clinical treatment of challenging bone defects often requires a suitable bone graft, yet extensive donor site morbidity and complication rates around 60% [1] pose significant problems for the use of autologous bone. Commercially available bone substitute materials typically lack intrinsic osteoinductive potential, and the long-term integration into bone defects is not always achieved [2].

The use of engineered hypertrophic cartilage is receiving increasing consideration as a possible bone substitute, because of many inherent advantages. As a bradytroph and hypoxia-resistant tissue [3], it does not require immediate vascularization. Moreover, it has some initial mechanical stability, and it embeds the biological signals for remodeling into a complete bone organ, resembling the processes of embryonic bone development [4]. Although the bone-forming capacity of engineered hypertrophic cartilage has been demonstrated in stringent ectopic implantation models as well as in an orthotopic nonunion model [5–9], clinical translation can be hampered by the required use of autologous cells, their known and unpredictable variability across different donors, and the long times for in vitro construct generation.

Devitalization and off-the-shelf storage of engineered, allogeneic hypertrophic cartilage could offer an attractive bone substitute material, on the basis of the assumption that the deposited extracellular matrix (ECM) would physiologically deliver a suitable combination of cytokines and morphogens to recruit and instruct endogenous osteoprogenitors at the repair site [10]. Previous work has shown that the signals necessary for osteoinduction can be preserved in the ECM, provided a mild but effective devitalization strategy is used [11]. Yet the efficiency of bone formation remains reduced in comparison with the vital tissue. Moreover, this difference is expected to become increasingly relevant along with the graft size, because of the time required by host cells to penetrate and reactivate the matrix, a prerequisite for tissue remodeling into bone [12].

Inspired by the "developmental engineering" concept of modularity, whereby "the interfaces between developing entities are initially uncoupled" [13], here we investigated the possibility of using multiple small organoids of engineered and devitalized hypertrophic cartilage to generate a larger bone volume. The strategy is based on the rationale that each construct would efficiently develop into bone tissue as an independent module, because of the large surface-area-to-volume ratio, and the tissues would then fuse into a monolithic trabecular structure.

To enhance the reactivation and remodeling of the devitalized ECM, we further introduced the use of stromal vascular fraction (SVF) cells, freshly harvested from human adipose tissue and embedded within a gel along with the devitalized cartilage matrix. The rationale was based on the fact that SVF cells contain endothelial cells, monocytes, and mesenchymal stromal cells [14], with the respective capacity to potentially enhance tissue vascularization, osteoclast-mediated remodeling, and bone formation. Previous experiments have demonstrated that SVF cells implanted subcutaneously in a fibrin gel with hydroxyapatite granules do not form bone unless they are primed with bone morphogenetic protein (BMP)-2 [15].

The goal of the present study was thus to test the hypothesis that the supplementation of human SVF cells with multiple pellets of engineered and devitalized hypertrophic cartilage leads to a composite construct with enhanced capacity to form de novo bone tissue, both ectopically (i.e., subcutaneously in nude mice) and orthotopically (i.e., in a calvarial defect model in nude rats).

Materials and Methods

All human samples were collected with informed patient consent and after approval by the local ethical committee, in accordance with Swiss law. Animal procedures were approved by the Swiss Federal Veterinary Office (Kantonal permit BS-2590).

Preparation of Devitalized Hypertrophic Constructs

Human bone marrow stromal cells from five donors (35.4 $\pm$ 11.3 years, all male) were expanded for two passages in complete medium (α-minimum essential medium, 10% fetal bovine serum, 10 mM HEPES, 1 mM sodium pyruvate, 100 U/ml penicillin, 100 μg/ml streptomycin, 0.29 mg/ml glutamate; all from Invitrogen, Carlsbad, CA, USA, https://www.thermofisher.com) containing fibroblast growth factor-2 (5 ng/ml; R&D Systems, Minneapolis, MN, USA, https://www.rndsystems.com), as previously described [16]. Cells from different donors were used in independent experiments. Pellets were prepared by centrifuging 0.5×10^6 cells in 1.5-ml screw cap Eppendorf tubes at 300*g* for 5 minutes and cultured in serum-free medium (Dulbecco's modified Eagle's medium, 1.25 mg/ml human serum albumin, 10 mM HEPES, 1 mM sodium pyruvate, 100 U/ml penicillin, 100 μg/ml streptomycin, 0.29 mg/ml glutamate, and ITS-A [10 μg/ml insulin, 5.5 μg/ml transferrin, 5 ng/ml selenium, 0.5 mg/ml bovine serum albumin]; from Invitrogen), supplemented with 10 ng/ml transforming growth factor-β1 (R&D Systems), 10^{-7} M dexamethasone, and 0.1 mM ascorbic acid 2-phosphate (Sigma-Aldrich, St. Louis, MO, USA, https://www.sigmaaldrich.com) (chondrogenic medium). After 3 weeks, resulting cartilaginous pellets were further cultured in hypertrophic medium (serum-free medium with 50 nM thyroxine, 10 mM β-glycerophosphate, 10^{-8} M dexamethasone, 0.1 mM ascorbic acid 2-phosphate, and 50 pg/ml interleukin-1β; Sigma-Aldrich) for 2 weeks, as has been previously described [16, 17]. The generated hypertrophic pellets were devitalized by using three cycles of freezing (−196°C for 10 minutes) and thawing (37°C for 10 minutes) and a final wash with deionized water. All fluids were removed and pellets stored at −80°C until further use. To determine variability of pellets among different batches of preparation, we assessed two pellets of each donor for glycosaminoglycan (GAG) content, as has been previously described [16], and one pellet of each donor was processed histologically, as is detailed below.

Isolation of SVF Cells

SVF cells from liposuctions or excision fat were isolated from 12 donors (33.7 $\pm$ 7.7 years, 2 males and 10 females) as described previously [18, 19]. Briefly, minced fat tissue was incubated for 60 minutes in 0.15% collagenase type 2 solution, centrifuged and supernatants discarded. Cells were resuspended, filtered through 100 μm mesh filters and counted in a Neubauer counting chamber using crystal violet. Fluorescence-activated cell sorting analysis for CD31, CD34, CD146, CD90, CD105 and CD15 (AbD Serotec, Bio-Rad, Raleigh, NC, USA, https://www.bio-rad-antibodies.com) was performed, as previously described [18]. Cells were frozen in fetal bovine serum and 10% dimethyl sulfoxide and kept in the gaseous phase of liquid nitrogen until further use. Cells from different donors were used in independent experiments.

Preparation of Grafts

SVF cells were thawed and counted, and the appropriate amount was resuspended in 40 μl fibrinogen (100 mg/ml; Tisseel, Baxter, Deerfield, IL, USA, http://www.tisseel.com/). Control samples contained no SVF cells. Multiple devitalized hypertrophic pellets (12 to 24, depending on the experiment, but constant for all groups in one experiment) were mixed with this solution, and 40 μl of thrombin (400 units per milliliter with 40 μM $CaCl_2$; Baxter) were added. Polymerization was allowed to occur for 30 minutes at 37°C, followed by immediate implantation.

Ectopic and Orthotopic Implantation

For ectopic implantations, grafts were inserted into subcutaneous pouches of nude mice (CD-1 nude/nude; Charles River Laboratories, Ashland, OH, USA, http://www.criver.com/) at four pouches per mouse, with duplicate grafts per donor and experimental group. The operation was performed with isoflurane (Attane Isoflurane; Provet AG, Lyssach, Switzerland, http://www.provet.ch/) anesthesia and buprenorphine (Temgesic; Reckitt Benckiser AG,

Wallisellen, Switzerland, http://www.rb.com/) analgesia, and animals were checked periodically. After 12 weeks, mice were euthanized with CO_2, and explants were assessed, as is described below. Our previous experience with similar-sized grafts [4] suggested that 12 weeks would be sufficient for the remodeling of the cartilage pellets into bone.

For orthotopic implantations, nude rats (Rowett nude; Charles River Laboratories) were anesthetized using isoflurane, and the calvaria were exposed by dissection of the subcutaneous tissue and periosteum. Bilateral 4-mm defects were created in the central area of each parietal bone by using a saline-cooled trephine bur. The defect was refined using a piezoelectric knife in order not to injure the dura mater. The sites were constantly irrigated with sterile NaCl 0.9% to prevent overheating of the bone margins and to remove the bone debris. Grafts were molded into the defect by using a small spoon and spatula. Incisions were closed in a double layer by sutures and clamps, which were removed after 10 days. Animals were carefully monitored for behavioral abnormalities after the operation. After 4 weeks, the rats were euthanized with CO_2, followed by decapitation, and the calvaria were stored and assessed as described below.

Microtomography

After explantation, samples were fixed in 4% paraformaldehyde overnight and then transferred to phosphate-buffered saline. Microtomography was performed by using a tungsten x-ray source at 70 kV and 260 μA with an aluminum filter of 0.5 mm (Nanotome; GE, Fairfield, CT, USA, http://www.ge.com/). Transmission images were acquired for 360° with an incremental step size of 0.25°. Volumes were reconstructed using a modified Feldkamp algorithm at a voxel size of 2.5–15 μm. Manual thresholding, segmentation, and three-dimensional (3D) measurements were made with the ImageJ [20] software with the BoneJ [21] and 3DShape [22] additions.

Histology

Samples were decalcified using a 7% EDTA 30% sucrose solution (Sigma-Aldrich) and either embedded in paraffin for histological staining or frozen in optimal cutting temperature medium for immunofluorescence. Sections (5- to 10-μm thick) were stained with hematoxylin and eosin (H&E), Masson trichrome, or Safranin-O. In situ hybridization for human *Arthrobacter luteus* (ALU) sequences was performed, as has been described previously [11], to detect the presence of human cells. Tartrate resistant acid phosphatase (TRAP) staining was performed, as has been described previously [23], to identify osteoclasts. Immunohistochemistry and immunofluorescence were performed by using primary antibodies for DIPEN (1042002, MDBiosciences, St. Paul, MN, USA, http://www.mdbiosciences.com/), type X collagen (ab49945), type II collagen (ab34712), MMP13 (ab39012), MMP9 (ab38898), CD31 (ab28364), human calcitonin receptor (ab175297; all from Abcam, Cambridge, UK, http://www.abcam.com/), and human CD34 (CBL496; Dako, Glostrup, Denmark, http://www.dako.com). Secondary antibodies labeled with Alexa Fluor 488, Alexa Fluor 546, or Alexa Fluor 647 (Invitrogen) were used, and 4′,6-diamidino-2-phenylindole (DAPI) (Sigma-Aldrich) was used to stain nuclei in fluorescence images. Immunohistochemistry was done with biotinylated secondary antibodies (Dako) and the Vectastain ABC kit (Vector Laboratories, Burlingame, CA, USA, https://vectorlabs.com/). The Olympus BX61, BX63, Zeiss LSM 710, and Nikon A1R microscopes were used to acquire images.

Quantification of Histological Features

H&E-stained sections were used for the histological quantification of bone, as has been described previously [24]. Briefly, six central sections per graft, covering a total depth of 750 μm, were analyzed. The total area of the graft and the area of each pellet were manually selected, and a threshold was set to segment bone from other tissues. The bone area was then quantified as a percentage of the selected area. Osteoclasts were manually counted under high magnification on total areas of sections stained for TRAP and human calcitonin receptor, using four central sections per graft to cover a depth of 450 μm. For vessel quantification, the vessels in two representative photographs of four sections per graft, covering a total depth of 450 μm, were identified by immunofluorescence for CD31 and human CD34 and manually traced. At least four grafts per group were analyzed.

Statistical Analysis

The data were visualized and analyzed with GraphPad Prism version 6 software. Parametric analysis of variance with the appropriate post hoc tests as well as linear regressions were performed. We considered p values below .05 to indicate statistically significant differences.

Results

Devitalized Hypertrophic Constructs Activated With SVF Cells Form Ectopic Bone

Hypertrophic cartilage pellets engineered from human bone marrow-derived mesenchymal stromal cells (between 300 and 800 pellets for each of the five donors used) were rather uniform in size (average pellet diameter: 1.0 $\pm$ 0.2 mm), with variable GAG content (GAG/pellet: 15.8 $\pm$ 9.5 μg). Positive staining for GAG, type II, and type X collagen (Fig. 1A) were consistent with previously reported morphological and molecular features [16]. SVF cells from the different donors displayed a typical phenotypic heterogeneity (Fig. 1B), with the largest variability observed for the percentage of CD90 expressing cells (39.6%–86.2% of the isolated cells). After freeze/thaw devitalization, 12 pellets were suspended in a fibrin gel with or without the addition of human SVF cells (6 million cells per milliliter of gel) and implanted into nude mice (Fig. 1C).

After 12 weeks, control grafts in cell-free fibrin gel displayed depletion of glycosaminoglycans and only limited, scattered areas of remodeling into bone tissue (Fig. 2A). Instead, SVF-activated grafts contained abundant osteoid matrix, embedding large areas occupied by bone marrow. In situ hybridization for human ALU sequences indicated that the SVF-activated grafts still contained human cells surrounding the pellets after 12 weeks in vivo, in contrast to the nonactivated, devitalized grafts (Fig. 2A). However, instances of human cells surrounded by osteoid matrix were rare. A closer immunohistochemical analysis showed that both the activated and nonactivated grafts were undergoing matrix metalloproteinase (MMP)-driven degradation of cartilage matrix, leading to aggrecan cleavage, as signaled by detection of the major MMP cleavage site DIPEN (Fig. 2B). Thus, aggrecan depletion did not appear to be directly related to the efficiency of bone and bone

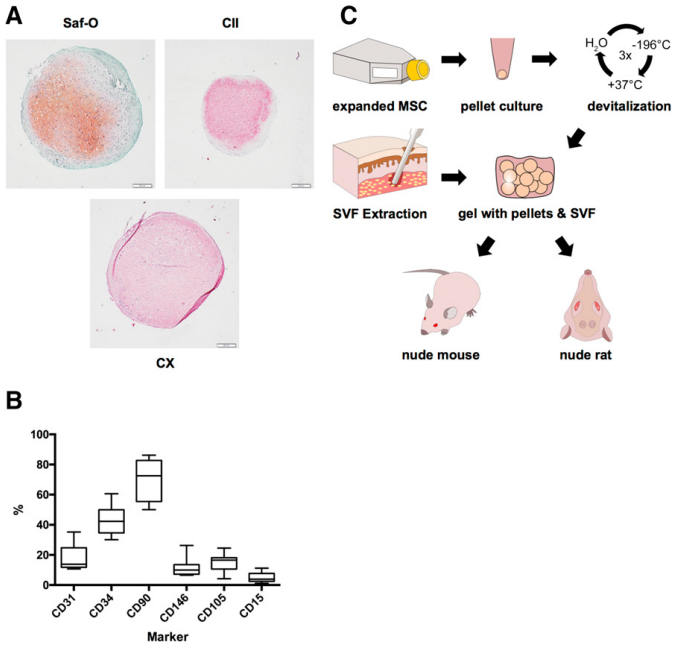

Figure 1. Starting material and experimental setup. **(A):** Representative staining of devitalized hypertrophic cartilage pellets. Scale bars = 200 μm. **(B):** Marker expression across stromal vascular fraction donors; boxes represent median with interquartile range; whiskers represent 97.5th and 2.5th percentiles. **(C):** Experimental setup for the generation of grafts, ultimately tested by implantation subcutaneously (nude mouse, ectopic model) or in calvarial defects (nude rat, orthotopic model). Abbreviations: CII, type II collagen (red/pink = positive); CX, type X collagen (red/pink = positive); MSC, mesenchymal stem cells; Saf-O, Safranin-O; SVF, stromal vascular fraction.

marrow development, which occurred to a markedly higher extent following SVF cell-based activation.

The Number of SVF Cells Correlates With Ectopic Bone Quantity

We then assessed a possible dose response in the effect of SVF cells. In up to 12 million cells per milliliter of gel, we identified a clear correlation between the number of SVF cells at implantation, and the resulting total amount of mineralized tissue, measured by microtomography (R^2 = 0.347, p = .01; Fig. 3A), or of bone matrix, quantified in histological sections (R^2 = 0.546, p = .0025; Fig. 3B). With 12 million SVF cells, the amount of bone formation was 2.9-fold higher (by histological measurements) than was the one obtained in the nonactivated grafts. It should be highlighted that quantification of the total space covered by bone structures, including bone marrow cavities embedded within the osteoid trabeculae (Fig. 3C), would lead to even more marked differences in the effect of SVF cells. The amount of bone formation was similar or even reduced by graft activation with more than 12 million SVF cells per milliliter of gel. Changes in the total amount of bone formation with the number of SVF cells were not associated with an increase in the amount of bone per pellet (Fig. 3D), but with an increase in the percentage of pellets including bone tissue (Fig. 3E). This result suggests a role of SVF cells in increasing the reproducibility of pellet remodeling.

SVF Cells Contribute to Osteoclast-Mediated Matrix Resorption

The number of implanted SVF cells correlated significantly with the density of TRAP-positive osteoclasts, histologically quantified after 12 weeks in vivo (R^2 = 0.31, p = .03; Fig. 4A, 4B). Immunofluorescence staining for the human isoform of calcitonin receptor identified some multinucleated positive cells in the vicinity of the osteoid matrix even after 12 weeks in vivo (Fig. 4C). The number of human origin osteoclasts correlated with the amount of SVF cells (R^2 = 0.32, p = .02) and represented an average of 18% of total osteoclasts when using the highest number of SVF cells (Fig. 4D). These data suggest that activation of devitalized hypertrophic cartilage by SVF cells may enhance its resorption and that SVF cells could not only attract resident osteoclasts but also offer a source for them.

Specific SVF Subpopulations of Endothelial Lineage Correlate With Total Bone Quantity

Considering the phenotypic heterogeneity of freshly isolated SVF cells, we addressed whether the amount of mineralized tissue could be correlated with the delivered dose of specific SVF subpopulations. Therefore, we analyzed data generated from graft activation by different SVF preparations (n = 9 donors) against cytofluorimetric analysis of their phenotype, performed in parallel using the markers CD31, CD34, CD146, CD90, CD105, and

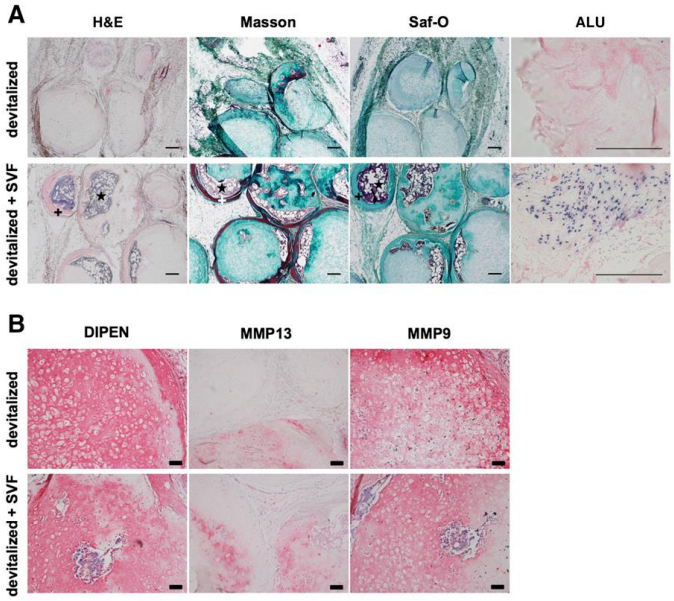

Figure 2. Ectopic bone formation. Grafts based on devitalized hypertrophic cartilage pellets were embedded in fibrin gel without or with stromal vascular fraction cells from adipose tissue and implanted subcutaneously in nude mice. **(A):** Representative hematoxylin and eosin, Masson-Tri-Chrome, and Safranin-O (Saf-O) staining and in situ hybridization for human ALU sequences (dark blue = positive) after 12 weeks in vivo. Saf-O stainings are blue-green because of lack of glycosaminoglycans and counterstaining with fast green. Osteoid matrix and bone marrow are visible. Scale bars = 200 μm. **(B):** Stainings for metalloproteinase (MMP)13 and MMP9, as well as for the N-terminal neoepitope at the major MMP cleavage site (DIPEN) after 12 weeks in vivo (red/pink = positive). Scale bars = 50 μm. +, osteoid matrix; ⋆, bone marrow. Abbreviations: ALU, *Arthrobacter luteus*; H&E, hematoxylin and eosin; Masson, Masson's trichrome; MMP, metalloproteinase; Saf-O, Safranin-O; SVF, stromal vascular fraction.

CD15. The ratio of mineralized volume to total volume correlated most strongly with the number of implanted CD31, CD34, CD146 triple-positive cells (R^2 = 0.4756, p = .013; Fig. 5A), which identify endothelial cells. No correlation was found with CD90 (R^2= 0.0226, p = .608; Fig. 5B), CD105 (R^2 = 0.0450, p = .467), or CD15 (R^2 = 0.0616, p = .392) positive cells. Staining for DAPI, type X collagen, and CD31 indicated that the activated grafts displayed a more advanced colonization of the hypertrophic matrix with uniformly organized vascular network than did the nonactivated grafts after 12 weeks in vivo (Fig. 5C, 5D). Quantification of the total length of vessels per square millimeter of section showed that grafts activated with 6 or 12 million cells per milliliter of gel were significantly more vascularized (up to 1.9-fold) than were nonactivated grafts (Fig. 5E). Immunohistochemistry for the human isoform of CD34 allowed us to identify that some of the endothelial cells lining the vessels were of human origin (Fig. 5F). The percentage of vessels including human CD34+ cells (average of 52%) and the percentage of vessel lengths formed by them (average of 29%) did not vary with the number of SVF cells seeded (Fig. 5G, 5H).

SVF-Activated Constructs Enhance Early Orthotopic Bone Formation and Bridging to Host Bone

To evaluate the orthotopic bone-regenerative capacity of SVF-activated grafts, we implanted devitalized hypertrophic cartilage pellets with or without (control) additional SVF cells (12 million per milliliter of gel) into 4 mm of rat calvarial defects (Fig. 1C). At the time of implantation the pellets were in contact with each other and with the rat calvarium. After 4 weeks, calcified volume inside the defects was nearly identical (Fig. 6A). However, more rigorous histological analysis revealed that the percentage of defect area filled by bone matrix was up to 7.3-fold larger in the SVF-activated graft than in the nonactivated grafts ($p < .0001$; Fig. 6B), with osteoid formation also reaching the center of the defect (Fig. 6C, 6D). Higher-magnification assessments indicated that bone formation in the SVF-activated group was developing by (a) remodeling of the pellets into trabecular bone organoids and (b) merging of those modular structures with each other and with the rat calvarium surrounding the defect (Fig. 6E). Both processes could not be recognized in the nonactivated grafts, also because of the minimal amounts of bone formed at the time point of observation. Pellet merging was observed in all orthotopic activated grafts, in 31% of ectopic activated grafts, and in none of the orthotopic or ectopic nonactivated grafts. In general, the size and shape of the pellets in both groups were almost identical to those of the grafts at implantation. In some areas of implants activated by SVF cells, human origin cells could be observed inside the osteoid matrix, including the areas corresponding to newly formed bone marrow sinusoids (Fig. 6F).

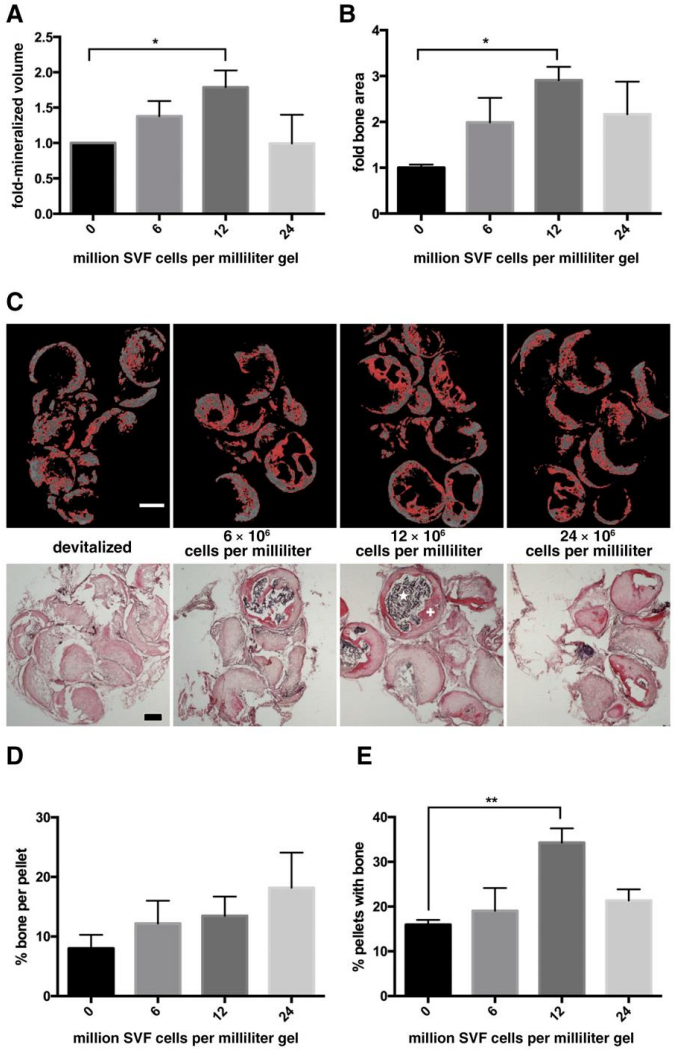

Figure 3. Effect of stromal vascular fraction (SVF) cell number. Following ectopic implantation, the amount of mineralized bone volume, quantified by microtomography **(A)** or the area covered by bone tissue, assessed in histological slides stained by hematoxylin and eosin (H&E) **(B)**, was expressed as fold difference of the nonactivated grafts and plotted versus the number of embedded SVF cells ($n = 5$–6 grafts assessed per group). *, $p < .05$, mean and standard error of the mean. **(C):** Representative microtomography sections, with pixels marked in red corresponding to the selected density threshold (top panels) and H&E-stained sections (bottom panels) used to generate the data displayed in panels A and B. Scale bars = 500 μm. Percentage of osteoid matrix area per total pellet area **(D)** and percentage of implanted pellets with osteoid matrix formation **(E)** ($n = 5$–6 grafts assessed per group). **, $p < .01$, mean and standard error of the mean. +, osteoid matrix; ⋆, bone marrow. Abbreviation: SVF, stromal vascular fraction.

Discussion

In this study we investigated the bone-forming capacity of constructs generated by the combination of devitalized engineered hypertrophic cartilage pellets with freshly isolated SVF cells from human adipose tissue. SVF activation of the hypertrophic cartilage strongly enhanced its bone-formation efficiency, tested in subcutaneous ectopic implantation and calvarial defect models. The density of SVF cells was correlated with that of osteoclasts in the grafts, and the percentage of SVF-derived endothelial lineage cells was correlated with the amount of deposited mineralized matrix.

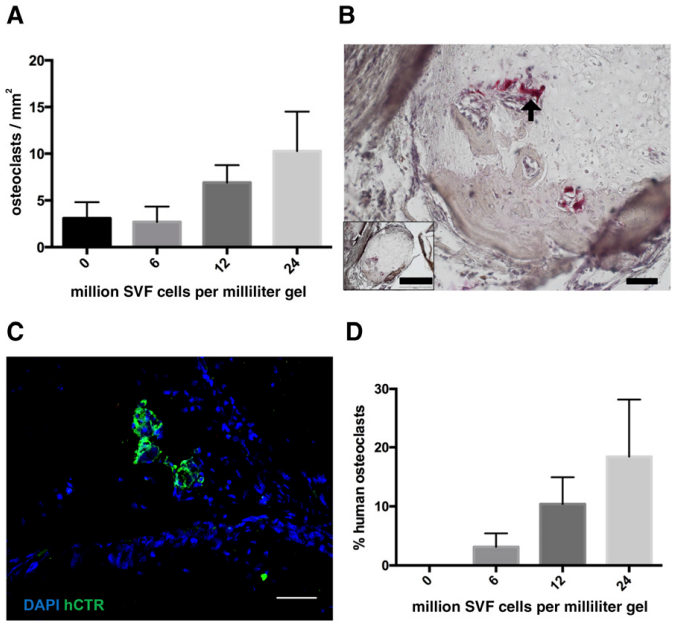

Figure 4. Osteoclast characterization. **(A):** The density of osteoclasts, assessed by tartrate resistant acid phosphatase staining (TRAP), was plotted versus the number of embedded stromal vascular fraction (SVF) cells ($n = 3$ grafts assessed per group). **(B):** Representative TRAP staining (arrow = multinucleated osteoclast). Scale bars = 50 μm or 500 μm (inset). **(C):** Staining for human calcitonin receptor (green fluorescence) indicates the direct contribution of SVF cells to osteoclast formation. Scale bar = 50 μm. **(D):** Human osteoclasts as percentage of the total number of identified osteoclasts ($n = 4$–6 grafts per group). Abbreviations: DAPI, 4′,6-diamidino-2-phenylindole; hCTR, green fluorescence; SVF, stromal vascular fraction.

The concept of using multiple pellets formed by chondrogenic differentiation of human mesenchymal stem cells (MSCs) for the engineering of bone substitute materials has been previously proposed for the treatment of segmental bone defects in immunodeficient mice [7] or rats [5]. In both studies, the cartilage grafts resulted in the generation of vascularized bone tissue, thereby supporting the idea that recapitulation of endochondral ossification is a valid strategy for bone repair at orthotopic sites. However, despite the overall good performance, limited integration across the implanted pellets was observed [7], indicating that scaling up bone graft materials by the principle of bringing together smaller modules may require further improvement. Moreover, the implantation of living tissues required the use of autologous cells, with associated cost and logistics issues.

In this context, the possibility of using engineered and then devitalized hypertrophic cartilage pellets described here would offer the distinct advantage of having "off-the-shelf" units, possibly engineered by allogeneic cells. Our results indicate that the MSC-deposited, cell-free extracellular matrix does contain the cues to trigger bone and bone marrow formation and that its effect is strongly potentiated by the activation through living progenitors derived from fat tissue. Interestingly, we observed highly efficient integration among the different pellets and with the surrounding bone areas in an orthotopic environment. The gel embedding the pellets could facilitate the ingrowing cells and the seeded SVF cells to interconnect the structures during the remodeling process. The fact that merging was more limited in an ectopic environment and absent if no SVF cells were seeded indicates that SVF cells had an effect on graft remodeling, which was enhanced by factors or cells present at a site of bone injury.

One relevant contribution of SVF cells was demonstrated to be related to the endothelial subpopulation that they include. In fact, SVF-activated grafts displayed a qualitatively more uniformly organized and quantitatively larger vascular network. Moreover, a quantitative correlation could be established between the amount of mineralized matrix formed and the density of delivered endothelial cells, phenotypically identified as expressing CD31, CD34, and CD146 [25–27]. Surprisingly, the amount of SVF cells did not correlate with the amount of human cells contributing to the vasculature after 12 weeks, despite the previously recognized role of SVF cells in establishing functional endothelial structures within engineered tissues [19, 28]. Our findings thus suggest the formation of a transitory human vasculature, followed by pruning and replacement with host vessels, or a paracrine role of the SVF-derived endothelial cells, leading to more efficient activation of resident endothelial/osteoblast lineage cell populations. Regardless of the effective mechanism, which should be addressed by analyzing early time points, our findings suggest that the number of endothelial cells in SVF preparations could be used as a quality control parameter, to ensure efficient graft activation.

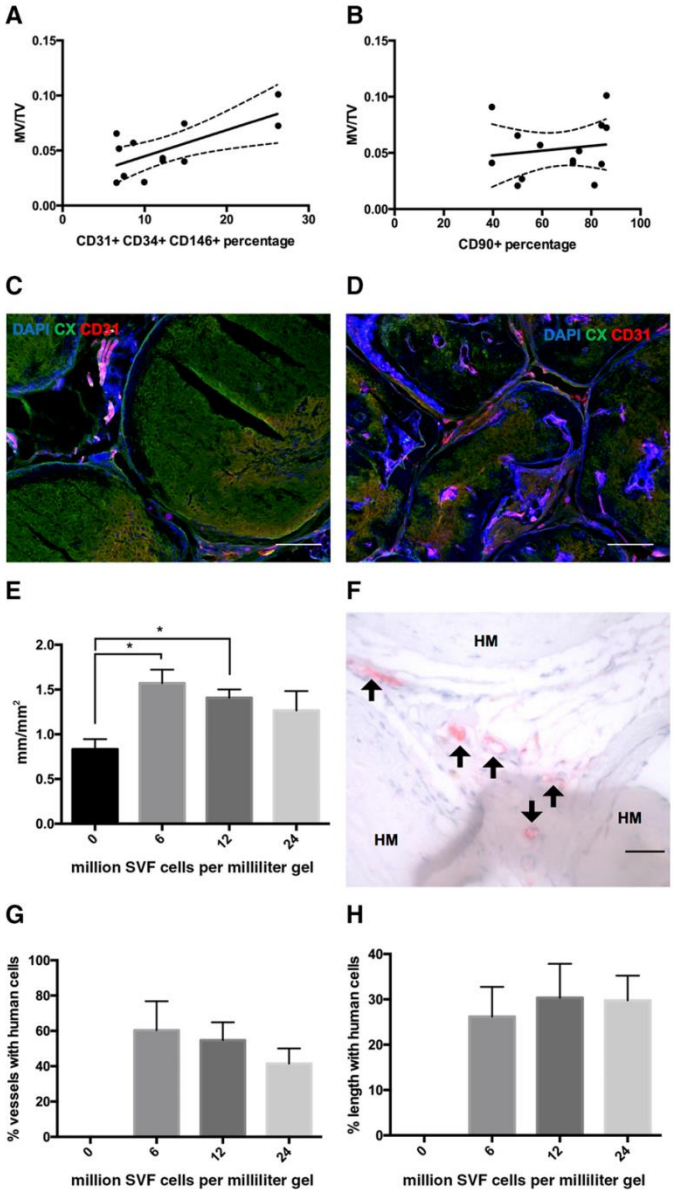

Figure 5. Contribution of stromal vascular fraction (SVF) cell lineages. Plots of mineralized tissue volume per total tissue volume versus the percentage of embedded CD31+ CD34+ CD146+ (R^2 = 0.4756, p = .013) **(A)** or CD90+ SVF cells (R^2 = 0.0226, p = .608) **(B)**. Dots represent single grafts. **(C, D):** Representative immunofluorescence staining for type X collagen, CD31, and 4′,6-diamidino-2-phenylindole of devitalized samples without **(C)** or with **(D)** SVF activation after 12 weeks in vivo. Scale bars = 200 μm. **(E):** Vessel length density calculated as total length of visible vessels per square millimeter of section (n = 5–6 grafts per group). *, $p < .05$, mean and standard error. **(F):** Immunohistochemistry and immunofluorescence staining for human CD34, identifying positive cells (arrows) between remnants of hypertrophic matrix. Scale bars = 50 μm. Percentage of vessels with human cells **(G)** and percentage of vessel length covered by human cells **(H)** (n = 5–6 grafts per group, mean and standard error). Abbreviations: CX, type X collagen; DAPI, 4′,6-diamidino-2-phenylindole; HM, hypertrophic matrix; MV, mineralized tissue volume; SVF, stromal vascular fraction; TV, total tissue volume.

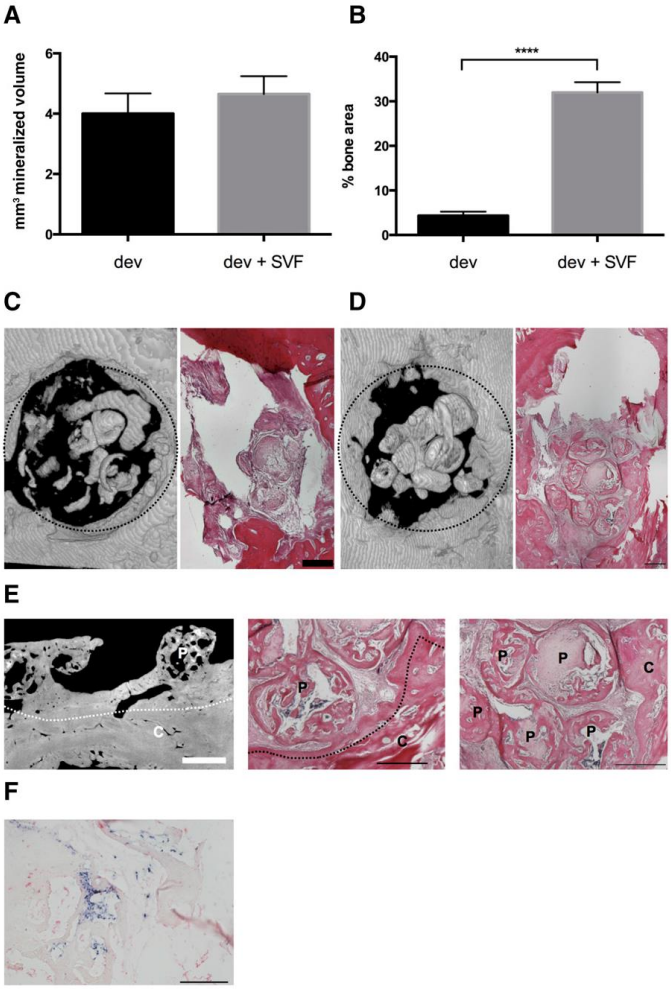

Figure 6. Bone repair capacity. Devitalized hypertrophic cartilage pellets were embedded in fibrin gel without or with stromal vascular fraction (SVF) cells from adipose tissue and implanted in rat calvarial defects. **(A):** Mineralized volume quantified by microtomography (n = 9 grafts assessed per group). **(B):** Bone area assessed in histological sections, expressed as percentage of total defect area (n = at least 24 sections assessed per group). ****, $p < .0001$. **(C, D):** Representative three-dimensional microtomography reconstructions (left) and hematoxylin/eosin (H&E) staining (right) of the calvarial defects filled with devitalized grafts, implanted without **(C)** or with **(D)** activation by SVF cells after 4 weeks. Dotted circles indicate the defect borders (4 mm diameter). Scale bars = 500 μm. **(E):** Microtomography (left) and H&E staining (middle and right) displaying the bridging between hypertrophic matrix and bone of the calvarium, or the fusion of single pellets (right) in activated grafts. White bar = 850 μm; black bars = 500 μm. Dotted lines indicate the edge of the calvarium. **(F):** In situ hybridization for *Arthrobacter luteus* sequences showing the presence of human cells (dark blue, positive) in the explants. Scale bar = 200 μm. Abbreviations: C, calvarium; dev, fibrin gel without stromal vascular fraction; dev + SVF, fibrin gel with stromal vascular fraction; P, hypertrophic matrix; SVF, stromal vascular fraction.

An increasing number of delivered SVF cells was associated with a higher density of chondroclasts/osteoclasts in the grafts. These cells were in part (5%–18% of the total) of human origin, thus derived from the monocytic population of the SVF and in part from the host, likely recruited thanks to the enhanced blood vessel invasion. A moderate increase in the density of osteoclasts from baseline values, achieved by the delivery of 12 million SVF cells per milliliter of gel, could have been pivotal at early stages in enhancing the efficiency of hypertrophic cartilage remodeling, leading to bone formation. In fact, osteoclasts would mediate release of cytokines and morphogens contained in the devitalized hypertrophic cartilage [11], in turn activating resident osteoprogenitor cells. On the other hand, a larger increase in the density of osteoclasts, corresponding to the delivery of 24 million SVF cells

per milliliter of gel, was associated with reduced bone formation. It is possible that excessive graft colonization by osteoclasts at early time points, as previously observed upon delivery of vascular endothelial growth factor [29], would disrupt bone homeostasis toward excessive degradation, ultimately resulting in more limited net amounts of bone matrix. In future studies, the timing and extent of osteoclast activity, both from the SVF donor and host, will need to be more thoroughly investigated.

Although SVF cells contain progenitors for osteoblasts, their direct contribution to the osteoid formation appeared marginal. The fact that SVF cell delivery strongly enhanced the total density of osteoblastic cells ultimately forming abundant bone matrix suggests their role in recruiting local osteoprogenitors from the host through the paracrine effect of trophic factors. An analog mode of action was recently proposed for Wharton jelly-derived mesenchymal progenitors, upon implantation in a calvarial defect [30]. Importantly, ectopic implantation of freshly harvested SVF cells in combination with calcium phosphate-based materials was previously reported to yield dense connective tissue but no bone formation [31], unless BMP-2 was additionally delivered [15]. These findings underline the strong regulatory/inductive role of the devitalized hypertrophic extracellular matrix in comparison with ceramic materials in the process of ossification. Cell populations derived from SVF culture, commonly referred to as adipose stromal cells (ASC), typically lose both endothelial and monocytic lineages and retain predominantly mesenchymal/osteoblast progenitors [19]. In light of the observed role of endothelial cells in our grafts and the almost complete absence of human osteoblasts, it will be relevant to test the hypothesis that ASC would not improve bone-forming efficiency unless a method for endothelial lineage cell preservation/expansion is used.

In our study, hypertrophic cartilage matrix was engineered, starting from bone marrow-derived MSC and subsequently devitalized. Gawlitta et al. previously proposed the use of decellularized xenogenic cartilage-derived matrix particles, also incorporated within a gel material in combination with MSC [32], and found that it induced no increase in bone tissue formation. The difference from our findings may be related to the use of articular as opposed to hypertrophic cartilage, whereby the former is phenotypically stable and developmentally not competent to support bone formation. The general approach of using engineered instead of native tissue as a source of devitalized extracellular matrix could be associated with additional advantages. In fact, an engineered matrix may be customized and enriched in defined factors (e.g., osteoinductive, angiogenic, or chemotactic cues) by using (a) specific culture medium supplements, (b) cells transduced to undergo apoptosis upon exposure to chemical agents, thereby achieving a devitalization with better preservation of the matrix [11] or (c) customized cells lines engineered to express larger amounts of the target factors [10]. Finally, it would be tempting to speculate that a devitalized extracellular matrix can be most effective in instructing formation of bone if it does not derive from the fully developed tissue but rather from the earlier stages of its development, as is the case for hypertrophic cartilage [33].

Conclusion

Our findings support a novel strategy for bone repair or augmentation, whereby allogeneic hypertrophic cartilage is engineered, devitalized, and then clinically used as an off-the-shelf material in combination with autologous SVF cells, intraoperatively derived from a lipoaspirate. Manufacturing of hypertrophic cartilage could take place within bioreactor systems, whereby biological processes could be monitored, controlled, automated, and standardized [34]. Toward clinical fruition, further studies are necessary in more relevant animal models, which should include the critical factors of immunocompetence and mechanical loading.

Acknowledgments

This work was supported by the Swiss National Science Foundation (SNF 310030_133110), the AO Foundation (AO S-11-13P), the Osteology Foundation (13-059), and the European Union (Eurostars E!7865 Endomatrix). P.E.B. is currently affiliated with the Department of Biosystems, Science, and Engineering, ETH Zurich, Basel, Switzerland.

Author Contributions

A.T. and M.K.: conception and design, collection and assembly of data, data analysis and interpretation, manuscript writing, final approval of manuscript; A.H. and P.E.B.: collection of data, data analysis and interpretation, final approval of manuscript; C.S.: conception and design, data analysis and interpretation, final approval of manuscript; A.B.: conception and design, data analysis and interpretation, manuscript writing, final approval of manuscript; A.S.: data analysis and interpretation, administrative support, provision of study material, final approval of manuscript; C.J.: data analysis and interpretation, administrative and financial support, overall supervision of animal experiments; I.M.: conception and design, data analysis and interpretation, administrative and financial support, manuscript writing, final approval of manuscript.

Disclosure of Potential Conflicts of Interest

The authors indicated no potential conflicts of interest.

References

1 Li P, Fang Q, Qi J et al. Risk factors for early and late donor-site morbidity after free fibula flap harvest. J Oral Maxillofac Surg 2015;73:1637–1640.

2 Kneser U, Schaefer DJ, Polykandriotis E et al. Tissue engineering of bone: The reconstructive surgeon's point of view. J Cell Mol Med 2006;10:7–19.

3 Grimshaw MJ, Mason RM. Bovine articular chondrocyte function in vitro depends upon oxygen tension. Osteoarthritis Cartilage 2000;8:386–392.

4 Scotti C, Piccinini E, Takizawa H et al. Engineering of a functional bone organ through endochondral ossification. Proc Natl Acad Sci USA 2013;110:3997–4002.

5 van der Stok J, Koolen MK, Jahr H et al. Chondrogenically differentiated mesenchymal stromal cell pellets stimulate endochondral bone regeneration in critical-sized bone defects. Eur Cell Mater 2014;27:137–148; discussion 148.

6 Kuhn LT, Liu Y, Boyd N Let al. Developmental-like bone regeneration by human embryonic stem cell-derived mesenchymal cells. Tissue Eng Part A 2014;20:365–377.

7 Bahney CS, Hu DP, Taylor AJ et al. Stem cell-derived endochondral cartilage stimulates bone healing by tissue transformation. J Bone Miner Res 2014;29:1269–1282.

8 Harada N, Watanabe Y, Sato K et al. Bone regeneration in a massive rat femur defect through endochondral ossification achieved

with chondrogenically differentiated MSCs in a degradable scaffold. Biomaterials 2014;35: 7800–7810.

9 Yang W, Yang F, Wang Y et al. In vivo bone generation via the endochondral pathway on three-dimensional electrospun fibers. Acta Biomater 2013;9:4505–4512.

10 Papadimitropoulos A, Scotti C, Bourgine P et al. Engineered decellularized matrices to instruct bone regeneration processes. Bone 2015; 70:66–72.

11 Bourgine PE, Scotti C, Pigeot S et al. Osteoinductivity of engineered cartilaginous templates devitalized by inducible apoptosis. Proc Natl Acad Sci USA 2014;111:17426–17431.

12 Kojima T, Hasegawa T, de Freitas PH et al. Histochemical aspects of the vascular invasion at the erosion zone of the epiphyseal cartilage in MMP-9-deficient mice. Biomed Res 2013; 34:119–128.

13 Lenas P, Moos M, Luyten FP. Developmental engineering: a new paradigm for the design and manufacturing of cell-based products: Part I. From three-dimensional cell growth to biomimetics of in vivo development. Tissue Eng Part B Rev 2009;15:381–394.

14 Riordan NH, Ichim TE, Min WP et al. Non-expanded adipose stromal vascular fraction cell therapy for multiple sclerosis. J Transl Med 2009;7:29.

15 Mehrkens A, Saxer F, Güven S et al. Intraoperative engineering of osteogenic grafts combining freshly harvested, human adipose-derived cells and physiological doses of bone morphogenetic protein-2. Eur Cell Mater 2012; 24:308–319.

16 Scotti C, Tonnarelli B, Papadimitropoulos A et al. Recapitulation of endochondral bone formation using human adult mesenchymal stem cells as a paradigm for developmental engineering. Proc Natl Acad Sci USA 2010;107: 7251–7256.

17 Mumme M, Scotti C, Papadimitropoulos A et al. Interleukin-1β modulates endochondral ossification by human adult bone marrow stromal cells. Eur Cell Mater 2012;24:224–236.

18 Güven S, Karagianni M, Schwalbe M et al. Validation of an automated procedure to isolate human adipose tissue-derived cells by using the Sepax® technology. Tissue Eng Part C Methods 2012;18:575–582.

19 Güven S, Mehrkens A, Saxer F et al. Engineering of large osteogenic grafts with rapid engraftment capacity using mesenchymal and endothelial progenitors from human adipose tissue. Biomaterials 2011;32:5801–5809.

20 Schneider CA, Rasband WS, Eliceiri KW. NIH image to ImageJ: 25 years of image analysis. Nat Methods 2012;9:671–675.

21 Doube M, Kłosowski MM, Arganda-Carreras I et al. BoneJ: Free and extensible bone image analysis in ImageJ. Bone 2010;47:1076–1079.

22 Sheets KG, Jun B, Zhou Y et al. Microglial ramification and redistribution concomitant with the attenuation of choroidal neovascularization by neuroprotectin D1. Mol Vis 2013;19: 1747–1759.

23 Papadimitropoulos A, Scherberich A, Güven S et al. A 3D in vitro bone organ model using human progenitor cells. Eur Cell Mater 2011;21:445–458; discussion 458.

24 Martin I, Mastrogiacomo M, De Leo G et al. Fluorescence microscopy imaging of bone for automated histomorphometry. Tissue Eng 2002;8:847–852.

25 Ingram DA, Mead LE, Tanaka H et al. Identification of a novel hierarchy of endothelial progenitor cells using human peripheral and umbilical cord blood. Blood 2004;104: 2752–2760.

26 Rohde E, Bartmann C, Schallmoser K et al. Immune cells mimic the morphology of endothelial progenitor colonies in vitro. STEM CELLS 2007;25:1746–1752.

27 Yoder MC, Mead LE, Prater D et al. Redefining endothelial progenitor cells via clonal analysis and hematopoietic stem/progenitor cell principals. Blood 2007;109:1801–1809.

28 Klar AS, Güven S, Biedermann T et al. Tissue-engineered dermo-epidermal skin grafts prevascularized with adipose-derived cells. Biomaterials 2014;35:5065–5078.

29 Helmrich U, Di Maggio N, Güven S et al. Osteogenic graft vascularization and bone resorption by VEGF-expressing human mesenchymal progenitors. Biomaterials 2013;34: 5025–5035.

30 Todeschi MR, El Backly R, Capelli C et al. Transplanted umbilical cord mesenchymal stem cells modify the in vivo microenvironment enhancing angiogenesis and leading to bone regeneration. Stem Cells Dev 2015;24: 1570–1581.

31 Müller AM, Mehrkens A, Schäfer DJ et al. Towards an intraoperative engineering of osteogenic and vasculogenic grafts from the stromal vascular fraction of human adipose tissue. Eur Cell Mater 2010;19: 127–135.

32 Gawlitta D, Benders KE, Visser J et al. Decellularized cartilage-derived matrix as substrate for endochondral bone regeneration. Tissue Eng Part A 2015;21:694–703.

33 Martin I. Engineered tissues as customized organ germs. Tissue Eng Part A 2014;20: 1132–1133.

34 Martin I, Baldomero H, Bocelli-Tyndall C et al. The survey on cellular and engineered tissue therapies in Europe in 2011. Tissue Eng Part A 2014;20:842–853.

Chapter V:

Prefabrication of vascularized bone grafts

Prefabrication of a large pedicled bone graft by engineering the germ for de novo vascularization and osteoinduction.

Haumer A & Epple C, Ismail T, Lunger A, Scherberich A, Schaefer DJ, Martin I

Abstract

Large and complex bone defects represent challenging clinical scenarios. Autologous vascularized bone is typically used for reconstruction, but entails bottlenecks such as limited availability, donor site morbidity and restricted ability to be shaped into the desired form. Here, we thus aimed at ectopically prefabricating a pedicled bone graft surrogate.

A form-stable outer shell of devitalized bone was used to define a space which was filled with bone-inducing engineered hypertrophic cartilage, in the form of vital or devitalized pellets, in combination or not with progenitor cells from the stromal vascular fraction (SVF) of adipose tissue. Vascularization of the space was targeted through axial insertion of an arterio-venous (AV) bundle. Constructs were subcutaneously implanted in nude rats and assessed after 12 weeks for bone formation and vascularization, using histological and microtomography imaging techniques.

Retrieved constructs were efficiently vascularized in all conditions, with vessels sprouting from the AV bundle and reaching a higher density and larger diameter in the axially central volume. Bone tissue was formed through remodeling of hypertrophic cartilage (60%-75% of the implanted pellets), with no significant difference among experimental groups but in tight correlation with de novo vascularization.

Our study demonstrates feasibility to prefabricate large, pedicled, form-stable bone grafts. The combination of an AV bundle with engineered hypertrophic cartilage provided a *germ* for the coupled processes of vascularization and bone formation. The demonstrated osteoinductive properties of devitalized hypertrophic cartilage offer the opportunity of implementing the proposed regenerative surgery strategy through off-the-shelf materials.

Introduction

Large and complex bone defects represent challenging clinical scenarios. As diverse the pathogenesis and resulting clinical need is, so are its treatment strategies. The most effective standard of treatment for complex bone defects, for example in the maxillo-facial region, relies on the use of autologous vascularized bone grafts (e.g., pedicled fibula). This is associated with several bottlenecks, such as limited availability and significant donor site morbidity. Furthermore, shaping of complex, three-dimensional structures with available autologous bone can be cosmetically and functionally insufficient with restrained functional rehabilitation. An engineered osteogenic material, combined with a vascular bundle would represent an attractive alternative to develop a pedicled bone graft surrogate. In this regard arteriovenous fistulas have proved to be efficient in neovascularization of tissues for the past 40 years and it has been demonstrated that the performance of arteriovenous (AV) bundles is superior to AV-loops in terms of tissue remodeling and regeneration, entailing less complications [1–5].

In a recently established rat model, we demonstrated that stromal vascular fraction (SVF) cell-seeded hydroxyapatite scaffold, combined with a vascular AV bundle, efficiently vascularized necrotic bone and formed bone tissue de novo by direct ossification [6]. However, the procedure required culturing of the SVF cells in osteogenic medium for 5 days prior to implantation and newly formed bone ossicles were found in limited amounts and restricted regions.

In the past, recapitulating the endochondral route of ossification has proved to be a robust strategy for bone formation in ectopic models as well as in orthotopic non-union models [7–11]. The endochondral route of ossification can be recapitulated by generation of hypertrophic cartilage templates in vitro which embed the biological signals for the remodeling into a complete bone organ when implanted in vivo. Recently, we demonstrated that these hypertrophic cartilage templates can form bone ectopically and orthotopically after devitalization and ‘reactivation’ by stromal vascular (SVF) fraction cells [12]. Using multiple small modules - engineered & devitalized hypertrophic cartilage chips - would allow for reconstruction of complex, three-dimensional defects.

The aim of this study was to prefabricate an engineered, vascularized, pedicled bone graft substitute in an in vivo rodent model. The concept is based on following three pillars: a form-stable outer shelf consisting of devitalized cancellous bone (Tutobone©), which is shapeable to specific needs and an inner core of hypertrophic cartilage, able to undergo bone formation in vivo. An AV bundle was axially implemented to provide a strong and reliable vascularization of the graft, as well as the pedicle for anastomosis to the recipient site.

Methods

Micromass culture and devitalization

Human bone marrow derived stromal cells (hBMSCs) from three donors (all male, 33.3 ± 11.7 years) were expanded as monolayers for two to four passages as previously described [13]. hBMSCs were detached and distributed in 1.5 ml screw cap Eppendorf tubes with $0.5x10^3$ cells per tube and centrifuged at 300g for 5 minutes. The resulting micromass pellets were then cultured in serum-free medium (Dulbecco's modified Eagle's medium, 1.25 mg/ml human serum albumin, 10 mM HEPES, 1 mM sodium pyruvate, 100 U/ml penicillin, 100 mg/ml streptomycin, 0.29 mg/ml glutamate, and ITS-A [10 mg/ml insulin, 5.5 mg/ml transferrin, 5 ng/ml selenium, 0.5 mg/ml bovine serum albumin]; all from Invitrogen), supplemented with 10 ng/ml transforming growth factor-b3 (R&DSystems), 10^{-7} M dexamethasone, and 0.1 mM ascorbic acid 2-phosphate (Sigma-Aldrich, St. Louis, MO, USA, https://www.sigmaaldrich.com) (chondrogenic medium). After 3 weeks of chondrogenic differentiation the resulting cartilaginous pellets were further cultured in hypertrophic medium (serum-free medium with 50 nM thyroxine, 10 mM b-glycerophosphate, 10^{-8} M dexamethasone, 0.1 mM ascorbic acid 2-phosphate, (Sigma-Aldrich) for 2 weeks as previously described with medium changes twice weekly [12]. A part of the resulting pellets were devitalized by three cycles of freezing (-196°C for 10 minutes) and thawing (37°C for 10 minutes) and a final wash with deionized water. All fluids were removed and pellets stored at -80°C until further use (devitalized pellets conditions).

SVF isolation

SVF cells were isolated from two liposuction and one excision fat samples from 3 donors (28.3 ± 3.7 years, two females and one male). The fractionated adipose tissue was incubated with 0.15% collagenase type 2 solution (Worhtington-Biochem.com, Ref: LS004176, 345 u/mg dw) for 60 minutes, centrifuged at 300g for 10 minutes and the supernatants discarded. Cells were washed with complete medium to deactivate the collagenase, filtered through a sterilized tea strainer and a 100 µm mesh filter to remove undissolved tissue debris, and finally counted in a Neubauer counting chamber using crystal violet. The isolated SVF cells were then frozen in medium consisting of fetal bovine serum and 10% dimethyl sulfoxide and kept in the gaseous phase of liquid nitrogen until construct manufacturing.

Grafts manufacturing

The constructs were generated as described in Fig 1 A. Fibrinogen (Fibrinkleber SD TIM3, VNK4J002) and thrombin (SD TIM5 500 IE/ml, VNF4H023, both Baxter AG) were separately dissolved in sterile water, 40 mM of calcium chloride dihydrate (Fluka, now Sigma-Aldrich Ref. 21102) added to the thrombin and both solutions frozen at -20°C for later use. 40 hypertrophic cartilage pellets were resuspended in 600 µL of fibrin gel (1:2 thrombin:fibrinogen). For the devitalized group with SVF cells, $12x10^6$ SVF cells were added to each construct. The constructs were inserted in a hollow cylinder of processed bovine cancellous bone (Tutobone, Tutogen Medical, Neunkirchen, Germany), provided with a 1.5 mm drill hole at the base to allow later insertion of the arteriovenous bundle. The whole graft was wrapped in semipermeable anorganic-based silicone membrane to prevent ingrowth of host cells from the outside (Biobrane, UDL Laboratories Inc., Rockford, IL, USA) [14] . An 18G peripheral venous catheter with needle (B. Braun Melsungen AG, Melsungen, Germany) was then used to pierce through the packed construct to allow for an easy introduction of the vascular bundle into the construct [6].

Implantation

For in vivo implantation, 18 young athymic nude rats (RH-Foxn1rnu, Envigo, Venray, The Netherlands) were operated with permission of the Federal Veterinary Office (permit BS 2598). Animals were held in groups of three with unrestricted access to food and water. Before surgery, 0.05 mg/kg buprenorphine (Temgesic, Reckitt Benckiser, Wallisellen, Switzerland) was injected subcutaneously for analgesia. Then inhalation anesthesia was induced and maintained with 1.5-3 % Isofluran (Baxter, Volketswil, Switzerland) in 1 l/min oxygen. The rats were placed in a supine position on an electrically heated mat, the operation area disinfected and a sterile operating field established. An incision of approximately 15 mm was made along the left groin and the superficial inferior epigastric artery and vein dissected free with help of an operation microscope, making sure to leave a small amount of connective tissue in place around the bundle. After distal ligation and transection of the bundle, the ligature thread was used to gently pull the vascular bundle through the prepared construct, using the peripheral venous catheter as a guide and removing it in the process. A subcutaneous pouch was then created by blunt dissection and the pedicled construct inserted carefully. The wound was then closed by layered subdermal and intradermal suturing with absorbable material (5-0 Monocryl, Ethicon, US) and the animal returned to the cage, closely monitored and treated with analgesia according to the veterinary study guidelines.

Construct harvesting

After 12 weeks, deep anesthesia of the animals was induced by intraperitoneal injection of mg/kg ketamine (Ketasol 100, Dr. E. Graeub AG, Switzerland) and 10 mg/kg xylazine (Xylasol, Dr. E. Graeub AG). Additionally an inhalation anesthesia with 1.5.-3 % Isoflurane in 1 l/min oxygen was used. The animals were again placed in a supine position and through a median laparotomy the abdominal aorta was exposed and dissected free from the inferior vena cava. The aorta was then cannulated with a 23G butterfly cannula (BD, Heidelberg, Germany) and a heparinized saline solution (100 IU/ml, 0.9 % NaCl, B. Braun AG, Switzerland), followed by a dark-blue contrasting agent (5% w/v Gelatine-Gold, Carl Roth GmbH, Karlsruhe, Germany; 50% v/v Indian Ink, Lefranc & Bourgeois, Le Mans, France; 4% w/v D-Mannitol, Carl Roth

GmbH; distilled water) was injected until the skin of the lower extremities turned black, followed by immediate euthanasia of the rat by exsanguination. The cadavers were refrigerated at 4°C overnight to allow for polymerization of the contrast agent-containing gelatin. The constructs were then cautiously dissected free from the surrounding tissue, the state of the vascular bundle macroscopically assessed and the constructs including the bundle transferred to a solution of 1% PFA in distilled water for 24 hours, followed by immersion in PBS and preparation for microtomography.

Histology

All histological samples were embedded in paraffin using a TES Valida embedding station and sectioned using a Microm HM 340E Microtome.

To check for successful differentiation into hypertrophic cartilage of the expanded hBMSCs, 6 randomly picked pellets were processed histologically and stained with Safranin-O (Sigma Ref. 84120), fast green FCF (Sigma Ref. F-7252) and immunohistochemically stained with collagen II (Abcam ab49945) and collagen X (Abcam ab185430) antibodies. For immunological stainings, a goat anti-mouse IgG/ Biotin antibody (Dako E 0433) was used as a secondary antibody and the staining developed with the Vectastain ABC / AP Kit (Linaris AK-5000) and Vector Red AP Substrate kit 1 + Levamisole (Linaris SK-5100) and then counterstained with hematoxylin.

After tomography, constructs were sectioned into a proximal and distal half, processed, embedded in paraffin and sections cut with 5-10 µm slice thickness. To achieve a close histological representation of the constructs, slides were made on three levels per half construct to cover 290 µm per level and 670 µm in total. Hematoxylin-eosin (HE Papanicolaou J.T.BAKER, Eosin 2% + Erythrosin B 1%; from Biosystems: Hematoxylin 38-7025-00/38-73, Eosin 84-0012-00 Erythrosin 84-0013-00) and Masson's trichrome staining (Réactifs RAL, Martillac, France) were performed to assess tissue morphology, bone formation and maturation. ALU-sequence staining (Zytovision GmbH, Bremerhaven, Germany) for cells of human origin and immunohistochemistry for human CD34+ endothelial cells (Millipore CBL

496 from DAKO) were performed to investigate their presence and contribution in SVF-seeded constructs [6].

Image acquisition

Single images for illustration purposes were taken with Olympus BX61, BX63 and IX83 microscopes. Serial pictures for quantification were taken with a Nikon up right Ni, connected to a Prior robot and with 4x and 10x objectives.

Quantification

Images were analyzed with Olympus cellSens Dimension 1.15 (Build 14760) and Nikon NIS-Elements AR 4.51 (build 1143) software. For vessel quantification, structures were counted on pictures taken with 10x magnification. Vessels were defined by endothelial cell lining, a well-defined lumen and the presence of either red blood cells or contrasting agent (Indian ink) inside the lumen. Counting was done by two independent observers in blinded samples. Bony regions were identified by the presence of densely organized, homogenous, cell-poor areas with or without bone marrow. These regions, total pellet area and the inside area of the Tutobone cylinder were selected manually and the area provided by the imaging software. Percentages of remodeled area to total pellet area and of pellet area to total construct area were calculated to account for the distribution of the pellets in the constructs.

Microtomography

For microtomography, constructs were placed in a 10-ml syringe barrel containing 1 ml of HistoGel (HG-4000-012, Thermo Fisher Scientific, 168 Third Avenue, Waltham, MA USA 02451) to conserve and stabilize the sample during transport and scanning. All samples were scanned twice: first without any contrast agent (for imaging of mineralization/bone) and a second time after decalcification with a 15% w/v EDTA (Sigma-Aldrich) solution in distilled water at 37°C for one week and consecutive radio-dense contrasting of the vessels with 5% w/v phosphotungstic acid (Sigma-Aldrich) in distilled water at room temperature for 24 hours, to image the vascular bed, as previously described [15]. All samples were scanned at 360° using a tungsten x-ray source with a voltage of 70kV and a current of 260 µA (Nanotom M,

GE, USA). To reduce beam hardening artifacts, a 0.5 mm aluminum filter was applied. Volumes were reconstructed with 8.5-12 µm voxel size using the manufacturer's software and analyzed with VGStudio Max version 2.2 (Volume Graphics, Heidelberg, Germany).

Bone/ mineralization assessment

Total mineralization of the implanted construct was assessed by creating a cylindrical region of interest (ROI) of the Tutobone's inside and using VGStudio Max Volume analysis tool. Gray values thresholds were chosen with help of the histogram and visual control to eliminate all non-dense material and background signal. Voxels of the selected gray values were counted by the software and corresponding volumes automatically calculated, giving the total mineralized volume of the constructs. Absolute bone volume was quantified by matching the µCT data on mineralized tissue with histologically-proven bone tissue. The number and volume of all pellets was counted and measured manually by creating ROIs for each pellet. The morphology of the pellets was assessed for the presence of bone-like structures like vascular ingrowth perforation of the mineralized shell, trabeculae inside the pellets, fused pellets and round shaped osteoid deposits, and compared with corresponding histological sections. Number and volumes of pellets with signs of remodeling into bone were measured.

Vascularization assessment

Vascularization was assessed in reconstructed volumes of PTA-stained constructs with a focus on characterizing the AV-bundle and its branching vessels. The AV-bundle and branching vessels were identified by radiodensity, and the diameters and numbers measured or counted on transversal planes. Measurement of the largest vessel was performed on short and long axes on three levels: the proximal entry point of the bundle into the Tutobone, in the middle and at the distal end of the Tutobone just over the drill hole. Furthermore, the shortest and longest distance between remodeled pellets and the central vessel were measured. By superimposing µCT-datasets taken with and without phosphotungstic acid, it was possible to subtract the signal of the radio-dense pellets from the 3D-reconstruction to visualize selectively the PTA stained structures.

Statistical analysis

All statistical analyses were performed using GraphPad Prism software (GraphPad Software, Inc., California, USA). Kruscal-Wallis test, Dunn's multiple comparisons test and Spearman's rank correlation coefficient were performed considering a p-value of <0.05 significant. Results are reported as mean ± standard deviation unless otherwise indicated.

Results

Successful in vitro cartilaginous differentiation and hypertrophy of the hBMSC micromass pellets was demonstrated by high glycosaminoglycan content (red in Saf-O staining) and positive immunohistochemical stainings for collagen II and X (Fig. 1 B). Vital and devitalized (with and without SVF) pellets were then inserted in the cancellous bone cylinder together with an AV bundle and implanted in nude rats (Fig. 1 A). All 18 implanted constructs (6 constructs containing vital pellets without SVF cells, 6 constructs containing devitalized pellets without SVF cells and 6 constructs containing devitalized pellets with SVF cells) were explanted after 12 weeks in vivo. A visual inspection revealed signs of thrombosis in AV-bundles of four constructs (2 vital, 1 devitalized and 1 devitalized + SVF). These constructs showed signs of limited engraftment with fibrotic tissue and marked inflammatory response. Due to the surgery-related technical failure, these 4 constructs were excluded from the study and not further analyzed.

Bone assessment and quantification

Bone tissue was formed in 3 out of the 4 constructs containing vital pellets and in 3 out of the 5 constructs containing devitalized pellets, both in the presence and in absence of SVF cells (Fig. 2 A). H&E-stained sections demonstrated, beyond a dense collagen matrix, fused pellets and formation of bone marrow elements, indicating the maturation into trabecular bone (Fig. 2 A). µCT imaging confirmed fusion of the pellets and voids in the mineralized structures, indicating ingrowing vessels, and osteoid tissue vascularization (Fig. 3 B). Bone tissue formation was not homogenous all over the implanted constructs, but only took place at a radial distance of 0.2-2.2 mm from the central vessel (on a maximal potential radius of 5 mm, Supp.

Fig. 1). In all construct types, bone formation was rather variable along the longitudinal axis, with a tendency for higher amounts of bone in the proximal half of the construct (Supp. Fig. 2).

Quantification of the percentage of the average pellet area remodeled into bone tissue by histological morphometry revealed a stronger level of bone formation in constructs containing vital hypertrophic pellets (17.2 ± 9.7 %; Fig. 2 B) than in constructs containing devitalized pellets (2.8 ± 4.3 %) or devitalized pellets with SVF cells (1.5 ± 2.4 %). However, given the high variability of bone formation within the experimental groups (e.g. varying from 0 - 43 % in the vital pellets' group) and the limited number of analyzed replicates, the difference in terms of bone formation was not statistically significant among the groups. All three conditions exhibited the same density of infiltrating $CD68^+$ macrophages (Supp. Fig. 3). $CD68^+/CD163^+$, M2-like macrophages were significantly more frequent in the vital constructs, representing 40% of all macrophages. In constructs with devitalized pellets, M2-like macrophages were more abundant when SVF cells were added (29%), while only 6% of the invading macrophages were polarized towards an M2 phenotype when only devitalized pellets were implanted.

Total mineralized volume was quantified by µCT. Thresholding for densities corresponding to mineralization, eliminating the signal due to soft tissue and background, was possible on the gray value histogram by visually controlling the selected voxels (Supp. Fig. 4). Mineralization was not different among the three groups (12.8 ± 3.2 mm^3, 11.8 ± 2.4 mm^3 and 14.5 ± 3.8 mm^3; Fig. 3 A). Bone volume, calculated by adjusting the imaging threshold to the histologically proven bone, was maximal in the control group with 5.1 ± 2.2 mm^3, whereas the devitalized pellets only generated 1.2 ± 0.7 mm^3 of bone tissue and the devitalized pellets + SVF 1.4 ± 0.7 mm^3 (Fig. 3 C). However, differences were not statistically significant. The average pellet volume transformed into bone was also evaluated by µCT and was consistent with histomorphometry data, with 24.6 ± 11.7 % in the vital group, 3.9 ± 2.7 % in the devitalized group and 6.1 ± 3.4 % in the devitalized + SVF group, but again with no significant difference among the groups (Fig. 3 D). Staining for human ALU-sequences evidenced the presence of human cells inside the pellets (Supp. Fig. 5) after 12 weeks in vivo, documenting the survival

of a fraction of the implanted SVF cells, with a possible contribution in cartilage matrix remodeling and bone formation.

Vascularization analysis

We then assessed the vascularization inside the bone grafts after 12 weeks in vivo implantation time. Phosphotungstic acid-contrast enhanced µCT showed that in all constructs included for analysis, the graft was fully vascularized with small and intermediate sized vessels arising from the central arteriovenous bundle, spreading towards the surrounding devitalized bone (Fig. 4 A). Histological analysis confirmed the high level of vascularization in every experimental condition, as documented by the uniform distribution of vascular lumens filled by Indian ink (black arrows in Fig. 4 B) around the vascular bundle and in vicinity of the devitalized pellets. The radial distribution of vessels showed a statistically significant difference in all groups between the central (0-2.5 mm) and the peripheral (2.5-5 mm) half of the construct. In particular, the central part close to the main bundle was better vascularized with an up to 5-fold higher vessel density than the peripheral part (Supp. Fig. 6).

Quantification of vessels' diameter showed no significant difference between the experimental groups, although the mean diameter of central vessels in the constructs containing living pellets was in average twice larger (468 ± 111 µm) than in the devitalized (243 ± 68 µm) or devitalized pellets + SVF (190 ± 70 µm) groups (Fig. 4 C). The number of vessels branching from the central bundle also did not statistically differ among groups (Fig. 4 D).

Correlation of vascularization and bone formation

Despite no statistical difference could be evidenced among the groups in either diameter of central vessel or density of vascular network, a correlation could be established between vascularization and bone formation. The size of the central vessel diameter was positively correlated to an increased bone formation, with a linear correlation of r2=0.74 (Fig. 5 A). An even higher positive linear correlation of r2=0.77 could be demonstrated between the vascular density and the newly formed bone volume (Fig. 5 B).

Discussion

This study demonstrates that by combining engineered hypertrophic cartilage with an AV bundle within a form-stable outer shell it is possible to prefabricate a vascularized bone graft with an inherent germ of osteoinduction and vascularization. The vessels sprouting from the AV bundle strongly influenced the bone forming capacity, underlined by the fact that in the peripheral areas where vascularization decreased, bone formation was not observed.

The implementation of an axial AV bundle gave a thorough vascularization of the entire construct, indispensable for large bone grafts [16–18]. Also, the pedicle of this prefabricated bone graft surrogate offers the advantage that once anastomosed to the recipient vessels, it is entirely perfused through the already existing vascular network. In clinical translation of large tissue engineered bone grafts this has been a major limiting factor [19]. The high vessel density in the area surrounding the central AV bundle, together with the high number of branches arising from the main trunk, indicate an efficient vascularization process. In mature individuals, luminal vessel sprouting is believed to be the major process during angiogenesis and in AV bundles it typically occurs from the central vein [5,20]. The process underlying angiogenic luminal sprouting begins with promoting factors urging detachment of pericytes and endothelial cells [21]. The initial hypoxic and inflammatory environment within our constructs, as well as VEGF present in the hypertrophic cartilage, are strong promoters for the detached, reactive endothelial cells. Proteases further liberate proangiogenic factors from the ECM such as VEGF and FGF and endothelial sprouting is initiated by migrating and proliferating endothelial cells [22]. To avoid aberrant, random endothelial cell migration and ensure the generation of a functional neo-lumen, one endothelial cell is selected to become a tip cell by factors such as VEGF receptors, neuropilins (NRPs) and the NOTCH ligands DLL4 and JAGGED1 [23]. Endothelial cells in the vicinity of the tip cell are stimulated by NOTCH, Notch-regulated ankyrin repeat protein (NRARP), WNTs, placental growth factor (PlGF) and FGFs, to become elongated stalk cells and finally form the lumen, mediated by VE-cadherin, CD34, sialomucins, VEGF and hedgehog [24]. In our study, we could observe a limit in efficiency of vascularization at a radial distance of 2.5 mm from the AV bundle. The vessel density in the peripheral area

beyond this point was significantly lower than in the central part. A possible explanation for this decrease in vascularization could lie in the nature of tip cells. These cells are equipped with filopodia which sense environmental cues to guide them, such as ephrins and semaphorins [25]. In absence of these factors in the peripheral zone of our construct, tip cells become quiescent and stabilize. Ones stabilized, endothelial cells are covered by pericytes and a basal membrane is deposited, marking the end of the sprouting process.

Besides a solid vascularization, we generated a germ of bone formation within our constructs by using engineered hypertrophic cartilage. It has been shown that cartilaginous tissues engineered from hBMSC can act as a template for bone formation derived from the synergy of donor and host cells in both ectopic and orthotopic animal models [7,10]. Moreover, freeze and thaw (F&T) devitalized hypertrophic cartilage pellets were so far shown to undergo endochondral ossification upon in vivo implantation if reactivated by addition of SVF cells [12]. In order for devitalized cartilaginous tissue to undergo ossification in vivo without the addition of external cells, it was reported that a devitalization method able to maintain important biological cues in the ECM is required [26]. It is noteworthy that in our constructs, hypertrophic cartilage pellets devitalized by F&T and thus with compromised composition of the ECM were still able to form bone, in a quantity which was not statistically significant inferior as compared to the vital ones. A possible explanation for this finding lies in the privileged environment created by the AV bundle. The surrounding tissue transplanted together with vessels, where capillaries and fibroblasts proliferate, may provide osteoclasts and osteoblasts which resorb avital bone and at the same time stimulate bone formation and bone remodeling.

Often, this tissue remodeling is associated with specifically increased immunological cell subtypes, such as alternatively activated (pro-regenerative/M2-like) macrophages [27]. However, we could not observe any correlation between M2 polarization of invading macrophages and new bone formation. As previously observed, transplanted SVF cells are able to induce an M2 phenotype in macrophages [6]. In the constructs containing devitalized pellets they could revert absence of M2 macrophages, however this phenotype switch did not entail increased bone formation. This emphasizes the fact that to enhance a regenerative

process in bone tissue engineering a precise understanding of the role and dynamics of immunological cell populations is necessary [28,29] and the specific role of macrophagic populations, with phenotypes hardly categorized in artificial classes, is still elusive.

In our generated bone graft, the functional AV bundle was sufficient to lead to bony remodeling of the implanted pellets, since addition of SVF cells could not enhance the bone quantity. In fact, what emerged to have the strongest influence on the bone forming capacity was vascularization of the construct. Central vessel diameter and vessel density tightly correlated to bone formation. This finding is consistent with the knowledge that increased vascularization of a tissue can increase its regenerative capacity, since vascularization is a “critical obstacle in engineering metabolically active tissues”, [30]. Not only does vascularization enhance regenerative capacity, it also plays a major role in bony transformation of a cartilaginous template. Two mechanisms are mainly responsible for this: Oxygen tension plays an important role in regulating chondrocyte behavior and regulates its hypertrophy and transformation into bone. The mostly avascular cartilage thrives under hypoxic conditions, while in the ossification front of developing bone, invading blood vessels increase the oxygen tension driving the equilibrium towards bone formation [31]. Secondly, vessels play an indirect role in the remodeling of the cartilaginous matrix to bone. Attracted by VEGF secreted from the hypertrophic chondrocytes, the invading vessels provide chondroclasts for the degradation of cartilage as well as osteoblasts and osteoclasts, responsible for the deposition and remodeling of true bone matrix [32].

The here gained knowledge could inspire possible improvement to extend bone formation beyond the central zone. The observed decrease of vascularization, and thus vanishing of bone formation, could be explained by the high content of fibrin gel present. It is known that a material’s properties strongly influences the vascularization [33]. For example, pore structure and size of the hydroxyapatite scaffold used in Ismail et al.’s work was shown to be permissive for guided vascularization [6]. In fact, with the same axial AV bundle technique, bone formation was observed up to 4.5 mm. Thus, to increase vessel density beyond 2.5 mm from the central AV bundle, one could either increase the ratio of scaffolding material, i.e. pellet volume

(decreasing the amount of fibrin), or stimulate vessel formation by a growth factor-enhanced environment. Increasing the cartilage pellets number, which in our study was limited to 40 per construct, could enhance both vascular guidance and bone forming foci. In this regard, switching to a different in vitro culture method could provide the solution. It was demonstrated that hBMSC can undergo endochondral ossification when seeded on type I collagen sponges of variable sizes [13,35]. Seeding hBMSC on collagen sponges would allow generating larger pellets and thus facilitating production of large quantities of matrix, which would be then devitalized as possibly used as off-the-shelf filler material.

Conclusion

In this study we showed that an axially implemented central arteriovenous bundle plays a key role in the bone formation capacity of engineered hypertrophic cartilage. In challenging clinical scenarios, e.g. in the maxillo-facial region, the complexity of the defects often limit conventional reconstruction with autologous tissue. For these cases, our proposed approach could provide an alternative bone graft surrogate as a prefabricated, pedicled, large bone graft with a form-stable, outer shell and an inner core containing a germ for bone and vascularization. While this inner core represents the biological backbone allowing physiological behavior of the graft, the outer shell can be adapted to the defect by 3D CAD-CAM techniques and thus fit the defect site exactly in size and shape.

References

[1] A. Haumer, T. Ismail, A. Lunger, R. Osinga, A. Scherberich, D.J. Schaefer, I. Martin, From Autologous Flaps to Engineered Vascularized Grafts for Bone Regeneration, in: W. Holnthoner, A. Banfi, J. Kirkpatrick, H. Redl (Eds.), Vasc. Tissue Eng. Regen. Med., Springer International Publishing, Cham, 2017: pp. 1–34. doi:10.1007/978-3-319-21056-8_16-1.

[2] S. Akita, N. Tamai, A. Myoui, M. Nishikawa, T. Kaito, K. Takaoka, H. Yoshikawa, Capillary Vessel Network Integration by Inserting a Vascular Pedicle Enhances Bone Formation in Tissue-Engineered Bone Using Interconnected Porous Hydroxyapatite Ceramics, Tissue Eng. 10 (2004) 789–795. doi:10.1089/1076327041348338.

[3] O.O. Erol, M. Sira, New capillary bed formation with a surgically constructed arteriovenous fistula., Plast. Reconstr. Surg. 66 (1980) 109–15. doi:10.1097/00006534-198208000-00093.

[4] O. Kloeters, I. Berger, H. Ryssel, K. Megerle, U. Leimer, G. Germann, Revitalization of

cortical bone allograft by application of vascularized scaffolds seeded with osteogenic induced adipose tissue derived stem cells in a rabbit model., Arch. Orthop. Trauma Surg. 131 (2011) 1459–1466. doi:10.1007/s00402-011-1306-5.

[5] Y. Tanaka, K.-C. Sung, A. Tsutsumi, S. Ohba, K. Ueda, W. a Morrison, Tissue engineering skin flaps: which vascular carrier, arteriovenous shunt loop or arteriovenous bundle, has more potential for angiogenesis and tissue generation?, Plast. Reconstr. Surg. 112 (2003) 1636–44. doi:10.1097/01.PRS.0000086140.49022.AB.

[6] T. Ismail, R. Osinga, A.J. Todorov, A. Haumer, L.A. Tchang, C. Epple, N. Allafi, N. Menzi, R.D. Largo, A. Kaempfen, I. Martin, D.J. Schaefer, A. Scherberich, Engineered, axially-vascularized osteogenic grafts from human adipose-derived cells to treat avascular necrosis of bone in a rat model., Acta Biomater. (2017). doi:10.1016/j.actbio.2017.09.003.

[7] C.S. Bahney, D.P. Hu, A.J. Taylor, F. Ferro, H.M. Britz, B. Hallgrimsson, B. Johnstone, T. Miclau, R.S. Marcucio, Stem cell-derived endochondral cartilage stimulates bone healing by tissue transformation, J. Bone Miner. Res. 29 (2014) 1269–1282. doi:10.1002/jbmr.2148.

[8] N. Harada, Y. Watanabe, K. Sato, S. Abe, K. Yamanaka, Y. Sakai, T. Kaneko, T. Matsushita, Bone regeneration in a massive rat femur defect through endochondral ossification achieved with chondrogenically differentiated MSCs in a degradable scaffold, Biomaterials. 35 (2014) 7800–7810. doi:10.1016/j.biomaterials.2014.05.052.

[9] L.T. Kuhn, Y. Liu, N.L. Boyd, J.E. Dennis, X. Jiang, X. Xin, L.F. Charles, L. Wang, H.L. Aguila, D.W. Rowe, A.C. Lichtler, A.J. Goldberg, Developmental-like bone regeneration by human embryonic stem cell-derived mesenchymal cells., Tissue Eng. Part A. 20 (2014) 365–77. doi:10.1089/ten.TEA.2013.0321.

[10] J. van der Stok, M.K.E. Koolen, H. Jahr, N. Kops, J.H. Waarsing, H. Weinans, O.P. van der Jagt, Chondrogenically differentiated mesenchymal stromal cell pellets stimulate endochondral bone regeneration in critical-sized bone defects, Eur. Cells Mater. 27 (2014) 137–148.

[11] W. Yang, F. Yang, Y. Wang, S.K. Both, J.A. Jansen, In vivo bone generation via the endochondral pathway on three-dimensional electrospun fibers, Acta Biomater. 9 (2013) 4505–4512. doi:10.1016/j.actbio.2012.10.003.

[12] A. Todorov, M. Kreutz, A. Haumer, C. Scotti, A. Barbero, P.E. Bourgine, A. Scherberich, C. Jaquiery, I. Martin, Fat-Derived Stromal Vascular Fraction Cells Enhance the Bone-Forming Capacity of Devitalized Engineered Hypertrophic Cartilage Matrix., Stem Cells Transl. Med. (2016). doi:10.5966/sctm.2016-0006.

[13] C. Scotti, B. Tonnarelli, A. Papadimitropoulos, A. Scherberich, S. Schaeren, A. Schauerte, J. Lopez-Rios, R. Zeller, A. Barbero, I. Martin, Recapitulation of endochondral bone formation using human adult mesenchymal stem cells as a paradigm for developmental engineering., Proc. Natl. Acad. Sci. U. S. A. 107 (2010) 7251–7256. doi:10.1073/pnas.1000302107.

[14] M. Wiedmann-Al-Ahmad, R. Gutwald, N.C. Gellrich, U. Hübner, R. Schmelzeisen, Search for ideal biomaterials to cultivate human osteoblast-like cells for reconstructive surgery, J. Mater. Sci. Mater. Med. 16 (2005) 57–66. doi:10.1007/s10856-005-6447-z.

[15] S. Sutter, A. Todorov, T. Ismail, A. Haumer, I. Fulco, G. Schulz, A. Scherberich, A. Kaempfen, I. Martin, D.J. Schaefer, Contrast-enhanced microtomographic characterisation of vessels in native bone and engineered vascularised grafts using

ink-gelatin perfusion and phosphotungstic acid, Contrast Media Mol. Imaging. 2017 (2017). doi:10.1155/2017/4035160.

[16] M. Deschepper, M. Manassero, K. Oudina, J. Paquet, L.E. Monfoulet, M. Bensidhoum, D. Logeart-Avramoglou, H. Petite, Proangiogenic and prosurvival functions of glucose in human mesenchymal stem cells upon transplantation, Stem Cells. 31 (2013) 526–535. doi:10.1002/stem.1299.

[17] a W. Orr, C. a Elzie, D.F. Kucik, J.E. Murphy-Ullrich, Thrombospondin signaling through the calreticulin/LDL receptor-related protein co-complex stimulates random and directed cell migration., J. Cell Sci. 116 (2003) 2917–27. doi:10.1242/jcs.00600.

[18] M.I. Santos, R.L. Reis, Vascularization in bone tissue engineering: Physiology, current strategies, major hurdles and future challenges, Macromol. Biosci. 10 (2010) 12–27. doi:10.1002/mabi.200900107.

[19] J.M. Kanczler, R.O.C. Oreffo, Osteogenesis and angiogenesis: The potential for engineering bone, Eur. Cells Mater. 15 (2008) 100–114. doi:10.22203/eCM.v015a08.

[20] L. Beck, P. a D'Amore, Vascular development: cellular and molecular regulation., FASEB J. (1997) 365–373. doi:10.1002/term.394.

[21] P. Carmeliet, R.K. Jain, Molecular mechanisms and clinical applications of angiogenesis, Nature. 473 (2011) 298–307. doi:10.1038/nature10144.

[22] N. Ferrara, VEGF-A: A critical regulator of blood vessel growth, Eur. Cytokine Netw. 20 (2009) 158–163. doi:10.1684/ecn.2009.0170.

[23] L.K. Phng, H. Gerhardt, Angiogenesis: A Team Effort Coordinated by Notch, Dev. Cell. 16 (2009) 196–208. doi:10.1016/j.devcel.2009.01.015.

[24] P. Carmeliet, L. Moons, A. Luttun, V. Vincenti, V. Compernolle, M. De Mol, Y. Wu, F. Bono, L. Devy, H. Beck, D. Scholz, T. Acker, T. Dipalma, M. Dewerchin, A. Noel, I. Stalmans, A. Barra, S. Blacher, T. Vandendriessche, A. Ponten, U. Eriksson, K.H. Plate, J.M. Foidart, W. Schaper, D.S. Charnock-Jones, D.J. Hicklin, J.M. Herbert, D. Collen, M.G. Persico, Synergism between vascular endothelial growth factor and placental growth factor contributes to angiogenesis and plasma extravasation in pathological conditions, Nat. Med. 7 (2001) 575–583. doi:10.1038/87904.

[25] G. Neufeld, O. Kessler, The semaphorins: Versatile regulators of tumour progression and tumour angiogenesis, Nat. Rev. Cancer. 8 (2008) 632–645. doi:10.1038/nrc2404.

[26] P.E. Bourgine, C. Scotti, S. Pigeot, L. a Tchang, A. Todorov, I. Martin, Osteoinductivity of engineered cartilaginous templates devitalized by inducible apoptosis., Proc. Natl. Acad. Sci. U. S. A. (2014) 1–6. doi:10.1073/pnas.1411975111.

[27] C. Schlundt, T. El Khassawna, A. Serra, A. Dienelt, S. Wendler, H. Schell, N. van Rooijen, A. Radbruch, R. Lucius, S. Hartmann, Macrophages in bone fracture healing: their essential role in endochondral ossification, Bone. (2015).

[28] K.L. Spiller, T.J. Koh, Macrophage-based therapeutic strategies in regenerative medicine, Adv. Drug Deliv. Rev. (2017).

[29] A. Haumer, P.E. Bourgine, P. Occhetta, G. Born, R. Tasso, I. Martin, Delivery of cellular factors to regulate bone healing., Adv. Drug Deliv. Rev. (2018). doi:10.1016/j.addr.2018.01.010.

[30] R.K. Jain, P. Au, J. Tam, D.G. Duda, D. Fukumura, Engineering vascularized tissue, Nat. Biotechnol. 23 (2005) 821–823. doi:10.1038/nbt0705-821.

[31] E. Schipani, H.E. Ryan, S. Didrickson, T. Kobayashi, M. Knight, R.S. Johnson, Hypoxia in cartilage: HIF-1α is essential for chondrocyte growth arrest and survival, Genes Dev. 15 (2001) 2865–2876. doi:10.1101/gad.934301.

[32] H.M. Kronenberg, Developmental regulation of the growth plate, Nature. 423 (2003) 332–336. doi:10.1038/nature01657.

[33] B. Feng, Z. Jinkang, W. Zhen, L. Jianxi, C. Jiang, L. Jian, M. Guolin, D. Xin, The effect of pore size on tissue ingrowth and neovascularization in porous bioceramics of controlled architecture in vivo., Biomed. Mater. 6 (2011) 015007. doi:10.1088/1748-6041/6/1/015007.

[34] J. Dai, A.B.M. Rabie, VEGF: An essential mediator of both angiogenesis and endochondral ossification, J. Dent. Res. 86 (2007) 937–950. doi:10.1177/154405910708601006.

[35] C. Scotti, E. Piccinini, H. Takizawa, A. Todorov, P. Bourgine, A. Papadimitropoulos, A. Barbero, M.G. Manz, I. Martin, Engineering of a functional bone organ through endochondral ossification., Proc. Natl. Acad. Sci. U. S. A. 110 (2013) 3997–4002. doi:10.1073/pnas.1220108110.

[36] P. Yang, X. Huang, J. Shen, C. Wang, X. Dang, H. Mankin, Z. Duan, K. Wang, Development of a new pre-vascularized tissue-engineered construct using pre-differentiated rADSCs, arteriovenous vascular bundle and porous nano-hydroxyapatide-polyamide 66 scaffold, BMC Musculoskelet. Disord. 14 (2013). doi:10.1186/1471-2474-14-318.

[37] H. Ito, M. Koefoed, P. Tiyapatanaputi, K. Gromov, J.J. Goater, J. Carmouche, X. Zhang, P.T. Rubery, J. Rabinowitz, R.J. Samulski, T. Nakamura, K. Soballe, R.J. O'Keefe, B.F. Boyce, E.M. Schwarz, Remodeling of cortical bone allografts mediated by adherent rAAV-RANKL and VEGF gene therapy, Nat. Med. 11 (2005) 291–297. doi:10.1038/nm1190.

[38] S. Kumar, C. Wan, G. Ramaswamy, T.L. Clemens, S. Ponnazhagan, Mesenchymal stem cells expressing osteogenic and angiogenic factors synergistically enhance bone formation in a mouse model of segmental bone defect., Mol. Ther. 18 (2010) 1026–1034. doi:10.1038/mt.2009.315.

[39] K. Lee, E.A. Silva, D.J. Mooney, Growth factor delivery-based tissue engineering: general approaches and a review of recent developments, J. R. Soc. Interface. 8 (2011) 153–170. doi:10.1098/rsif.2010.0223.

[40] M. Ehrbar, S.M. Zeisberger, G.P. Raeber, J.A. Hubbell, C. Schnell, A.H. Zisch, The role of actively released fibrin-conjugated VEGF for VEGF receptor 2 gene activation and the enhancement of angiogenesis, Biomaterials. 29 (2008) 1720–1729. doi:10.1016/j.biomaterials.2007.12.002.

[41] M. Ehrbar, R. Schoenmakers, E.H. Christen, M. Fussenegger, W. Weber, Drug-sensing hydrogels for the inducible release of biopharmaceuticals, Nat. Mater. 7 (2008) 800–804. doi:10.1038/nmat2250.

[42] J.R. García, A.Y. Clark, A.J. García, Integrin-specific hydrogels functionalized with VEGF for vascularization and bone regeneration of critical-size bone defects, J. Biomed. Mater. Res. - Part A. 104 (2016) 889–900. doi:10.1002/jbm.a.35626.

Figure Legend:

Figure 1: Constructs generation and in vitro differentiation of hBMSC pellets. Figure 1A shows how constructs were generated prior to implantation. Either vital or devitalized pellets were used within a fibrin gel together or not with SVF cells from human adipose tissue. Finally the pellet/fibrin mix was introduced in a hollow cylinder of devitalized cancellous bone together with an axially implemented AV bundle generated from the epigastric vessel sof a nude rat. The construct was the inserted subcutaneously. Fig 1B shows Successful in vitro cartilaginous differentiation and hypertrophy of the hBMSC micromass pellets was demonstrated by high glycosaminoglycan content (red in Saf-O staining) and positive immunohistochemical stainings for collagen II and X.

Figure 2: Bone formation in vivo. Figure 2 A demonstrates bone formation in all three conditions. H&E and Masson Trichrome stained sections demonstrated a dense collagen matrix, fused pellets and formation of bone marrow elements, indicating the maturation into trabecular bone Figure 2 B shows the percentage of pellet area transformed into bone after 12 weeks in vivo. Vital pellets did not generate a significantly higher percentage of bone compared to devitalized and devitalized pellets with SVF cells.

Figure 3: Assessment of mineralization and bone formation with uCT. A shows that mineralized volume was the same in all three groups. Bone volume in fig. 3B, assessed by adjusting uCT data with histologically proven bone, did also not show a statistical difference among the groups. Percentage of bone volume transformed into bone (3C) confirms the trend seen in the percentage of the pellet area transformed into bone calculated with histological means.

Figure 4: Assessment of vascularization. Contrast enhanced uCT in figure 4A shows vessels spreading from the central AV bundle to the periphery of the constructs. Histological analysis confirmed the high level of vascularization in every experimental condition, as documented by the uniform distribution of vascular lumens filled by Indian ink (arrows). Although the mean diameter of central vessels in the constructs containing living pellets was in average twice larger than in the devitalized or devitalized pellets + SVF groups (Fig. 4 C). The number of

vessels branching from the central bundle, shown in figure 4D also did not statistically differ among groups.

Figure 5: Correlation between bone formation and vascularization. Figure 5 A shows a direct positive correlation (P=0.0002; r2=0.742) between the bone volume and the proximal vessel diameter. Figure 5 B shows a positive correlation (p< 0.0001; r2=0.77) between the vessel density and bone formation. A higher vessel density could also be evidenced in the radially central part of the construct compared to the periphery (p=0.0016). This tightly correlated with the pellet area transformed into bone which was strictly in the central part (Fig. 5D; p=0.0002)

Supplementary figure 1: Bone formation along the transversal axis. Bone tissue formation was not homogenous all over the implanted constructs, but only took place at a radial distance of 0.2-2.2 mm from the central vessel

Supplementary figure 2: Bone formation along the longitudinal axis. Bone tended to be formed more in the proximal part of the construct.

Supplementary figure 3: Polarization of invading macrophages. All three conditions exhibited the same density of infiltrating CD68+ macrophages (Supp. Fig. 3). CD68+/CD163+, M2-like macrophages were significantly more frequent in the vital constructs (Vital vs Devitalized: p=0.0049) representing 40% of all macrophages. In constructs with devitalized pellets, M2-like macrophages were more abundant when SVF cells were added (29%; Devitalized + SVF vs. Devitalized: p=0.04), while only 6% of the invading macrophages were polarized towards an M2 phenotype when only devitalized pellets were implanted.

Supplementary figure 4: Thresholding for densities corresponding to mineralization, eliminating the signal due to soft tissue and background, was possible on the gray value histogram by visually controlling the selected voxels.

Supplementary figure 5: Staining for human ALU-sequences evidenced the presence of human cells inside the pellets

Figure 1:

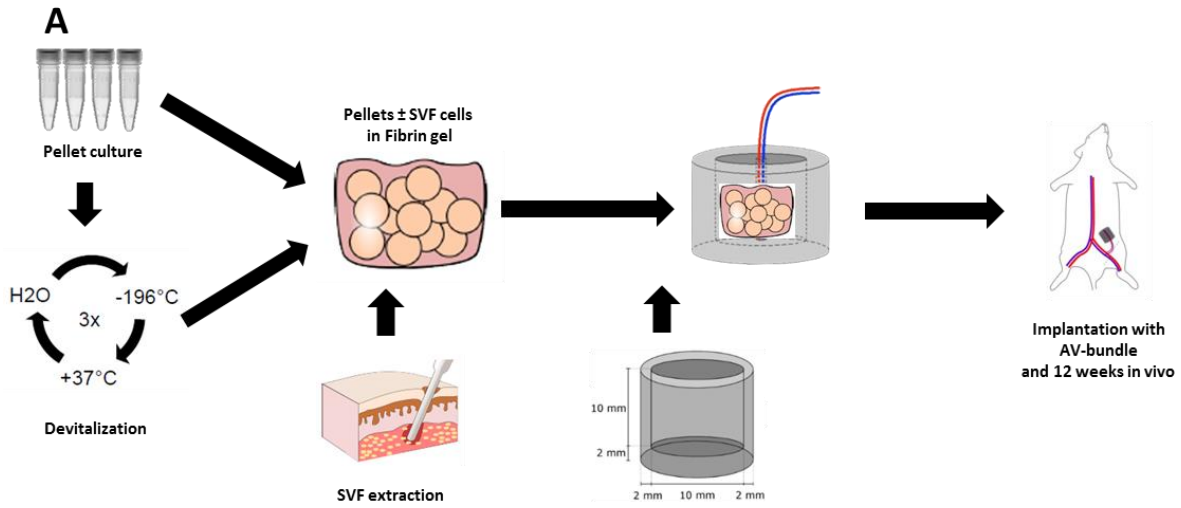
A
Pellet culture
H2O
-196°C
3x
+37°C
Devitalization
Pellets ± SVF cells
in Fibrin gel
SVF extraction
10 mm
2 mm
2 mm
10 mm
2 mm
Implantation with
AV-bundle
and 12 weeks in vivo

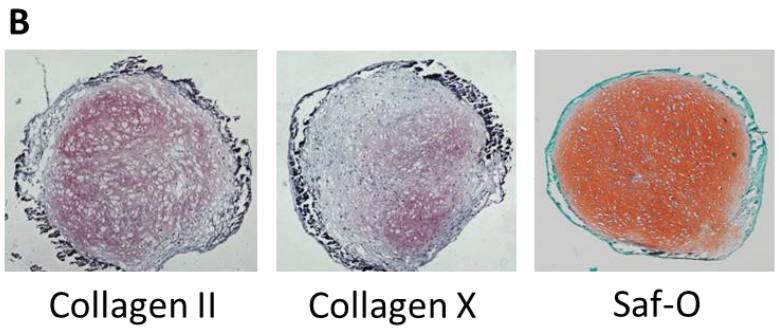
B
Collagen II
Collagen X
Saf-O

Figure 2:

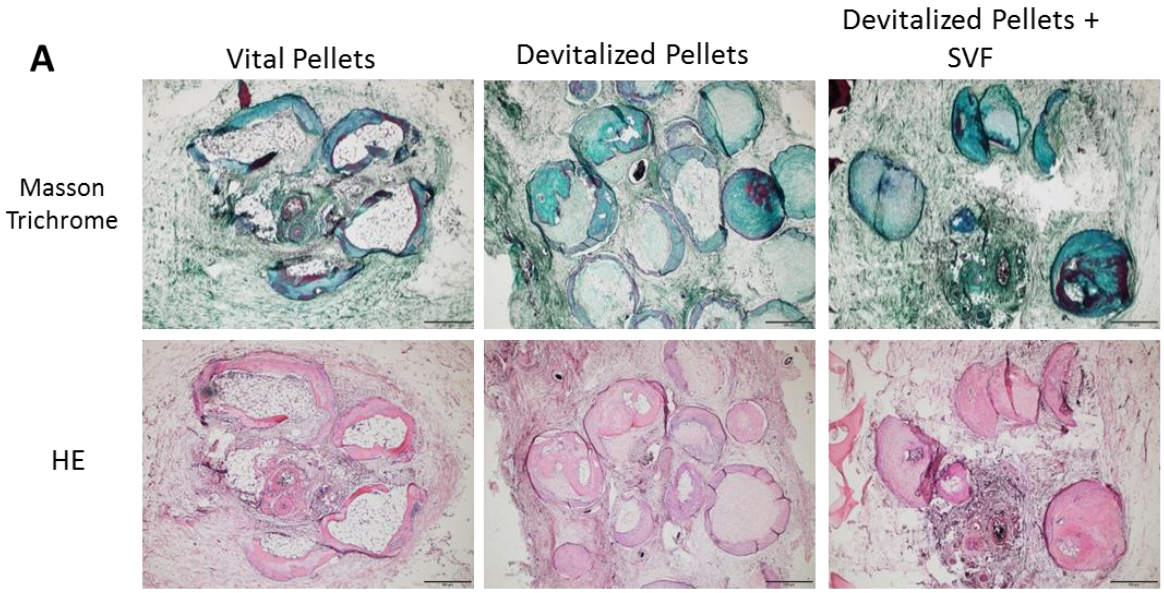
A
Vital Pellets
Devitalized Pellets
Devitalized Pellets + SVF
Masson Trichrome
HE


B
Percentage of pellet area remodeled into bone
Percentage [%]
50
40
30
20
10
0
Vital Pellets
Devital Pellets
Devital Pellets + SVF

Figure 3:

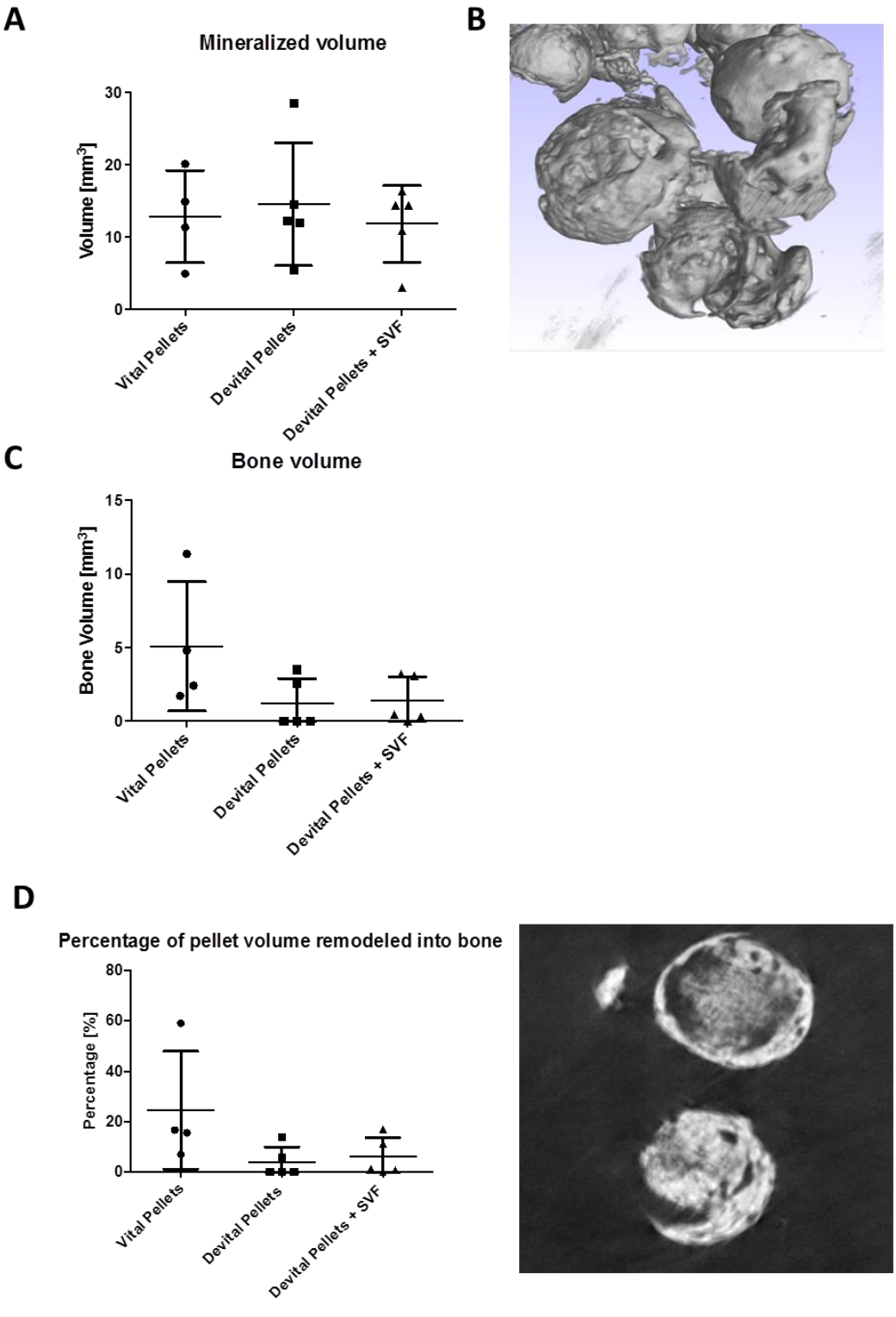
A
Mineralized volume
Volume [mm3]
30
20
10
0
Vital Pellets
Devital Pellets
Devital Pellets + SVF
B
C
Bone volume
Bone Volume [mm3]
15
10
5
0
Vital Pellets
Devital Pellets
Devital Pellets + SVF
D
Percentage of pellet volume remodeled into bone
Percentage [%]
80
60
40
20
0
Vital Pellets
Devital Pellets
Devital Pellets + SVF

Figure 4:

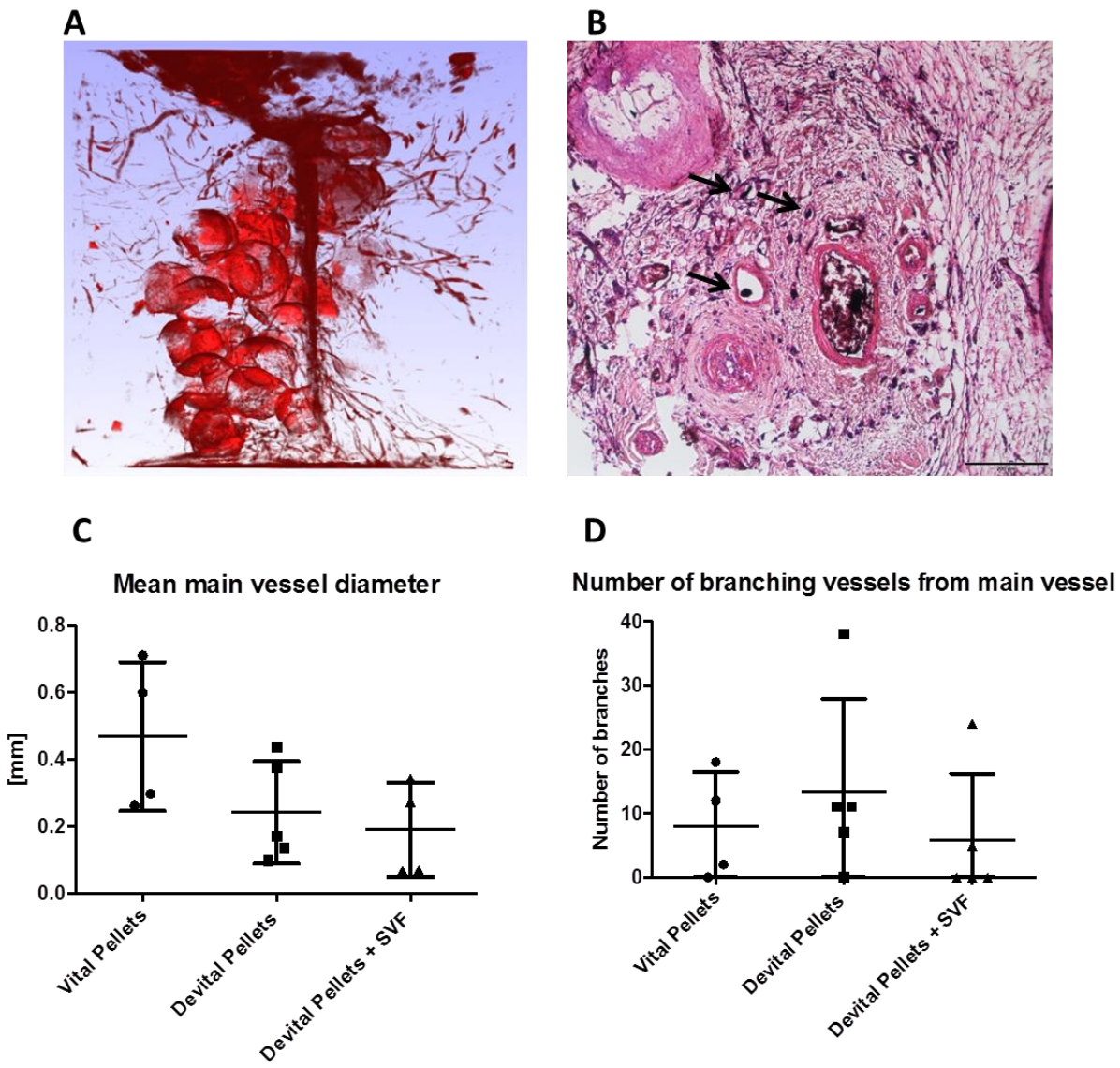
A
B
C
Mean main vessel diameter
[mm]
0.8
0.6
0.4
0.2
0.0
Vital Pellets
Devital Pellets
Devital Pellets + SVF
D
Number of branching vessels from main vessel
Number of branches
40
30
20
10
0
Vital Pellets
Devital Pellets
Devital Pellets + SVF

Figure 5:

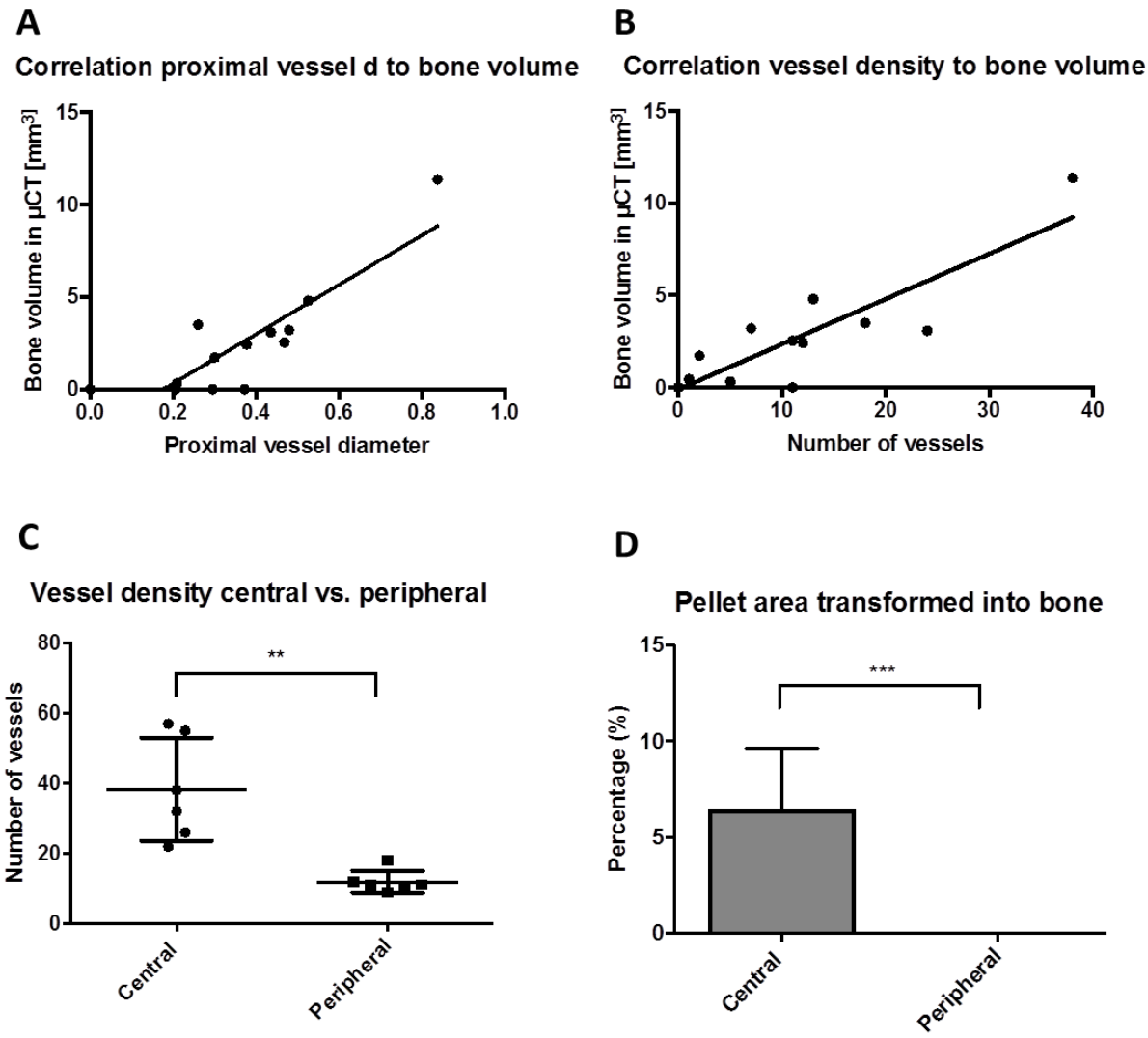
A
Correlation proximal vessel d to bone volume
Bone volume in µCT [mm³]
Proximal vessel diameter
B
Correlation vessel density to bone volume
Bone volume in µCT [mm³]
Number of vessels
C
Vessel density central vs. peripheral
Number of vessels
**
Central
Peripheral
D
Pellet area transformed into bone
Percentage (%)
***
Central
Peripheral

Supplementary material

Supplemental Fig. 1

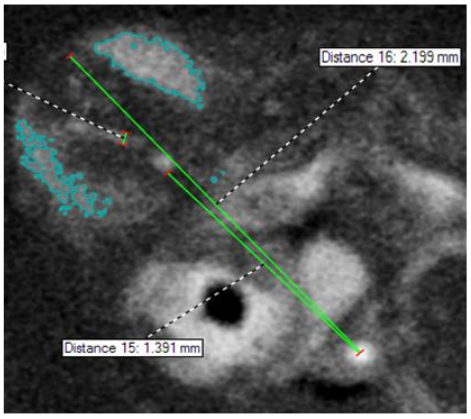

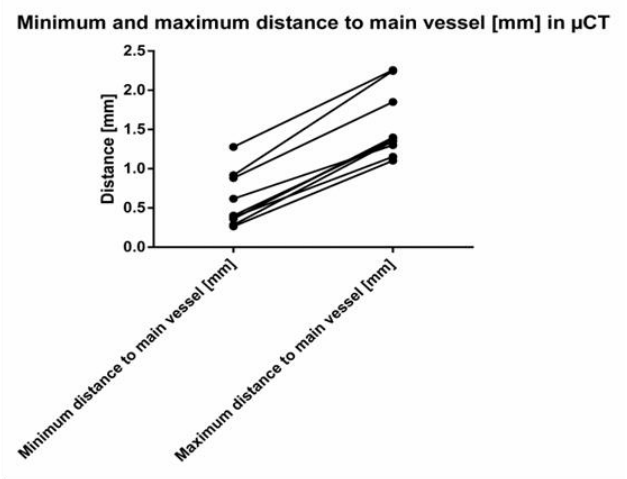

Supplemental Fig. 2

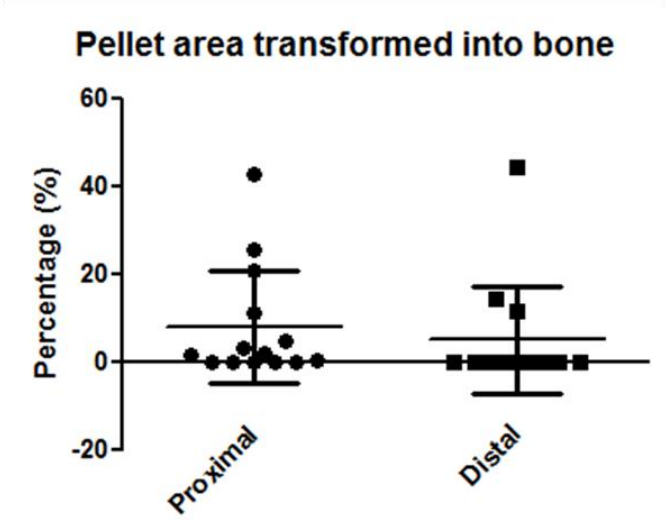

Supplemental Fig. 3:

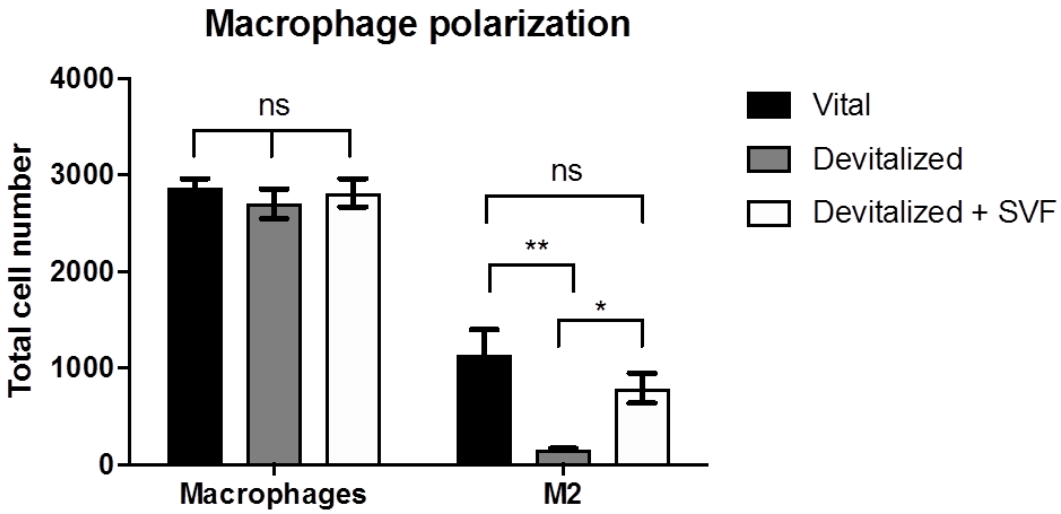

Supplemental Fig. 4:

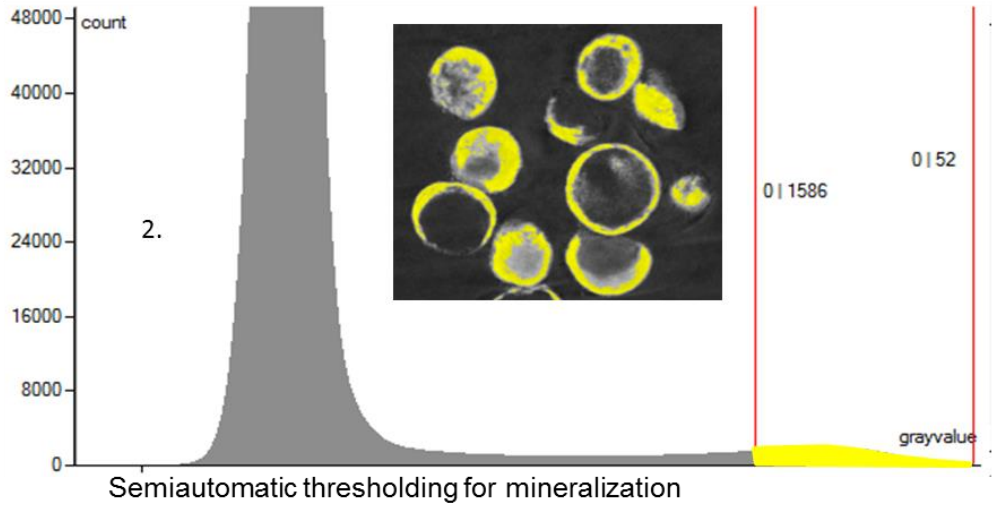

Semiautomatic thresholding for mineralization

Supplemental Fig. 5:

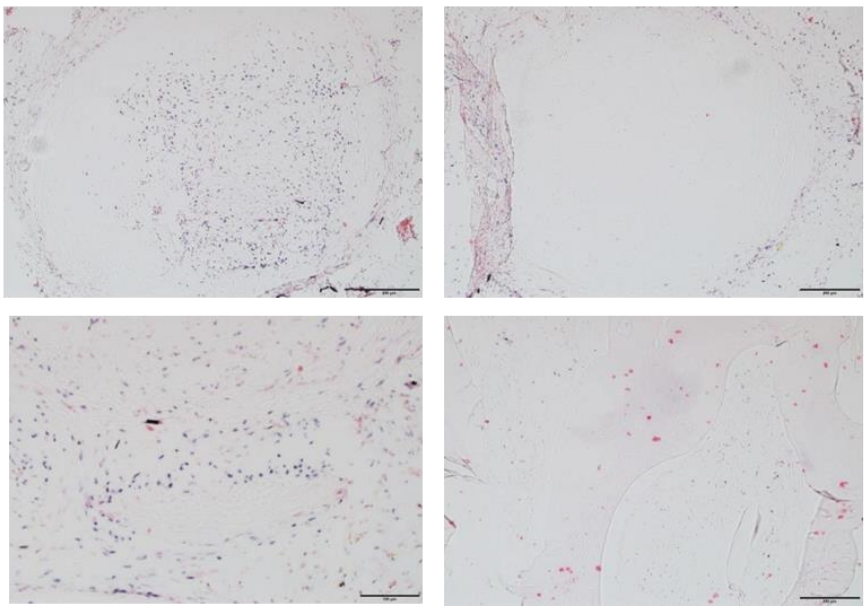

Chapter VI:

Delivery of cellular factors to regulate bone healing

ARTICLE IN PRESS
ADR-13247; No of Pages 10
Advanced Drug Delivery Reviews xxx (2018) xxx–xxx
Contents lists available at ScienceDirect
Advanced Drug Delivery Reviews
journal homepage: www.elsevier.com/locate/addr

Delivery of cellular factors to regulate bone healing ☆

Alexander Haumer [a,b], Paul Emile Bourgine [a,b], Paola Occhetta [a,b], Gordian Born [a,b], Roberta Tasso [c], Ivan Martin [a,b,*]

[a] Department of Biomedicine, University Hospital Basel, University of Basel, Switzerland
[b] Department of Biomedical Engineering, University of Basel, Switzerland
[c] Ospedale Policlinico San Martino-IST, IRCCS per l'Oncologia, Genova, Italy

ARTICLE INFO

Article history:
Received 29 September 2017
Received in revised form 8 January 2018
Accepted 13 January 2018
Available online xxxx

Keywords:
Regenerative medicine
Extracellular matrix
Extracellular vesicles
Mesenchymal stem cells
Immunomodulation
Inflammation
Bone repair
Paracrine factors
Tissue engineering

ABSTRACT

Bone tissue has a strong intrinsic regenerative capacity, thanks to a delicate and complex interplay of cellular and molecular processes, which tightly involve the immune system. Pathological settings of anatomical, biomechanical or inflammatory nature may lead to impaired bone healing. Innovative strategies to enhance bone repair, including the delivery of osteoprogenitor cells or of potent cytokines/morphogens, indicate the potential of 'orthobiologics', but are not fully satisfactory. Here, we review different approaches based on the delivery of regenerative cues produced by cells but in cell-free, possibly *off-the-shelf* configurations. Such strategies exploit the paracrine effect of the secretome of mesenchymal stem/stromal cells, presented in soluble form, shuttled through extracellular vesicles, or embedded within the network of extracellular matrix molecules. In addition to osteoinductive molecules, attention is given to factors targeting the resident immune cells, to reshape inflammatory and immunity processes from scarring to regenerative patterns.

1. Introduction

Tissue regeneration is a complex and highly dynamic process, requiring the interplay between blood and parenchymal cells, soluble mediators and extracellular matrix (ECM) molecules [1]. In the past 20 years, advances in cellular and molecular biology allowed deeper analysis and better understanding of the multi-staged wound healing process, where inflammation leads to new tissue formation and remodeling. These phases partially overlap in time and are accompanied by concomitant revascularization of the injury site together with a local and systemic defense activation, involving both the innate and adaptive immunity [2,3]. After injury, platelets or the activated-complement pathway (in absence of hemorrhage) initiate the healing cascade. This triggers the release of vasoactive mediators and chemotactic factors that attract the first cellular actors to the injury site: neutrophils, macrophages and fibroblasts [4]. These cell populations will in turn secrete a variety of factors and chemokines necessary for the priming of new tissue formation and the regulation of repair events. The timely orchestration of these processes, including primary inflammation, has revealed to be essential for an effective regeneration.

In the skeletal context, following an injury or a fracture, bone tissue has the capacity to heal without scar formation by recapitulation of the outlined wound healing phases. However, increasing severity of the trauma, comorbidities of the patient or biomechanical instability can cause an imbalance in the physiological healing cascade, leading to incomplete repair and functional failure (e.g., non-unions) [5]. In order to enhance fracture healing when compromised, cellular therapies have been extensively considered using mesenchymal stromal/stem

Abbreviations: BMP, bone morphogenetic protein; CCL, chemokine (C-C motif) ligand; CCR, chemokine receptor; CM, conditioned medium; CXCR, CXC chemokine receptors; DAMP, damage-associated molecular patterns; ECM, extracellular matrix; EV, extracellular vesicle; FGF, fibroblast growth factor; GF, growth factor; hES, human embryonic stem cells; IFN, interferon; IHH, Indian hedgehog; IGF, insulin-like growth factor; IL, interleukin; MCSF, macrophage colony-stimulating factor; MMP, matrix metalloproteinase; MSC, mesenchymal stem/stromal cell; MSC-CM, mesenchymal stem/stromal cell-conditioned medium; NLR, NOD-like receptors; OPG, osteoprotegerin; PDGF, platelet derived growth factor; PTHrP, parathyroid hormone-related protein; RANKL, receptor activator of nuclear factor kappa-B ligand; SDF, stromal cell-derived factor; TGF, transforming growth factor; TLR, toll-like receptors; TNF, tumor necrosis factor; VEGF, vascular endothelial growth factor; WT, wild type.

☆ Funding: This work was supported by the People Programme (Marie Curie Actions) of the European Union 7th Framework Programme FP7/2007-2013/under REA grant agreement No. 607868 (iTERM, to A. Scherberich), by the Swiss National Science Foundation (Grant number NBM 1579, to Prof. Ivan Martin) and by the Italian Ministry of Health ("Young Investigator Grant" - GR-2013-323 02357519).

* Corresponding author at: Department of Biomedicine, University Hospital Basel, Laboratory for Tissue Engineering, Hebelstrasse 20, Basel 4031, Switzerland.
E-mail addresses: alexander.haumer@usb.ch (A. Haumer), paul.bourgine@usb.ch (P.E. Bourgine), paola.occhetta@usb.ch (P. Occhetta), gordian.born@unibas.ch (G. Born), ivan.martin@usb.ch (I. Martin).

https://doi.org/10.1016/j.addr.2018.01.010
0169-409X/

cells (MSCs). These cells have been identified as progenitor population differentiating into cells directly involved in the replacement of skeletal tissue at the injury site. [6].

Autologous MSCs have been tested in several pre-clinical studies and even used in clinical cases (keywords "mesenchymal stem cells" and "bone" yield 264 results on clinicaltrial.gov), but major drawbacks still hamper the use of such procedures in the routine treatment of challenging bone defects [7]. First, the enhancement of clinical outcome could not be demonstrated to be repeatable. This may be related not only to the patient-to-patient heterogeneity of bone defects and of autologous MSCs, but also to the variability of protocols for MSCs isolation and preparation [8]. Second, the production of MSCs for clinical use is extremely complex and costly, such that demonstration of cost-effectiveness cannot be provided. Many groups have tried to avoid high costs and complex logistics linked to good manufacturing practice-based approaches by directly applying MSCs intraoperatively [9,10]. However, the success of this method was strictly related to the concentration and engrafting capacity of the injected cells and the absence of an experimental control group receiving a placebo treatment contributed to the weakness of the reports.

Despite promising results, the mechanisms by which MSCs exert beneficial effects towards a damaged tissue remain unclear even in seemingly successful studies. The scientific hypothesis underlying the above mentioned studies relied on the notion that MSCs exert their functions by directly replacing damaged cells. However, proper labeling and tracking of donor cells in vivo suggested that therapeutic effects provided by implanted MSCs are often short-lived, and most times related to dynamic paracrine interactions between MSCs and endogenous cells [11,12]. These experimental findings contributed to a new concept, whereby MSCs not only participate to direct tissue replacement, but also indirectly orchestrate the repair cascade by secretion of soluble "regenerative" factors [13–15]. Together with increasing evidences of their participation to all phases of tissue repair, MSCs progressively emerged as a pivotal cell population "paracrinally" modulating the endogenous environment and the immune response [16,17].

Leveraging the paracrine regulatory role of MSCs offers the possibility to develop a standardized and cost-effective clinical procedure. This approach would bypass the use of living cells by harnessing their so-called "secretome", representing the combination of secreted structural and bioactive molecules [18,19]. However, the exploitation of this scenario requires the suitable engineering of delivery strategies, in order to efficiently prime/modulate inflammation, tissue formation and remodeling events. In this context, beyond the injection of soluble factors, extracellular vesicles (EVs) and the ECM have been proposed as delivery vehicles.

In this manuscript, we will first review the successive phases of bone healing and the associated regulatory molecules. A special emphasis is given to those at the interplay with the immunological system. We will then describe how restoration of such processes in cases of impaired healing can be addressed by delivery of factors produced by MSCs. We report that such pro-regenerative factors can be delivered through cell-free approaches as soluble mediators, channeled through EVs or coupled within engineered ECMs.

2. Key regulators of bone healing

Bone healing occurs through the classical healing cascade characterized by the inflammatory, the repair and the remodeling phases. In parallel, a progressive revascularization of the injury site develops from the very first days after injury. While these phases occur successively, they also partially overlap in time. However, each phase is distinguishable by the stage-specific tissue status, as well as the cellular and molecular factors involved (Fig. 1). Deciphering the role and timing of actions of such factors during bone morphogenetic developmental events can be source of inspiration for tailoring new delivery strategies prompting bone fracture healing [20,21].

2.1. The role of the immune compartment in bone healing

Upon bone fracture, disruption of the vascular supply results in hematoma formation at the injury site, with initiation of the acute inflammatory response [22–24]. The initial inflammatory phase, reaching a peak 24 h post-injury [25,26], plays a pivotal role in the response to injury, since it initiates the repair cascade by stimulating angiogenesis, attracting and promoting MSC differentiation, and enhancing ECM deposition [27–29]. These features result from the tight interaction of molecular factors and resident progenitor cells in interplay with a well-orchestrated immune response. The local inflammation is induced in response to damage-associated molecular patterns (DAMPs, or alarmins) that bind specific receptors such as Toll-like Receptors (TLRs) and NOD-like receptors (NLRs). Distinctive for this early phase is a surge of a vast variety of proinflammatory cytokines, such as interleukin (IL)-1, IL-6, tumor necrosis factor-α (TNF-α), receptor activator of nuclear factor kappa-B ligand (RANKL) and macrophage colony-stimulating factor 1 (MCSF-1) as well as transforming growth factor-β (TGF-β) superfamily members including bone morphogenetic protein (BMP)-2, -4, -5, and -6 [27,30]. During the initial inflammatory phase, short-lived inflammatory cells, such as polymorphonuclear neutrophils, are recruited to the site of injury where the fibrin clot acts as a scaffold for the invading cells. These acute-phase inflammatory cells then recruit more long-lived monocytes and macrophages by secretion of chemokines such as monocyte chemoattractant protein 1 (i.e. C-C motif chemokine 2 (CCL2)) and IL-6 [24,31,32]. These signals, together with the danger signals TLRs and NLRs, activate tissue-resident macrophages and promote the expression of various cytokines and chemokines, such as IL-6, IL-1β, IL-1 receptor, type 1 (IL-1R1) ligands and CCL2, which direct the myeloid cell response. Macrophages are key players in different phases of bone regeneration [33]. Two distinct macrophage populations act in this phase of the healing cascade and influence the bone formation pathways: while bone tissue resident macrophages (osteomacs) appear to play an important role in intramembranous ossification, pro-inflammatory macrophages, recruited to the site, affect the endochondral bone formation route [24,34]. The varied functions of macrophages during bone tissue regeneration are realized through the tremendous plasticity of these cells. Throughout the normal healing process, macrophages adopt phenotypes ranging from a pro-inflammatory or "M1"

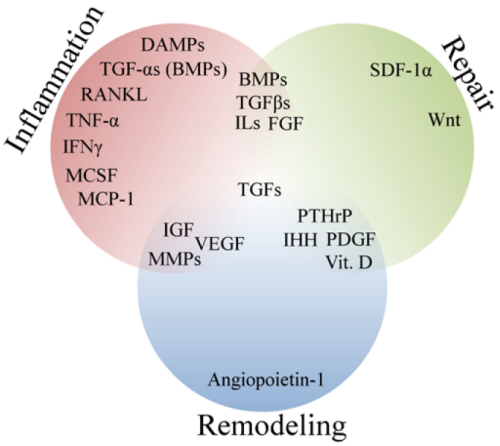

Fig. 1. Key factors involved in the bone healing phases, based on the current status of knowledge. The regulatory function of a factor to a specific phase of bone healing is represented by its proximity to the external part of one of the three circles, displaying inflammation, repair and remodeling. Positioning of the factor at the interfaces among the circles indicates overlapping functions.

Please cite this article as: A. Haumer, et al., Delivery of cellular factors to regulate bone healing, Adv. Drug Deliv. Rev. (2018), https://doi.org/10.1016/j.addr.2018.01.010

phenotype, to an anti-inflammatory/pro-regenerative or "M2" phenotype [35]. It is now generally accepted that a broad variety of stimuli can influence macrophage phenotype, resulting in a wide spectrum of different phenotypes characterized by diverse behaviors, particularly in vivo [33,36]. Nonetheless, the M1/M2 paradigm remains useful for describing the divergent effects of relatively pro-inflammatory (M1-like) and anti-inflammatory (M2-like) macrophages as they progress through the stages of tissue repair. During acute inflammation upon injury, macrophages exhibit mainly an M1-like pro-inflammatory phenotype. M1-like phenotype is driven by exposure to TNF-α and interferon gamma (IFN-γ), produced by T helper 1 (TH1) cells and CD8+ T cells from the adaptive immune system, which are in turn maintained by interleukin-12 [37]. M1-like macrophages secrete inflammatory and chemotactic mediators, such as TNF-α, IL-1β, IL-6, and CCL2 [38]. Although it is known that chronic expression of such cytokines have a negative effect on bone repair, a brief and highly regulated secretion of pro-inflammatory molecules following an acute injury is critical for tissue regeneration [27,39–41]. For instance, TNF-α has been shown also to induce apoptosis of stem cells, thus inhibiting their regenerative potential, but it can enhance the recruitment of muscular stromal cells, improving bone regeneration [39,42].

At later stages, anti-inflammatory cytokines such as IL-4 and IL-13 produced by T helper 2 (T_H2) cells, in combination with cellular processes such as phagocytosis of apoptotic cells, contribute to polarize macrophages towards an M2-like pro-regenerative (or anti-inflammatory) phenotype [43]. Activation of pro-regenerative macrophages has revealed to speed up the resolution of acute inflammation responses and eventually the bone healing process [44,45]. However, several studies demonstrated that sequential and balanced activation of both M1-like and M2-like macrophage is a critical factor for tissue repair [46]. For instance, TNF-alpha activates M1-like macrophages. Its local injection immediately after injury accelerates bone healing in murine models, but impairs it when given in high and prolonged doses [47]. In addition, while prolonged activation of pro-inflammatory macrophages worsens tissue healing, sustained mobilization of IL-4 recruited macrophages contributes to the generation of non-functional fibrotic tissue [35]. Factors delivery strategies for modulating macrophages polarization should thus take this delicate balance into account.

Beyond the macrophage compartment, the adaptive immune system also plays a crucial role in tissue repair. Indeed T cell responses can be polarized to different phenotypes by signals from the microenvironment. While the precise function of T cells in tissue regeneration is still largely debated, it appears clear that different subsets of T cells are involved in different stages of tissue healing and their function varies from tissue to tissue. $CD4^+$ T_H1 and $CD8^+$ cytotoxic T cells, both characterized by a TNF-α and IFN-γ secretory profile, were shown to negatively affect bone healing. Indeed, fracture healing was accelerated in $Rag1^{-/-}$ mice lacking T and B cells, while intravenous infusion of $CD4^+CD25^-$ T cells totally blocked mesenchymal progenitor-mediated bone formation in nude mice [39,48]. $CD8^+$ effector memory T cell (T_{EMRA}, $CD3^+CD8^+CD11a^+CD28^-CD57^+$ T cells) recruitment was shown to correlate with delayed fracture healing in humans [49]. In contrast, different T cell subsets have been reported to exhibit an anti-inflammatory phenotype. Regulatory T cells ($CD4^+CD25^+FoxP3^+$) (T_{reg}) have recently been correlated with tissue reparative functions through a panel of chemokine receptors (CCR6, CCR2, CXCR3, CCR4 and CCR10) supporting their attraction to the site of injury. Moreover, a critical role of T_{reg} has been postulated lately [50]. Taken together these findings lead to investigate on the combined infusion of T_{reg} and bone marrow-MSCs, reported to enhance healing in mice calvarial defects [39]. T_{reg} can indeed modulate local inflammation by secreting immunosuppressive cytokines, such as IL-10, IL-35 and TGF-β, and by inducing an M2-like macrophage phenotype. Anti-inflammatory macrophages in turn regulate the development and maintenance of IL-10 and TGF-β1-producing T_{reg}. As additional T cell subset, γδT cells are also important in tissue healing processes, peaking between 2 and 7 days after mouse bone injury and secreting IL-17A, shown to enhance osteoblast function [51].

2.2. Factors and cells for differentiation, remodeling and vascularization

Due to the rupture of blood vessels and the vasoconstriction following bone fracture, blood flow is markedly decreased in the injury area [52]. The initial hypoxic environment post-trauma is a strong trigger for the release of pro-angiogenic factors, leading to the formation of new capillaries growing into the fibrin clot formed at the injury site. Beyond vascular endothelial growth factor (VEGF), other factors such as angiopoetin-1 and platelet-derived growth factor (PDGF) contribute in promoting vessel invasion in new-formed bone [53,54]. Although the primary function of VEGF is related to vasculature, it was also suggested to be implicated in the recruitment and differentiation of osteoprogenitor cells and in the regulation of various osteoinductive factors (i.e. TGF-β1, insulin-like growth factors (IGF), fibroblast growth factor (FGF-2)), which in turn regulate its expression pattern. PDGF is another key regulator of fracture healing, stimulating both angiogenic and osteogenic pathways. PDGF is released by degranulating platelets, it is chemotactic for osteoblasts and it has both direct and indirect (e.g. through upregulation of VEGF expression) pro-angiogenic functions [55]. Moreover, it has been demonstrated that mechanical loading within the new formed bone leads to matrix metalloproteinase (MMP) secretion and this further enhances angiogenesis [56]. Ingrowing vessels also provide an important source of circulating factors crucial for bone homeostasis such as parathyroid hormone and vitamin D [55].

Over time, the increased intra- and extra-osseous vascularization leads to re-establishment of normoxic conditions. Cells and nutrients are delivered to the tissue and breakdown products removed. Fibroblasts then start remodeling the site by stepwise replacement of the hematoma with dense granulation tissue, rich in small vessels [57,58].

The repair phase can take different paths based on the anatomical location and mechanical conditions present at the injury site. Primary healing, characterized by direct deposition of a mineralized matrix, requires compression between the two fractured fragments as well as low interfragmentary movement [59]. Compression and stability of the two bony surfaces allow bridging by Haversian systems, which are in turn infiltrated by osteoclasts [57,59,60]. The osteoclasts build tunnels connecting the two bone segments, which can eventually be colonized by blood vessels. Cells from the innate immune system (e.g. macrophages) immediately start to secrete a pool of chemotactic mediators that initiate the recruitment of fibroblasts, MSCs, and osteoprogenitor cells from local niches [29,61].

Processes involved in indirect bone healing tightly recapitulate the sequential events of the endochondral ossification route, typically occurring during long bone development. In contrast to the direct route, bone heals through this healing path when the fracture site is mechanically instable [57,62,63]. Indirect bone healing comprises both intramembranous and endochondral ossification, but bone formation through transformation of a cartilaginous callus, which undergoes mineralization to bone, is the central part of the process. Intramembranous ossification starts approximately 3–7 days after injury by osteoblasts directly derived from the periosteum, where it has been spared from the traumatic event [64,65]. Following direct matrix deposition by periosteal progenitors, cartilaginous tissue is formed 7–10 days after the injury occurred [25,62]. Two mechanisms are considered to be responsible for cartilage tissue formation. The increased mechanical strain on tissue in the injury area leads to a decrease in new vessel formation [66,67]. Eventually, it is the low oxygen content in the fracture site that drives the equilibrium towards chondrogenic differentiation of progenitor cells [24,57,68]. The associated factors participate to the course of the endochondral ossification route, comprising sequentially processes of progenitor cell recruitment and condensation, cellular proliferation, chondrogenic differentiation, cartilage mineralization, vascularization and remodeling. Stromal cell-derived factor-1α (SDF-1α) is

Please cite this article as: A. Haumer, et al., Delivery of cellular factors to regulate bone healing, Adv. Drug Deliv. Rev. (2018), https://doi.org/10.1016/j.addr.2018.01.010

one of the key chemokines mediating the recruitment of progenitor cells both from local and systemic sources [69,70]. It has been demonstrated that osteoprogenitor cells mobilized from the bone marrow express CD44 and CXCR4, receptors of osteopontin and SDF-1, respectively [69]. SDF-1α, which is highly released by the periosteum during the acute phase of bone healing, induces efficient migration of mobilized cells to the region of bone formation [70]. As during long bone development, condensation, expansion and chondrogenic differentiation of progenitor cells are then driven by an orchestrated combination of Wnt, FGF, and BMP pathways. During proliferative expansion of mesenchymal progenitors, FGF and Wnt signaling play a synergistic role in controlling limb growth and inhibiting chondrogenesis, while maintaining progenitor cells in a proliferative and potential osteogenic state [71,72]. In contrast, BMP and TGFβ signaling are required for the aggregation and chondrogenic differentiation of the Sox9-positive chondrogenic progenitors [73]. During progression of skeletal development, BMP signaling is also involved in triggering the hypertrophic route of differentiated chondrocytes towards bone, together with the negative regulatory feedback loop between Indian Hedgehog (IHH) and Parathyroid Hormone-related Protein (PTHrP) [74,75]. Due to its key role in guiding bone formation, BMP is the most widely used inductive factor in bone tissue engineering applications. However, BMPs signaling should be carefully considered when designing a BMP-based delivering strategy to effectively enhance bone formation due to its great variety of context- and temporal-dependent functions (i.e. its role in chondrocyte specification, cartilage template growth, and endochondral bone development). Also, it has been shown that BMPs contribute to significant soft tissue swelling and inflammation, hampering their clinical application [76–80]. Moreover, together with BMP, Wnt activity has revealed essential to promote osteoblast differentiation during both endochondral and intramembranous ossification [81,82].

The remodeling phase represents the final phase of bone fracture healing and can take up to years in human adults to yield a fully loadable bone. Approximately two weeks after bone fracture, chondrocytes undergo hypertrophy and become apoptotic while releasing calcium, as observed in the endochondral ossification process [62,83,84]. Hypertrophic cartilage and the increasing calcium content of the callus enhance the fracture site's mechanical stability, reducing the high tissue strain and thus favoring vessel ingrowth into the now bridged gap [66,85,86]. The newly formed vessels bring MSCs and circulating monocytes to the site, which then differentiate into osteoblasts and osteoclasts respectively and start remodeling the soft callus towards bone [62]. Osteoclastic activity enables the transformation of deposited woven bone into lamellar bone as in primary bone healing. Osteoclast induction, survival, and activity are tightly regulated by the osteoblast-secreted cytokines MCSF, involved in osteoclast differentiation, and RANKL, responsible for osteoclast differentiation and the coordination of bone formation and bone resorption [87]. This phase, which outlines the return to a pre-injury status of the bone, is characterized by a decrease of most inflammatory cytokines, except IL-1, TNF-α and BMP-2 [24]. When the first bony bridging of the gap is completed, the initially high tissue strain is low enough to allow for intramembranous ossification to happen - this typically occurs 4–6 weeks after bone fracture [63,88].

3. Cell-free strategies to deliver MSC-produced regenerative factors

From the overview provided in Section 2, it is clear that bone regeneration processes are strictly controlled by a wide variety of regulatory molecules, which may be potentially used to enhance healing when impaired. Upon immune activation, activated MSCs secrete factors that arrange a regenerative environment [14]. The use of activated MSCs as 'drugstores' producing many of such molecules has possible advantages over the delivery of single recombinant factors through synthetic devices. However, the manufacturing and biological challenges of using living MSCs has so far limited consolidated evidences of efficacy and discouraged clinical adoption. Thus, in the remainder of this manuscript we will describe possible strategies to deliver MSC-based products using cell-free materials (Fig. 2).

3.1. Delivery of MSC-secreted soluble factors

The idea that MSCs possess the capacity to sustain the growth and the viability of other cell types through the secretion of trophic factors has been already postulated in the 1970s, when Dexter and colleagues demonstrated for the first time that adherent stromal cells were able to enhance hematopoietic stem cell growth, maintaining their multipotent status [89]. Throughout the years further studies demonstrated that the effects of MSCs on regulation of other cell types, as well as on regenerative processes, are highly related to their paracrine interactions [12]. This paracrine hypothesis led to a new definition for MSCs, described as "injury drugstores" [14]. MSCs produce a wide range of cytokines, chemokines, and growth factors that have shown extensive therapeutic potential, investigated in a vast variety of animal models [90]. As a result, a growing body of work exploits the administration of MSC-derived conditioned media (MSC-CM) to capture the beneficial effects of stem cell transplantation.

MSCs possess the ability to regulate immune responses, an important feature during bone repair [91]. To exert this important task, the dynamic interplay between MSCs and the innate immune system plays a fundamental role, governing MSC downstream modulatory effects [92]. Proof is that immediately after the onset of an inflammatory response, as the one generated following tissue injury, hypoxic conditions as well as Toll-like receptors (TLRs), which are expressed by innate effectors, trigger phagocytosis and mediator release, which in turn activates MSCs [93,94]. Activated MSCs acquire an immunomodulatory phenotype and exert their function secreting a panel of soluble factors, comprising, among the others, PGE2, TGF-β, and HGF, that contribute to the suppression of neutrophil and T lymphocyte proliferation [95,96]. Moreover, activated MSCs modulate the inflammatory response at the injury site, decreasing the levels of pro-inflammatory cytokines such as IL-1-β, TNF-α, and IL-6 or inducing a macrophage polarization towards a pro-resolving/anti-inflammatory profile, contributing to the generation of a suitable environment for bone repair [92,97]. In addition to the paracrine effects related to the regulation of immune responses, MSCs secrete pro-survival bioactive factors retaining the capacity to rescue damaged cells and foster tissue repair [90]. This pro-survival effect was first shown in studies of long-term co-cultures of irradiated MSCs with human embryonic stem (hES) cells [98]. Data obtained from rigorous transcriptome and proteome analysis indicated that MSCs secrete a repertoire of pro-survival signals, involved in the acceleration of adjacent progenitor cell self-renewal, migration of endogenous progenitors, and attenuation of apoptotic signals [45,99,100]. Moreover, it has been recently demonstrated that MSC-CM delivered in gelatin sponges stimulated angiogenesis and promoted fracture healing in a diabetic rat model [101]. In line with this, it has been shown that both adipose tissue-MSCs and their conditioned medium can induce bone regeneration in surgically created lesions in rabbit's jaws, indicating that MSCs can improve the process of bone regeneration by releasing paracrine factors [102].

3.2. Delivery of MSC-produced extracellular vesicles

EVs represent a particular form of the MSC secretome, reported to exhibit regenerative effects by communicating with and activating recipient cells through the delivery of lipids, proteins, and genetic information [103,104]. As such, their exploitation as delivery vehicles has raised increasing interest in the field of regenerative medicine.

EVs are classified based on their cellular origin and biological function, and on their biogenesis. They are cell-derived vesicles enclosed by a lipid bilayer, and exist in the form of microvesicles or exosomes. While microvesicles are generated by budding from the plasma

Please cite this article as: A. Haumer, et al., Delivery of cellular factors to regulate bone healing, Adv. Drug Deliv. Rev. (2018), https://doi.org/10.1016/j.addr.2018.01.010

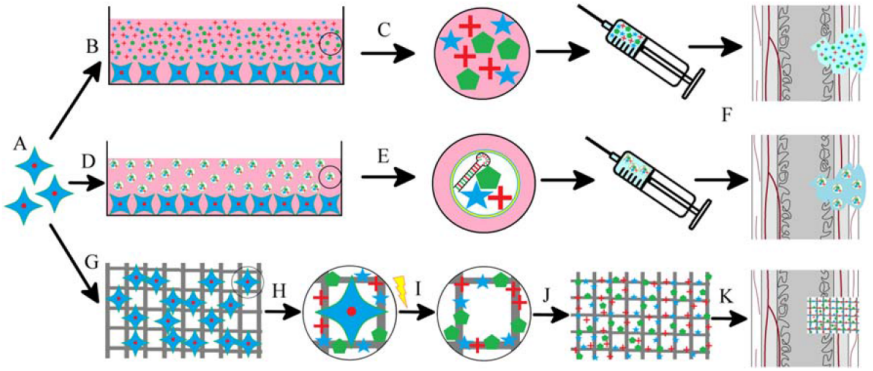

Fig. 2. Different application strategies of harvested MSCs for the generation of engineered grafts for bone regeneration. (A) MSCs can be isolated from different tissues of individuals. To avoid the use of living cells different strategies have been proposed: (B, magnified in C) The combination of growth factors secreted by MSCs in the supernatant, the so-called secretome, can be collected as MSC-CM. (D, magnified in E) From this MSC-CM one can also harvest MSC-derived EVs, which were proven to have reparative capacities similar to the MSCs themselves. (F) Both MSC-CM and MSC-derived EVs can be applied for the regeneration of the bone defects. Cytokines secreted by the MSCs are also entrapped and presented by the ECM. (G) MSCs are seeded on appropriate scaffolding materials, (H) where they secrete signaling molecules which remain entrapped in the ECM. (I) The process of devitalization yields a (J) cell-based, but cell-free graft, containing a cocktail of osteoinductive and immunomodulatory factors which may be relevant for the (K) enhancement of bone regeneration.

membrane and present a diameter ranging from 150 to 1000 nm, exosomes are derived from the endosomal compartment of the cell, ranging from 30 to 150 nm [105]. Encouraging data indicate that MSC-derived EVs have protective, modulatory, pro-angiogenic and reparative capacities similar to their cellular counterparts [106,107]. MSC-derived exosomes were demonstrated to induce naive stem cells osteogenic differentiation, and specific exosomal miRNAs were involved in the process of MSC osteoblastic differentiation [108]. Moreover, it has been shown that osteoblasts themselves secrete exosomes, establishing a positive feedback on bone growth [109]. Recent studies have revealed that exosomes derived from bone cells, including osteoclasts, osteoblasts and their precursors, play key roles on bone remodeling by transferring biologically active molecules to target cells, especially in the processes of osteoclast and osteoblast differentiation [110]. Exosomes can also be isolated from MSC-conditioned medium, and their role in the healing process has been evaluated in a femur fracture model conducted in CD9-/- mice, a strain known to produce reduced levels of exosomes [111]. The delayed callus formation observed in CD9-/- mice compared to wild type (WT) animals was rescued by the injection of MSC-derived exosomes, clearly indicating that these nano-vesicles can be considered important components and mediators of the MSC paracrine signaling.

To date, studies reporting the exploitation of exosomes as immunomodulators or as promoter of angiogenesis still lack in the bone context. However, MSC-derived exosomes were already demonstrated to be capable of stimulating endothelial cell proliferation, migration, and tube formation both in vitro and in vivo. Thus, deeper analysis of the roles of exosomes derived from specially activated MSCs in vessel formation and bone repair could pave the way for the development of novel treatments [112].

3.3. Delivery of MSC-deposited ECM

During the process of secretion of regenerative factors and their shuttling through EVs, MSCs produce abundant amounts of ECM. The ECM network is capable of embedding secreted factors, and appears to be an essential regulatory and presenting entity capable to foster tissue regeneration. Harnessing the potential of ECMs as presenting/delivery system thus represents a powerful approach for regenerative strategies.

The ECM is the acellular component of our tissues and as such possesses important structural, mechanical but also functional roles [113]. As primary cellular substrate, the ECM acts as a molecular niche capable to store and present growth factors [113]. This property is connected to the presence of major ECM proteins with a high binding affinity for growth factors (GFs) [114,115]. Their progressive embedding in the ECM leads to the constitution of a natural reservoir of cues whose activation, synthesis and degradability is tightly regulated. In the skeletal context, ECM proteins capable to interact with GFs include glycosaminoglycans and proteoglycans, abundantly found in cartilage tissue, but also fibronectin, osteopontin and collagens in bones [114,116–119]. Importantly, these ECM proteins regulate a wide range of GFs with distinct functions, from pro-angiogenic (e.g. VEGF), pro-mitotic (e.g. FGFs), master transcription regulators (e.g. TGFβ) but also inflammatory molecules (e.g. TNFα) [120–123]. The conformation through which these molecules are presented by the ECM is crucial, and even mandatory in some contexts for their subsequent activity (e.g. IL-1β) [124].

As such, while being primarily exploited as scaffolding material, ECM progressively raised interest also in regards to the biological properties associated with embedded factors [125,126]. The processing of native tissues has first been proposed in order to retrieve the ECM and exploit the growth factors and cytokines that are naturally stored within. Different decellularization strategies have been developed for the removal of the immunogenic cellular component, while preserving structural and/or bioactive elements of the ECM [127]. For skeletal repair, a variety of decellularized and demineralized bone/cartilage materials have been proposed, and the diversity of factors contained in these preparations was shown to prompt tissue regeneration at concentrations far lower than those required by single soluble factor injection [128–130].

However, so far the substantial heterogeneity of decellularized native ECM limits a robust clinical exploitation. The donor variability combined with the numerous preparation steps (e.g. decellularization, cleaning, lyophilization) lead to important batch-to-batch variations in terms of composition and ultimately of repair efficacy [131]. Taken together, this has driven the emergence of engineering strategies, with the aim to exploit ECM as smart factor-delivery entities through the tight control over their compositions and functions, including the flexibility to more specifically drive particular cascade of events occurring during tissue repair.

3.3.1. Synthetic ECM

ECM properties has been extensively exploited through synthetic approaches [132]. In this context, the use of ECM as effective storage and presenting interface has rapidly gained interests in regenerative medicine, for the improved delivery of molecules capable to drive

Please cite this article as: A. Haumer, et al., Delivery of cellular factors to regulate bone healing, Adv. Drug Deliv. Rev. (2018), https://doi.org/10.1016/j.addr.2018.01.010

endogenous tissue repair. Similarly to their native counterparts, engineered ECM has rapidly allowed bypassing some of the typical drawbacks associated with the direct injection of soluble GFs for regenerative therapies. Thus, the immobilization of factors by ECM was shown to increase the efficiency of delivery at local injury site, by avoiding diffusion and uptakes by surrounding cells [133]. This is of primary interest in context of bone repair, in order to reduce unsafe doses of BMPs resulting in ectopic site bone formation [134]. In this direction, grafts functionalized with fibronectin domains allowed reducing the required doses of BMP-2 to efficiently induce de novo bone formation in a rat ectopic model [135]. However, here the strategy was not directly correlated with a binding of BMP-2 to the fibronectin fragments. More recently, ECM binding properties were exploited in order to impact on the modulation of the immune microenvironment. As such, two different ECM-based approaches have been essentially followed so far: the (i) direct delivery of cytokines (pro-inflammatory and/or pro-regenerative) to polarize resident immune cells, and the (ii) recruitment of specific subsets of immune cells to the site of injury. The first one can be illustrated by the delivery of integrated inhibitors of IL-1R1 blocking pro-inflammatory signals. This resulted in the efficient promotion of MSC-driven bone regeneration in a mouse critical size calvarial defect model [40]. Moreover, synthetic matrices have for instance been recently demonstrated to induce a pro-regenerative environment in muscle wounds by activating T helper 2 cells, which in turn guide IL-4 dependent macrophage polarization [136]. The second strategy was achieved by the release of an SP-1 agonist in combination with platelet-rich plasma linked to the ECM. This was shown to increase the number of recruited macrophages in rat bone defects via promotion of a short term production of TNFα in the first three days, with subsequent increase of anti-inflammatory signals accumulation (osteoprotegerin (OPG) and IL-10) [137].

Importantly, synthetic ECMs offer a wide range of design flexibility, allowing to optimized GFs presentation and control their spatio-temporal delivery [138,139]. This was demonstrated to reduce the overall doses of GFs required to efficiently promote skeletal tissue regeneration [139–141].

Synthetic ECMs currently offer great levels of control associated with ease of engineering but are limited in their capacity to reflect the complexity of native ECM. In fact, so far only a limited number of biomolecules were immobilized on a synthetic substrate, which may be effective mainly in specific scenarios in which proteins have been identified as key trigger of the biological process to be induced (e.g. VEGF or BMP-2 in angiogenesis or osteogenesis respectively). Efforts have thus been made towards the development of more biological alternatives, through the generation of cell-laid ECM.

3.3.2. Cell-laid ECM

The in vitro generation of cell-laid ECM can be achieved by the directed proliferation/differentiation of progenitor cells in 2D or 3D substrates and accelerated matrix deposition using macromolecular crowding [142,143]. This is ultimately followed by a decellularization step for subsequent storage or use as *off-the-shelf* product. These templates can be re-seeded with patient-derived cells towards an autologous setting, or used as acellular grafts driving per se regeneration processes [144]. As opposed to their synthetic counterparts, cell-laid ECM offers a more complex environment composed of a multitude of factors "naturally embedded" along the in vitro maturation time. The type of ECM-graft produced can be adapted to specific clinical scenarios by selecting the type of cells and the culture conditions driving the secretion/deposition of ECM (e.g. osteogenic versus chondrogenic).

The exploitation of this approach was shown to bear particular relevance in a variety of contexts. For instance, 2D cell-derived osteogenic ECM could be generated out of MSCs, and were shown to be capable of enhancing the in vitro osteoblastic differentiation of marrow stromal cells, but also the repair of mouse calvarial defects [145–147].

By combination with 3D materials, cell-laid ECM were demonstrated to act as functionalization element, enhancing the basic properties of given scaffolds. This approach has been successfully implemented combining titanium material and rat MSC-derived ECM. The ECM was deposited along the differentiation of the cells towards the osteogenic lineage, which resulted in a scaffold homogenously covered with ECM [148]. Following decellularization and re-seeding with primary rat MSCs, ECM-coated scaffolds significantly enhanced their osteoblastic differentiation in vitro, as compared to "naked" titanium material. Along the same line, synthetic polymers were decorated with ECM deposited by human MSCs during 3D culture in perfusion bioreactor [149]. The resulting ECM-polymer hybrid constructs successfully recruited host progenitors forming mineralized tissue in a stringent ectopic model.

Of importance, the engineering of biological ECM with intrinsic regenerative properties may also largely depend on the decellularization method. This was illustrated in a study combining collagen scaffold and human MSCs to generate in vitro hypertrophic cartilage tissue. The resulting templates were shown to directly induce endochondral formation of bone and bone marrow in mouse models, only following a suitable decellularization method that preserves the ECM molecular components [150].

While biological ECMs have revealed to be promising, efforts are still being conducted in order to better control their composition/properties, towards approaching those of synthetic ECM. On this line, two different strategies are currently investigated. The first one relies on the modulation of culture conditions, leading to the generation of ECM with different molecular composition and structural features [151]. The second strategy consists in the generation of dedicated human MSCs lines overexpressing particular factors of interest, to generate customized ECM [152]. The study demonstrated the feasibility to design cell-laid ECM molecularly tuned in composition. This was exemplified by the engineering of VEGF-enriched matrices with superior angiogenic potential [152]. Importantly, the use of cell lines also introduces the notion of standardization which might reveal to be essential towards engineering of ECM with reproducible properties.

4. Conclusions

Convincing experimental evidences indicate that MSCs exert beneficial effects in the repair processes of injured tissues by means of their paracrine activity, opening new therapeutic perspectives in the field of regenerative medicine and specifically of bone tissue repair. The development of cell-free strategies based on the use of the MSC secretome, and in particular of the released vesicles, can be considered an interesting alternative to cell-therapy approaches. EV-based treatments present several potential advantages over the cell-based strategies, in terms of both efficacy and safety. These are related to their chemical and physical characteristics, to the ease of production in laboratory, and to the unique affinity for the cell targets. The delivery of MSC-produced signaling molecules through the deposited and subsequently devitalized ECM represents an alternative and highly attractive modality to exploit the MSC secretome, maintaining its entire potency within cell-free, possibly *off-the-shelf* devices. Collectively, these systems may be designed and customized to target not only recruitment and differentiation of osteoprogenitor cells, but also activation and regulation of immunological processes capable to shift fibrosis into regeneration. The present review has been focused on the specific context of bone healing, but obviously the same concepts could be extended and adapted to other indications.

Nevertheless, critical challenges have to be addressed in order to validate and exploit these alternative approaches towards clinical use. First of all, it is essential to develop more fundamental knowledge on which key components of the MSC secretome play which specific role in the healing cascade of clearly-defined pathological settings. Such understanding would enable definition of potency tests, in-process-controls

Please cite this article as: A. Haumer, et al., Delivery of cellular factors to regulate bone healing, Adv. Drug Deliv. Rev. (2018), https://doi.org/10.1016/j.addr.2018.01.010

and release criteria in the manufacturing of MSC-based products with standardized and repeatable therapeutic benefits. An 'all-purpose' product at a generic dose for diverse settings of impaired healing is unlikely to find scientifically and clinically sound adoption.

Further challenges are related to the production which would have to be scalable, standardized, cost-effective and compliant with regulatory constraints. MSC-product based therapeutic systems would avoid direct implantation of living cells and represent off-the-shelf therapeutic solutions. Thus they may allow overcoming critical issues of cell-based approaches in terms of clinical translation, eventually providing a less costly and easier to scale-up solution. However, especially with regard to regulatory constraints, it would be necessary to find consensus on whether a cell-based but cell-free product be considered as an Advanced Therapy Medicinal Product, regulated similar to a drug, or as a Biomaterial, regulated according to medical device criteria.

Beyond biological and manufacturing considerations, it is however clear that the outlined paradigms could offer an elegant alternative to conventional cellular therapies, as well as to conventional smart materials and implant devices.

References

[1] A.J. Singer, R.A. Clark, Cutaneous wound healing, N. Engl. J. Med. 341 (1999) 738–746, https://doi.org/10.1056/NEJM199909023411006.
[2] R.A.F. Clark, The Molecular and Cellular Biology of Wound Repair, http://books.google.com/books?hl=en&lr=&id=tt_ZHV1J_CAC&oi=fnd&pg=PA3&dq=roberts+sporn+molecular+and+cellular+biology+of+wound+repair&ots=KaPi6uWwJn&sig=ccssTbEn-FNLFCm7hXMgichwD8s 1996.
[3] S.A. Eming, P. Martin, M. Tomic-Canic, S. Of, T.H.E. Art, Wound repair and regeneration: mechanisms, signaling, and translation, Sci. Transl. Med. 6 (2014) 265sr6, https://doi.org/10.1126/scitranslmed.3009337.
[4] S. Van Linthout, K. Miteva, Crosstalk between fibroblasts and inflammatory cells, Cardiovasc. Res. 102 (2014) 258–269, https://doi.org/10.1093/cvr/cvu062 (C. Tsch??pe).
[5] M.A. Imam, J. Holton, L. Ernstbrunner, W. Pepke, F. Grubhofer, A. Narvani, M. Snow, A systematic review of the clinical applications and complications of bone marrow aspirate concentrate in management of bone defects and nonunions, Int. Orthop. (2017)https://doi.org/10.1007/s00264-017-3597-9.
[6] R. Berebichez-Fridman, R. Gómez-García, J. Granados-Montiel, E. Berebichez-Fastlicht, A. Olivos-Meza, J. Granados, C. Velasquillo, C. Ibarra, The holy grail of orthopedic surgery: Mesenchymal stem cells—their current uses and potential applications, Stem Cells Int. 2017 (2017) 1–14, https://doi.org/10.1155/2017/2638305.
[7] A.I. Caplan, Adult mesenchymal stem cells: when, where, and how, Stem Cells Int. 2015 (2015) 628766–628767, https://doi.org/10.1155/2015/628767.
[8] V. Tanavde, C. Vaz, M.S. Rao, M.C. Vemuri, R.R. Pochampally, Research using mesenchymal stem/stromal cells: quality metric towards developing a reference material, Cytotherapy 17 (2015) 1169–1177, https://doi.org/10.1016/j.jcyt.2015.07.008.
[9] F. Saxer, A. Scherberich, A. Todorov, P. Studer, S. Miot, S. Schreiner, S. Güven, L.A. Tchang, M. Haug, M. Heberer, D.J. Schaefer, D. Rikli, I. Martin, M. Jakob, Implantation of stromal vascular fraction progenitors at bone fracture sites: from A rat model to a first-in-man study, Stem Cells (2016)https://doi.org/10.1002/stem.2478.
[10] M.B. Coelho, J.M.S. Cabral, J.M. Karp, Intraoperative stem cell therapy, Annu. Rev. Biomed. Eng. 14 (2012) 325–349, https://doi.org/10.1146/annurev-bioeng-071811-150041.
[11] A. Sohni, C.M. Verfaillie, Mesenchymal stem cells migration homing and tracking, Stem Cells Int. (2013)https://doi.org/10.1155/2013/130763.
[12] B. Parekkadan, J.M. Milwid, Mesenchymal stem cells as therapeutics, Annu. Rev. Biomed. Eng. 12 (2010) 87–117, https://doi.org/10.1146/annurev-bioeng-070909-105309.
[13] D.J. Prockop, D.J. Kota, N. Bazhanov, R.L. Reger, Evolving paradigms for repair of tissues by adult stem/progenitor cells (MSCs), J. Cell. Mol. Med. 14 (2010) 2190–2199, https://doi.org/10.1111/j.1582-4934.2010.01151.x.
[14] A.I. Caplan, D. Correa, The MSC: an injury drugstore, Cell Stem Cell 9 (2011) 11–15, https://doi.org/10.1016/j.stem.2011.06.008.
[15] A. Armulik, G. Genové, C. Betsholtz, Pericytes: developmental, physiological, and pathological perspectives, problems, and promises, Dev. Cell 21 (2011) 193–215, https://doi.org/10.1016/j.devcel.2011.07.001.
[16] S. Maxson, E.A. Lopez, D. Yoo, A. Danilkovitch-Miagkova, M.A. LeRoux, Concise review: role of mesenchymal stem cells in wound repair, Stem Cells Transl. Med. 1 (2012) 142–149, https://doi.org/10.5966/sctm.2011-0018.
[17] P.R. Baraniak, T.C. McDevitt, Stem cell paracrine actions and tissue regeneration, Regen. Med. 5 (2010) 121–143, https://doi.org/10.2217/rme.09.74.
[18] F.J. Vizoso, N. Eiro, S. Cid, J. Schneider, R. Perez-Fernandez, Mesenchymal stem cell secretome: toward cell-free therapeutic strategies in regenerative medicine, Int. J. Mol. Sci. 18 (2017)https://doi.org/10.3390/ijms18091852.
[19] S. Bollini, C. Gentili, R. Tasso, R. Cancedda, The regenerative role of the fetal and adult stem cell secretome, J. Clin. Med. 2 (2013) 302–327, https://doi.org/10.3390/jcm2040302.
[20] B. Tonnarelli, M. Centola, A. Barbero, R. Zeller, I. Martin, Re-engineering development to instruct tissue regeneration, Curr. Top. Dev. Biol. 108 (2014) 319–338.
[21] P. Occhetta, C. Stüdle, A. Barbero, I. Martin, Learn, simplify and implement: developmental re-engineering strategies for cartilage repair, Swiss Med. Wkly. 146 (2016) w14346.
[22] P. Kolar, K. Schmidt-Bleek, H. Schell, T. Gaber, D. Toben, G. Schmidmaier, C. Perka, F. Buttgereit, G.N. Duda, The early fracture hematoma and its potential role in fracture healing, Tissue Eng. Part B Rev. 16 (2010) 427–434, https://doi.org/10.1089/ten.teb.2009.0687.
[23] J.B. WRAY, Acute changes in femoral arterial blood flow after closed tibial fracture in dogs, J. Bone Joint Surg. Am. 46 (1964) 1262–1268.
[24] L. Claes, S. Recknagel, A. Ignatius, Fracture healing under healthy and inflammatory conditions, Nat. Rev. Rheumatol. 8 (2012) 133–143, https://doi.org/10.1038/nrrheum.2012.1.
[25] R. Marsell, T.A. Einhorn, The biology of fracture healing, Injury 42 (2011) 551–555, https://doi.org/10.1016/j.injury.2011.03.031.
[26] T.-J. Cho, L.C. Gerstenfeld, T.A. Einhorn, Differential temporal expression of members of the transforming growth factor beta superfamily during murine fracture healing, J. Bone Miner. Res. 17 (2002) 513–520, https://doi.org/10.1359/jbmr.2002.17.3.513.
[27] L.C. Gerstenfeld, D.M. Cullinane, G.L. Barnes, D.T. Graves, T.A. Einhorn, Fracture healing as a post-natal developmental process: molecular, spatial, and temporal aspects of its regulation, J. Cell. Biochem. 88 (2003) 873–884.
[28] Z. Xing, C. Lu, D. Hu, Y. Yu, X. Wang, C. Colnot, M. Nakamura, Y. Wu, T. Miclau, R.S. Marcucio, R. Altman, L. Latta, R. Keer, K. Renfree, F. Hornicek, K. Banovac, N. Binder, B. Niederreiter, O. Hoffmann, R. Stange, T. Pap, T. Stulnig, M. Mack, R. Erben, J. Smolen, K. Redlich, F. Bonnarens, T. Einhorn, L. Boring, J. Gosling, S. Chensue, S. Kunkel, R. Farese, H. Broxmeyer, I. Charo, B. Capoccia, A. Gregory, D. Link, C. Champagne, J. Takebe, S. Offenbacher, L. Cooper, J. Chang, C. Li, S. Wu, C. Yeh, C. Chen, Y. Fu, G. Wang, M. Ho, V. Contreras-Shannon, O. Ochoa, S. Reyes-Reyna, D. Sun, J. Michalek, W. Kuziel, L. McManus, P. Shireman, S. Dimmen, L. Nordsletten, L. Engebretsen, H. Steen, J. Madsen, L. Engesaeter, B. Sudmann, E. Sudmann, L. Gerstenfeld, M. Thiede, K. Seibert, C. Mielke, D. Phippard, B. Svagr, D. Cullinane, T. Einhorn, F. Gonzalez, L. Vicioso, M. Alvarez, I. Sevilla, E. Marques, E. Gallego, L. Alonso, A. Matilla, E. Alba, S. Ito, N. Suzuki, S. Kato, T. Takahashi, M. Takagi, I. Kalfas, M. Kellinsalmi, V. Parikka, J. Risteli, T. Hentunen, H. Leskela, S. Lehtonen, K. Selander, K. Vaananen, P. Lehenkari, W. Kuziel, S. Morgan, T. Dawson, S. Griffin, O. Smithies, K. Ley, N. Maeda, J. Lloberas, A. Celada, C. Lu, T. Miclau, D. Hu, E. Hansen, K. Tsui, C. Puttlitz, R. Marcucio, C. Lu, E. Hansen, A. Sapozhnikova, D. Hu, T. Miclau, R. Marcucio, M. Ma, T. Wei, L. Boring, I. Charo, R. Ransohoff, L. Jakeman, S. Marks, C. Schmidt, J. Mazibrada, M. Ritta, M. Mondini, M. De Andrea, B. Azzimonti, C. Borgogna, M. Ciotti, A. Orlando, N. Surico, L. Chiusa, A. Mocsai, M. Humphrey, J. Van Ziffle, Y. Hu, A. Burghardt, S. Spusta, S. Majumdar, L. Lanier, C. Lowell, M. Nakamura, O. Ochoa, D. Sun, S. Reyes-Reyna, L. Waite, J. Michalek, L. McManus, P. Shireman, M. Ohta, Y. Kitadai, S. Tanaka, M. Yoshihara, W. Yasui, N. Mukaida, K. Haruma, K. Chayama, H. Oshina, S. Sotome, T. Yoshii, I. Torigoe, Y. Sugata, H. Maehara, E. Marukawa, K. Omura, K. Shinomiya, I. Pountos, T. Georgouli, T. Blokhuis, H. Pape, P. Giannoudis, C.R. Mdel, A. Bernad, M. Aracil, C. Schmidt, S. Marks, C. Jordan, L. Hawes, A. Schober, A. Zernecke, E. Liehn, P. von Hundelshausen, S. Knarren, W. Kuziel, C. Weber, A. Simon, J. O'Connor, E. Sudmann, E. Dregelid, A. Bessesen, J. Morland, Z. Thompson, T. Miclau, D. Hu, J. Helms, C. Tsou, W. Peters, Y. Si, S. Slaymaker, A. Aslanian, S. Weisberg, M. Mack, I. Charo, S. Werner, R. Grose, Multiple roles for CCR2 during fracture healing, Dis. Model. Mech. 3 (2010) 451–458, https://doi.org/10.1242/dmm.003186.
[29] T. Kon, T. Cho, T. Aizawa, M. Yamazaki, N. Nooh, D. Graves, L.C. Gerstenfeld, T.A. Einhorn, Expression of osteoprotegerin, receptor activator of NF-κB ligand (osteoprotegerin ligand) and related proinflammatory cytokines during fracture healing, J. Bone Miner. Res. 16 (2001) 1004–1014.
[30] Z.S. Al-Aql, A.S. Alagl, D.T. Graves, L.C. Gerstenfeld, T.A. Einhorn, Molecular mechanisms controlling bone formation during fracture healing and distraction osteogenesis, J. Dent. Res. 87 (2008) 107–118, https://doi.org/10.1177/154405910808700215.
[31] O. Bastian, J. Pillay, J. Alblas, L. Leenen, L. Koenderman, T. Blokhuis, Systemic inflammation and fracture healing, J. Leukoc. Biol. 89 (2011) 669–673, https://doi.org/10.1189/jlb.0810446.
[32] J.G. Andrew, S.M. Andrew, A.J. Freemont, D.R. Marsh, Inflammatory cells in normal human fracture healing, Acta Orthop. Scand. 65 (1994) 462–466http://www.ncbi.nlm.nih.gov/pubmed/7976298.
[33] J. Xue, S.V. Schmidt, J. Sander, A. Draffehn, W. Krebs, I. Quester, D. De Nardo, T.D. Gohel, M. Emde, L. Schmidleithner, Transcriptome-based network analysis reveals a spectrum model of human macrophage activation, Immunity 40 (2014) 274–288.
[34] K.A. Alexander, M.K. Chang, E.R. Maylin, T. Kohler, R. Müller, A.C. Wu, N. Van Rooijen, M.J. Sweet, D.A. Hume, L.J. Raggatt, A.R. Pettit, Osteal macrophages promote in vivo intramembranous bone healing in a mouse tibial injury model, J. Bone Miner. Res. 26 (2011) 1517–1532, https://doi.org/10.1002/jbmr.354.
[35] T.A. Wynn, K.M. Vannella, Macrophages in tissue repair, regeneration, and fibrosis, Immunity 44 (2016) 450–462.
[36] D.M. Mosser, J.P. Edwards, Exploring the full spectrum of macrophage activation, Nat. Rev. Immunol. 8 (2008) 958–969.
[37] K. Sadtler, A. Singh, M.T. Wolf, X. Wang, D.M. Pardoll, J.H. Elisseeff, Design, clinical translation and immunological response of biomaterials in regenerative medicine, Nat. Rev. Mater. 1 (2016) 16040.
[38] F. Loi, L.A. Córdova, J. Pajarinen, T. Lin, Z. Yao, S.B. Goodman, Inflammation, fracture and bone repair, Bone 86 (2016) 119–130.

Please cite this article as: A. Haumer, et al., Delivery of cellular factors to regulate bone healing, Adv. Drug Deliv. Rev. (2018), https://doi.org/10.1016/j.addr.2018.01.010

[39] Y. Liu, L. Wang, T. Kikuiri, K. Akiyama, C. Chen, X. Xu, R. Yang, W. Chen, S. Wang, S. Shi, Mesenchymal stem cell-based tissue regeneration is governed by recipient T lymphocytes via IFN-[gamma] and TNF-[alpha], Nat. Med. 17 (2011) 1594–1601.
[40] M.M. Martino, K. Maruyama, G.A. Kuhn, T. Satoh, O. Takeuchi, R. Müller, S. Akira, Inhibition of IL-1R1/MyD88 signalling promotes mesenchymal stem cell-driven tissue regeneration, Nat. Commun. 7 (2016).
[41] F.A. Fierro, J.A. Nolta, I.E. Adamopoulos, Concise review: stem cells in osteoimmunology, Stem Cells 35 (2017) 1461–1467.
[42] G.E. Glass, J.K. Chan, A. Freidin, M. Feldmann, N.J. Horwood, J. Nanchahal, TNF-promotes fracture repair by augmenting the recruitment and differentiation of muscle-derived stromal cells, Proc. Natl. Acad. Sci. 108 (2011) 1585–1590, https://doi.org/10.1073/pnas.1018501108.
[43] L. Bosurgi, Y.G. Cao, M. Cabeza-Cabrerizo, A. Tucci, L.D. Hughes, Y. Kong, J.S. Weinstein, P. Licona-Limon, E.T. Schmid, F. Pelorosso, Macrophage function in tissue repair and remodeling requires IL-4 or IL-13 with apoptotic cells, Science 356 (80) (2017) 1072–1076.
[44] C. Schlundt, T. El Khassawna, A. Serra, A. Dienelt, S. Wendler, H. Schell, N. van Rooijen, A. Radbruch, R. Lucius, S. Hartmann, Macrophages in bone fracture healing: their essential role in endochondral ossification, Bone 106 (2015) 78–89.
[45] R. Tasso, V. Ulivi, D. Reverberi, C. Lo Sicco, F. Descalzi, R. Cancedda, In vivo implanted bone marrow-derived mesenchymal stem cells trigger a cascade of cellular events leading to the formation of an ectopic bone regenerative niche, Stem Cells Dev. 22 (2013) 3178–3191, https://doi.org/10.1089/scd.2013.0313.
[46] K.L. Spiller, T.J. Koh, Macrophage-based therapeutic strategies in regenerative medicine, Adv. Drug Deliv., Rev, 2017.
[47] G.E. Glass, J.K. Chan, A. Freidin, M. Feldmann, N.J. Horwood, J. Nanchahal, TNF-α promotes fracture repair by augmenting the recruitment and differentiation of muscle-derived stromal cells, Proc. Natl. Acad. Sci. 108 (2011) 1585–1590.
[48] D. Toben, I. Schroeder, T. El Khassawna, M. Mehta, J. Hoffmann, J. Frisch, H. Schell, J. Lienau, A. Serra, A. Radbruch, Fracture healing is accelerated in the absence of the adaptive immune system, J. Bone Miner. Res. 26 (2011) 113–124.
[49] S. Reinke, S. Geissler, W.R. Taylor, K. Schmidt-Bleek, K. Juelke, V. Schwachmeyer, M. Dahne, T. Hartwig, L. Akyüz, C. Meisel, Terminally differentiated CD8+ T cells negatively affect bone regeneration in humans, Sci. Transl. Med. 5 (2013) 177ra36.
[50] H. Lei, K. Schmidt-Bleek, A. Dienelt, P. Reinke, H.-D. Volk, Regulatory T cell-mediated anti-inflammatory effects promote successful tissue repair in both indirect and direct manners, Front. Pharmacol. 6 (2015) 184.
[51] T. Ono, K. Okamoto, T. Nakashima, T. Nitta, S. Hori, Y. Iwakura, H. Takayanagi, IL-17-producing [gamma][delta] T cells enhance bone regeneration, Nat. Commun. 7 (2016).
[52] O. Grundnes, O. Reikeras, Blood flow and mechanical properties of healing bone, femoral osteotomies studied in rats, Acta Orthop. Scand. 63 (1992) 487–491, https://doi.org/10.3109/17453679209154720.
[53] U. Mayr-Wohlfart, J. Waltenberger, H. Hausser, S. Kessler, K.-P. Günther, C. Dehio, W. Puhl, R.E. Brenner, Vascular endothelial growth factor stimulates chemotactic migration of primary human osteoblasts, Bone 30 (2002) 472–477.
[54] K. Hu, B.R. Olsen, The roles of vascular endothelial growth factor in bone repair and regeneration, Bone 91 (2016) 30–38, https://doi.org/10.1016/j.bone.2016.06.013.
[55] K.D. Hankenson, M. Dishowitz, C. Gray, M. Schenker, Angiogenesis in bone regeneration, Injury 42 (2011) 556–561, https://doi.org/10.1016/j.injury.2011.03.035.
[56] A. Groothuis, G.N. Duda, C.J. Wilson, M.S. Thompson, M.R. Hunter, P. Simon, H.J. Bail, K.M. van Scherpenzeel, G. Kasper, Mechanical stimulation of the pro-angiogenic capacity of human fracture haematoma: involvement of VEGF mechano-regulation, Bone 47 (2010) 438–444.
[57] B. McKibbin, The biology of fracture healing in long bones, J. Bone Joint Surg. Br. 60-B (1978) 150–162.
[58] G. Kumar, B. Narayan, The biology of fracture healing in long bones, Class. Pap. Orthop 2014, pp. 531–533, https://doi.org/10.1007/978-1-4471-5451-8_139.
[59] S.M. Perren, Evolution of the internal fixation of long bone fractures. The scientific basis of biological internal fixation: choosing a new balance between stability and biology, J. Bone Joint Surg. Br. 84 (2002) 1093–1110, https://doi.org/10.1115/1.4026364.
[60] H. Willenegger, S.M. Perren, R. Schenk, Primary and secondary healing of bone fractures, Chirurg 42 (1971) 241–252.
[61] R. Bielby, E. Jones, D. McGonagle, The role of mesenchymal stem cells in maintenance and repair of bone, Injury 38 (2007) S26–S32.
[62] T.A. Einhorn, The cell and molecular biology of fracture healing, Clin. Orthop. Relat. Res. (1998) S7–S21, https://doi.org/10.1097/00003086-199810001-00003.
[63] L. Cleas, N. Maurer-Klein, T. Henke, H. Gerngross, M. McInyk, P. Augat, Moderate soft tissue trauma delays new bone formation only in the early phase of fracture healing, J. Orthop. Res. 24 (2006) 1178–1185, https://doi.org/10.1002/jor.
[64] L.E. Claes, C.A. Heigele, Magnitudes of local stress and strain along bony surfaces predict the course and type of fracture healing, J. Biomech. 32 (1999) 255–266, https://doi.org/10.1016/S0021-9290(98)00153-5.
[65] H. Nakahara, S.P. Bruder, S.E. Haynesworth, J.J. Holecek, M.A. Baber, V.M. Goldberg, A.I. Caplan, Bone and cartilage formation in diffusion chambers by subcultured cells derived from the periosteum, Bone 11 (1990) 181–188, https://doi.org/10.1016/8756-3282(90)90212-H.
[66] L. Claes, K. Eckert-Hübner, P. Augat, The effect of mechanical stability on local vasularization and tissue differentiation in callus healing, J. Orthop. Res. 20 (2002) 1099–1105.
[67] F.W. Rhinelander, Tibial blood supply in relation to fracture healing, Clin. Orthop. 105 (1974) 34–81, https://doi.org/10.1097/00003086-197411000-00005.
[68] C.A. Bassett, I. Herrmann, Influence of oxygen concentration and mechanical factors on differentiation of connective tissues in vitro, Nature 190 (1961) 460–461.
[69] S. Otsuru, K. Tamai, T. Yamazaki, H. Yoshikawa, Y. Kaneda, Circulating bone marrow-derived osteoblast progenitor cells are recruited to the bone-forming site by the CXCR4/stromal cell-derived Factor-1 pathway, Stem Cells 26 (2008) 223–234, https://doi.org/10.1634/stemcells.2007-0515.
[70] T. Kitaori, H. Ito, E.M. Schwarz, R. Tsutsumi, H. Yoshitomi, S. Oishi, M. Nakano, N. Fujii, T. Nagasawa, T. Nakamura, Stromal cell–derived factor 1/CXCR4 signaling is critical for the recruitment of mesenchymal stem cells to the fracture site during skeletal repair in a mouse model, Arthritis Rheum. 60 (2009) 813–823, https://doi.org/10.1002/art.24330.
[71] D. ten Berge, S.A. Brugmann, J.A. Helms, R. Nusse, Wnt and FGF signals interact to coordinate growth with cell fate specification during limb development, Development 135 (2008) 3247–3257.
[72] N. Quarto, M.T. Longaker, FGF-2 inhibits osteogenesis in mouse adipose tissue-derived stromal cells and sustains their proliferative and osteogenic potential state, Tissue Eng. 12 (2006) 1405–1418.
[73] J.-D. Bénazet, M. Bischofberger, E. Tiecke, A. Gonçalves, J.F. Martin, A. Zuniga, F. Naef, R. Zeller, A self-regulatory system of interlinked signaling feedback loops controls mouse limb patterning, Science 323 (80) (2009) 1050–1053.
[74] H.M. Kronenberg, Developmental regulation of the growth plate, Nature 423 (2003) 332–336.
[75] K.K. Mak, H.M. Kronenberg, P.-T. Chuang, S. Mackem, Y. Yang, Indian hedgehog signals independently of PTHrP to promote chondrocyte hypertrophy, Development 135 (2008) 1947–1956.
[76] A. Young, A. Mirarchi, Soft tissue swelling associated with the use of recombinant human bone morphogenetic protein-2 in long bone non-unions, J. Orthop. Case Rep. 5 (2015) 18–21, https://doi.org/10.13107/jocr.2250-0685.297.
[77] J.N. Zara, R.K. Siu, X. Zhang, J. Shen, R. Ngo, M. Lee, W. Li, M. Chiang, J. Chung, J. Kwak, B.M. Wu, K. Ting, C. Soo, High doses of bone morphogenetic protein 2 induce structurally abnormal bone and inflammation in vivo, Tissue Eng. A 17 (2011) 1389–1399, https://doi.org/10.1089/ten.tea.2010.0555.
[78] A.W. Ritting, E.W. Weber, M.C. Lee, Exaggerated inflammatory response and bony resorption from BMP-2 use in a pediatric forearm nonunion, J. Hand Surg. Am. 37 (2012) 316–321, https://doi.org/10.1016/j.jhsa.2011.10.007.
[79] K.-B. Lee, C.E. Taghavi, K.-J. Song, C. Sintuu, J.H. Yoo, G. Keorochana, S.-T. Tzeng, Z. Fei, J.-C. Liao, J.C. Wang, Inflammatory characteristics of rhBMP-2 in vitro and in an in vivo rodent model, Spine (Phila. Pa. 1976) 36 (2011) E149–54, https://doi.org/10.1097/BRS.0b013e3181f2d1ec.
[80] D. Benglis, M.Y. Wang, A.D. Levi, A comprehensive review of the safety profile of bone morphogenetic protein in spine surgery, Neurosurgery 62 (2008)https://doi.org/10.1227/01.neu.0000326030.24220.d8 (ONS423–31; discussion ONS431).
[81] Y. Chen, H.C. Whetstone, A. Youn, P. Nadesan, E.C.Y. Chow, A.C. Lin, B.A. Alman, β-catenin signaling pathway is crucial for bone morphogenetic protein 2 to induce new bone formation, J. Biol. Chem. 282 (2007) 526–533.
[82] T.F. Day, X. Guo, L. Garrett-Beal, Y. Yang, Wnt/β-catenin signaling in mesenchymal progenitors controls osteoblast and chondrocyte differentiation during vertebrate skeletogenesis, Dev. Cell 8 (2005) 739–750.
[83] T.A. Einhorn, The science of fracture healing, J. Orthop. Trauma 19 (2005) S4–S6, https://doi.org/10.1097/00005131-200511101-00002.
[84] E.M. Thompson, A. Matsiko, E. Farrell, D.J. Kelly, F.J. O'Brien, Recapitulating endochondral ossification: a promising route to in vivo bone regeneration, J. Tissue Eng. Regen. Med. 9 (2015) 889–902, https://doi.org/10.1002/term.1918.
[85] M. Melnyk, T. Henke, L. Claes, P. Augat, Revascularisation during fracture healing with soft tissue injury, Arch. Orthop. Trauma Surg. 128 (2008) 1159–1165, https://doi.org/10.1007/s00402-007-0543-0.
[86] F.W. Rhinelander, Tibial blood supply in relation to fracture healing, Clin. Orthop. 105 (1974) 34–81, https://doi.org/10.1097/00003086-197411000-00005.
[87] A. Schindeler, M.M. McDonald, P. Bokko, D.G. Little, Bone remodeling during fracture repair: the cellular picture, Semin. Cell Dev. Biol. 19 (2008) 459–466, https://doi.org/10.1016/j.semcdb.2008.07.004.
[88] L. Claes, Biomechanical principles and mechanobiologic aspects of flexible and locked plating, J. Orthop. Trauma 25 (Suppl. 1) (2011) S4–7, https://doi.org/10.1097/BOT.0b013e318207093e.
[89] T.M. Dexter, T.D. Allen, L.G. Lajtha, R. Schofield, B.I. Lord, Stimulation of differentiation and proliferation of haemopoietic cells in vitro, J. Cell. Physiol. 82 (1973) 461–473, https://doi.org/10.1002/jcp.1040820315.
[90] A.I. Caplan, J.E. Dennis, Mesenchymal stem cells as trophic mediators, J. Cell. Biochem. 98 (2006) 1076–1084, https://doi.org/10.1002/jcb.20886.
[91] Y. Shi, J. Su, A.I. Roberts, P. Shou, A.B. Rabson, G. Ren, How mesenchymal stem cells interact with tissue immune responses, Trends Immunol. 33 (2012) 136–143, https://doi.org/10.1016/j.it.2011.11.004.
[92] M.E. Bernardo, W.E. Fibbe, Mesenchymal stromal cells: sensors and switchers of inflammation, Cell Stem Cell 13 (2013) 392–402, https://doi.org/10.1016/j.stem.2013.09.006.
[93] A.N. Gornostaeva, E.R. Andreeva, P.I. Bobyleva, L.B. Buravkova, Interaction of allogeneic adipose tissue-derived stromal cells and unstimulated immune cells in vitro: the impact of cell-to-cell contact and hypoxia in the local milieu, Cytotechnology (2017) 1–14, https://doi.org/10.1007/s10616-017-0144-x.
[94] R.S. Waterman, S.L. Tomchuck, S.L. Henkle, A.M. Betancourt, A new mesenchymal stem cell (MSC) paradigm: Polarization into a pro-inflammatory MSC1 or an immunosuppressive MSC2 phenotype, PLoS One 5 (2010)https://doi.org/10.1371/journal.pone.0010088.
[95] M.A. Cassatella, F. Mosna, A. Micheletti, V. Lisi, N. Tamassia, C. Cont, F. Calzetti, M. Pelletier, G. Pizzolo, M. Krampera, Toll-like receptor-3-activated human mesenchymal stromal cells significantly prolong the survival and function of neutrophils, Stem Cells 29 (2011) 1001–1011, https://doi.org/10.1002/stem.651.

Please cite this article as: A. Haumer, et al., Delivery of cellular factors to regulate bone healing, Adv. Drug Deliv. Rev. (2018), https://doi.org/10.1016/j.addr.2018.01.010

[96] H. Mohammadpour, A.A. Pourfathollah, M.N. Zarif, M.T. Tahoori, TNF-a modulates the immunosuppressive effects of MSCs on dendritic cells and T cells, Int. Immunopharmacol. 28 (2015) 1009–1017, https://doi.org/10.1016/j.intimp.2015.07.045.
[97] V. Ulivi, R. Tasso, R. Cancedda, F. Descalzi, Mesenchymal stem cell paracrine activity is modulated by platelet lysate: induction of an inflammatory response and secretion of factors maintaining macrophages in a proinflammatory phenotype, Stem Cells Dev. 00 (2014) 1–12, https://doi.org/10.1089/scd.2013.0567.
[98] L. Cheng, H. Hammond, Z. Ye, X. Zhan, G. Dravid, Human adult marrow cells support prolonged expansion of human embryonic stem cells in culture, Stem Cells 21 (2003) 131–142, https://doi.org/10.1634/stemcells.21-2-131.
[99] F.E. Mercier, C. Ragu, D.T. Scadden, The bone marrow at the crossroads of blood and immunity, Nat. Rev. Immunol. 12 (2011) 49–60, https://doi.org/10.1038/nri3132.
[100] R.A. Boomsma, D.L. Geenen, Mesenchymal stem cells secrete multiple cytokines that promote angiogenesis and have contrasting effects on chemotaxis and apoptosis, PLoS One 7 (2012), e35685. https://doi.org/10.1371/journal.pone.0035685.
[101] C.Y. Wang, H.B. Yang, H.S. Hsu, L.L. Chen, C.C. Tsai, K.S. Tsai, T.L. Yew, Y.H. Kao, S.C. Hung, Mesenchymal stem cell-conditioned medium facilitates angiogenesis and fracture healing in diabetic rats, J. Tissue Eng. Regen. Med. 6 (2012) 559–569, https://doi.org/10.1002/term.461.
[102] I. Linero, O. Chaparro, Paracrine effect of mesenchymal stem cells derived from human adipose tissue in bone regeneration, PLoS One 9 (2014)https://doi.org/10.1371/journal.pone.0107001.
[103] S. Rani, A.E. Ryan, M.D. Griffin, T. Ritter, Mesenchymal stem cell-derived extracellular vesicles: toward cell-free therapeutic applications, Mol. Ther. 23 (2015) 812–823, https://doi.org/10.1038/mt.2015.44.
[104] C. Lo Sicco, D. Reverberi, C. Balbi, V. Ulivi, E. Principi, L. Pascucci, P. Becherini, M.C. Bosco, L. Varesio, C. Franzin, M. Pozzobon, R. Cancedda, R. Tasso, Mesenchymal stem cell-derived extracellular vesicles as mediators of anti-inflammatory effects: endorsement of macrophage polarization, Stem Cells Transl. Med. 6 (2017) 1018–1028, https://doi.org/10.1002/sctm.16-0363.
[105] S.E.L. Andaloussi, I. Mäger, X.O. Breakefield, M.J.A. Wood, Extracellular vesicles: biology and emerging therapeutic opportunities, Nat. Rev. Drug Discov. 12 (2013) 347–357, https://doi.org/10.1038/nrd3978.
[106] S. Koniusz, A. Andrzejewska, M. Muraca, A.K. Srivastava, M. Janowski, B. Lukomska, Extracellular vesicles in physiology, pathology, and therapy of the immune and central nervous system, with focus on extracellular vesicles derived from mesenchymal stem cells as therapeutic tools, Front. Cell. Neurosci. 10 (2016) 1–20, https://doi.org/10.3389/fncel.2016.00109.
[107] H. Xie, Z. Wang, L. Zhang, Q. Lei, A. Zhao, H. Wang, Q. Li, Y. Cao, W. Jie Zhang, Z. Chen, Extracellular vesicle-functionalized decalcified bone matrix scaffolds with enhanced pro-angiogenic and pro-bone regeneration activities, Sci. Rep. 7 (2017) 45622, https://doi.org/10.1038/srep45622.
[108] R. Narayanan, C.C. Huang, S. Ravindran, Hijacking the cellular mail: exosome mediated differentiation of mesenchymal stem cells, Stem Cells Int. 2016 (2016)https://doi.org/10.1155/2016/3808674.
[109] Y. Cui, J. Luan, H. Li, X. Zhou, J. Han, Exosomes derived from mineralizing osteoblasts promote ST2 cell osteogenic differentiation by alteration of microRNA expression, FEBS Lett. 590 (2016) 185–192, https://doi.org/10.1002/1873-3468.12024.
[110] Y. Xie, Y. Chen, L. Zhang, W. Ge, P. Tang, The roles of bone-derived exosomes and exosomal microRNAs in regulating bone remodelling, J. Cell. Mol. Med. 21 (2017) 1033–1041, https://doi.org/10.1111/jcmm.13039.
[111] T. Furuta, S. Miyaki, H. Ishitobi, T. Ogura, Y. Kato, N. Kamei, K. Miyado, Y. Higashi, M. Ochi, Mesenchymal stem cell-derived exosomes promote fracture healing in a mouse model, Stem Cells Transl. Med. 5 (2016) 1620–1630, https://doi.org/10.5966/sctm.2015-0285.
[112] C. Salomon, J. Ryan, L. Sobrevia, M. Kobayashi, K. Ashman, M. Mitchell, G.E. Rice, Exosomal signaling during hypoxia mediates microvascular endothelial cell migration and vasculogenesis, PLoS One 8 (2013)https://doi.org/10.1371/journal.pone.0068451.
[113] C. Frantz, K.M. Stewart, V.M. Weaver, The extracellular matrix at a glance, J. Cell Sci. 123 (2010) 4195–4200, https://doi.org/10.1242/jcs.023820.
[114] L. Macri, D. Silverstein, R.A.F. Clark, Growth factor binding to the pericellular matrix and its importance in tissue engineering, Adv. Drug Deliv. Rev. 59 (2007) 1366–1381, https://doi.org/10.1016/j.addr.2007.08.015.
[115] G.S. Schultz, J.M. Davidson, R.S. Kirsner, P. Bornstein, I.M. Herman, Dynamic reciprocity in the wound microenvironment, Wound Repair Regen. 19 (2011) 134–148, https://doi.org/10.1111/j.1524-475X.2011.00673.x.
[116] J.R. Bishop, M. Schuksz, J.D. Esko, Heparan sulphate proteoglycans fine-tune mammalian physiology, Nature 446 (2007) 1030–1037, https://doi.org/10.1038/nature05817.
[117] P.J. Roughley, E.R. Lee, Cartilage proteoglycans: structure and potential functions, Microsc. Res. Tech. 28 (1994) 385–397, https://doi.org/10.1002/jemt.1070280505.
[118] A.M. Moursi, C.H. Damsky, J. Lull, D. Zimmerman, S.B. Doty, S. Aota, R.K. Globus, Fibronectin regulates calvarial osteoblast differentiation, J. Cell Sci. 109 (Pt 6) (1996) 1369–1380.
[119] T.J. Nam, W.H. Busby, C. Rees, D.R. Clemmons, Thrombospondin and osteopontin bind to insulin-like growth factor (IGF)-binding protein-5 leading to an alteration in IGF-I-stimulated cell growth, Endocrinology 141 (2000) 1100–1106, https://doi.org/10.1210/en.141.3.1100.
[120] R.V. Iozzo, J.D. San Antonio, Heparan sulfate proteoglycans: heavy hitters in the angiogenesis arena, J. Clin. Invest. 108 (2001) 349–355, https://doi.org/10.1172/JCI200113738.
[121] D.M. Ornitz, FGFs, heparan sulfate and FGFRs: complex interactions essential for development, BioEssays 22 (2000) 108–112, https://doi.org/10.1002/(SICI)1521-1878(200002)22:2<108::AID-BIES2>3.0.CO;2-M.
[122] P. Sivakumar, New insights into extracellular matrix assembly and reorganization from dynamic imaging of extracellular matrix proteins in living osteoblasts, J. Cell Sci. 119 (2006) 1350–1360, https://doi.org/10.1242/jcs.02830.
[123] R. Alon, L. Cahalon, R. Hershkoviz, D. Elbaz, B. Reizis, S.K. Akiyama, K.M. Yamada, O. Liderlt, TNF-alpha binds to the N-terminal domain of fibronectin and augments the beta1-integrin-mediated adhesion of CD4+ T lymphocytes to the glycoproptein, J. Immunol. 152 (1994) 1304–1313.
[124] L. Summers, K. Kangwantas, L. Nguyen, C. Kielty, E. Pinteaux, Adhesion to the extracellular matrix is required for interleukin-1 beta actions leading to reactive phenotype in rat astrocytes, Mol. Cell. Neurosci. 44 (2010) 272–281, https://doi.org/10.1016/j.mcn.2010.03.013.
[125] P.M. Crapo, T.W. Gilbert, S.F. Badylak, An overview of tissue and whole organ decellularization processes, Biomaterials 32 (2011) 3233–3243, https://doi.org/10.1016/j.biomaterials.2011.01.057.
[126] B.N. Brown, S.F. Badylak, Extracellular matrix as an inductive scaffold for functional tissue reconstruction, Transl. Regen. Med. to Clin 2015, pp. 11–29, https://doi.org/10.1016/B978-0-12-800548-4.00002-4.
[127] P.E. Bourgine, B.E. Pippenger, A. Todorov, L. Tchang, I. Martin, Tissue decellularization by activation of programmed cell death, Biomaterials 34 (2013) 6099–6108, https://doi.org/10.1016/j.biomaterials.2013.04.058.
[128] C.W. Cheng, L.D. Solorio, E. Alsberg, Decellularized tissue and cell-derived extracellular matrices as scaffolds for orthopaedic tissue engineering, Biotechnol. Adv. 32 (2014) 462–484, https://doi.org/10.1016/j.biotechadv.2013.12.012.
[129] B. Wildemann, A. Kadow-Romacker, N.P. Haas, G. Schmidmaier, Quantification of various growth factors in different demineralized bone matrix preparations, J. Biomed. Mater. Res. A 81 (2007) 437–442, https://doi.org/10.1002/jbm.a.31085.
[130] M. Hinsenkamp, J.-F. Collard, Growth factors in orthopaedic surgery: demineralized bone matrix versus recombinant bone morphogenetic proteins, Int. Orthop. (2014) 137–147, https://doi.org/10.1007/s00264-014-2562-0.
[131] H. Bae, L. Zhao, D. Zhu, L.E. Kanim, J.C. Wang, R.B. Delamarter, Variability across ten production lots of a single demineralized bone matrix product, J. Bone Joint Surg. Am. 92 (2010) 427–435, https://doi.org/10.2106/JBJS.H.01400.
[132] M.P. Lutolf, J.A. Hubbell, Synthetic biomaterials as instructive extracellular microenvironments for morphogenesis in tissue engineering, Nat. Biotechnol. 23 (2005) 47–55, https://doi.org/10.1038/nbt1055.
[133] K. Lee, E.A. Silva, D.J. Mooney, Growth factor delivery-based tissue engineering: general approaches and a review of recent developments, J. R. Soc. Interface 8 (2011) 153–170, https://doi.org/10.1098/rsif.2010.0223.
[134] E.J. Carragee, E.L. Hurwitz, B.K. Weiner, A critical review of recombinant human bone morphogenetic protein-2 trials in spinal surgery: emerging safety concerns and lessons learned, Spine J. 11 (2011) 471–491, https://doi.org/10.1016/j.spinee.2011.04.023.
[135] M. Kisiel, M.M. Martino, M. Ventura, J.A. Hubbell, J. Hilborn, D.A. Ossipov, Improving the osteogenic potential of BMP-2 with hyaluronic acid hydrogel modified with integrin-specific fibronectin fragment, Biomaterials 34 (2013) 704–712, https://doi.org/10.1016/j.biomaterials.2012.10.015.
[136] K. Sadtler, K. Estrellas, B.W. Allen, M.T. Wolf, H. Fan, A.J. Tam, C.H. Patel, B.S. Luber, H. Wang, K.R. Wagner, Developing a pro-regenerative biomaterial scaffold microenvironment requires T helper 2 cells, Science 352 (80) (2016) 366–370.
[137] Y.H. Kim, H. Furuya, Y. Tabata, Enhancement of bone regeneration by dual release of a macrophage recruitment agent and platelet-rich plasma from gelatin hydrogels, Biomaterials 35 (2014) 214–224, https://doi.org/10.1016/j.biomaterials.2013.09.103.
[138] A. Page-McCaw, A.J. Ewald, Z. Werb, Matrix metalloproteinases and the regulation of tissue, Nat. Rev. Mol. Cell Biol. 8 (2007) 221–233, https://doi.org/10.1038/nrm2125.Matrix.
[139] M.M. Martino, P.S. Briquez, E. Güç, F. Tortelli, W.W. Kilarski, S. Metzger, J.J. Rice, G.A. Kuhn, R. Müller, M.A. Swartz, J.A. Hubbell, Growth factors engineered for super affinity to the extracellular matrix enhance tissue healing, Science 343 (80) (2014) 885–889.
[140] N. Nishi, O. Matsushita, K. Yuube, H. Miyanaka, A. Okabe, F. Wada, Collagen-binding growth factors: production and characterization of functional fusion proteins having a collagen-binding domain, Proc. Natl. Acad. Sci. U. S. A. 95 (1998) 7018–7023, https://doi.org/10.1073/pnas.95.12.7018.
[141] V. Sacchi, R. Mittermayr, J. Hartinger, M.M. Martino, K.M. Lorentz, S. Wolbank, A. Hofmann, R.A. Largo, J.S. Marschall, E. Groppa, R. Gianni-Barrera, M. Ehrbar, J.A. Hubbell, H. Redl, A. Banfi, Long-lasting fibrin matrices ensure stable and functional angiogenesis by highly tunable, sustained delivery of recombinant VEGF164, Proc. Natl. Acad. Sci. 111 (2014) 6952–6957, https://doi.org/10.1073/pnas.1404605111.
[142] M.C. Prewitz, A. Stißel, J. Friedrichs, N. Träber, S. Vogler, M. Bornhäuser, C. Werner, Extracellular matrix deposition of bone marrow stroma enhanced by macromolecular crowding, Biomaterials 73 (2015) 60–69, https://doi.org/10.1016/j.biomaterials.2015.09.014.
[143] C. Chen, F. Loe, A. Blocki, Y. Peng, M. Raghunath, Applying macromolecular crowding to enhance extracellular matrix deposition and its remodeling in vitro for tissue engineering and cell-based therapies, Adv. Drug Deliv. Rev. 63 (2011) 277–290, https://doi.org/10.1016/j.addr.2011.03.003.
[144] H. Lu, T. Hoshiba, N. Kawazoe, I. Koda, M. Song, G. Chen, Cultured cell-derived extracellular matrix scaffolds for tissue engineering, Biomaterials 32 (2011) 9658–9666, https://doi.org/10.1016/j.biomaterials.2011.08.091.
[145] S. Zeitouni, U. Krause, B.H. Clough, H. Halderman, A. Falster, D.T. Blalock, C.D. Chaput, H.W. Sampson, C.A. Gregory, Human mesenchymal stem cell-derived matrices for enhanced osteoregeneration, Sci. Transl. Med. 4 (2012) 132ra55, https://doi.org/10.1126/scitranslmed.3003396.

Please cite this article as: A. Haumer, et al., Delivery of cellular factors to regulate bone healing, Adv. Drug Deliv. Rev. (2018), https://doi.org/10.1016/j.addr.2018.01.010

[146] G. Tour, M. Wendel, I. Tcacencu, Cell-derived matrix enhances osteogenic properties of hydroxyapatite, Tissue Eng. A 17 (2011) 127–137, https://doi.org/10.1089/ten.tea.2010.0175.
[147] G. Tour, M. Wendel, I. Tcacencu, Human fibroblast-derived extracellular matrix constructs for bone tissue engineering applications, J. Biomed. Mater. Res. A 101 (2013) 2826–2837, https://doi.org/10.1002/jbm.a.34600.
[148] N. Datta, H.L. Holtorf, V.I. Sikavitsas, J.A. Jansen, A.G. Mikos, Effect of bone extracellular matrix synthesized in vitro on the osteoblastic differentiation of marrow stromal cells, Biomaterials 26 (2005) 971–977, https://doi.org/10.1016/j.biomaterials.2004.04.001.
[149] N. Sadr, B.E. Pippenger, A. Scherberich, D. Wendt, S. Mantero, I. Martin, A. Papadimitropoulos, Enhancing the biological performance of synthetic polymeric materials by decoration with engineered, decellularized extracellular matrix, Biomaterials 33 (2012) 5085–5093, https://doi.org/10.1016/j.biomaterials.2012.03.082.
[150] P.E. Bourgine, C. Scotti, S. Pigeot, L.A. Tchang, A. Todorov, I. Martin, Osteoinductivity of engineered cartilaginous templates devitalized by inducible apoptosis, Proc. Natl. Acad. Sci. U. S. A. (2014) 1–6, https://doi.org/10.1073/pnas.1411975111.
[151] M.C. Prewitz, F.P. Seib, M. von Bonin, J. Friedrichs, A. Stißel, C. Niehage, K. Müller, K. Anastassiadis, C. Waskow, B. Hoflack, M. Bornhäuser, C. Werner, Tightly anchored tissue-mimetic matrices as instructive stem cell microenvironments, Nat. Methods 10 (2013) 788–794, https://doi.org/10.1038/nmeth.2523.
[152] P.E. Bourgine, E. Gaudiello, B. Pippenger, C. Jaquiery, T. Klein, S. Pigeot, A. Todorov, S. Feliciano, A. Banfi, I. Martin, Engineered extracellular matrices as biomaterials of tunable composition and function, Adv. Funct. Mater. 1605486 (2017)https://doi.org/10.1002/adfm.201605486.

Please cite this article as: A. Haumer, et al., Delivery of cellular factors to regulate bone healing, Adv. Drug Deliv. Rev. (2018), https://doi.org/10.1016/j.addr.2018.01.010

5. Conclusion and perspectives:

Infection, trauma, tumor and burn sequelae can lead to varying degrees of tissue damage, resulting in complex defects including muscle and bone. At the beginning of the previous century, such damage often resulted in amputation of a limb or organ, or even death of the patient. Two of the most important medical advances of the 20th century have made it possible to offer these patients a better option. First, autologous tissue grafting, where tissue is transferred from an unharmed part of the own body to the injury site, allowed to restore crucial body function and coverage. Secondly, defined body areas with constant, independent and reliable blood supply were discovered. This promoted clinical implementation of the grafting concept by providing a fast and efficient vascularization of the transferred tissue, which in turn made graft and flap surgery possible. Technological development in microsurgery from the 1960ies on, allowed to constantly refine and broaden the surgical options in reconstructive surgery. Despite many sophisticated techniques have been developed to repair tissue defects, grafting in reconstructive surgery almost entirely relies on native tissues. However, these tissues are limited in availability and in its suitability to match the defect site in size and shape.

My thesis aimed at overcoming these shortcomings by developing a prefabricated, large, vascularized bone graft for the treatment of complex bone defects.

In chapter II a vascularization method, suitable for prefabricating a large bone graft, was tested in a relevant animal model. The concept of prefabrication relies on the process of neovascularization of a tissue by introducing a vascular pedicle in a defined tissue segment, allowing for reimplantation of the tissue as free graft [113]. In order to observe bone formation in such a setting, living cells from the stromal vascular fraction (SVF) are required to be seeded on an osteoconductive ceramic material. In the third chapter a contrast-enhanced microtomographic imaging technique was developed to

critically assess vascularization and bone formation in this large-sized constructs, to provide a comprehensive overview by computed reconstruction of the data.

The fourth chapter addresses the bone formation in the inner core of the graft. After extensively reviewing the literature, described in the last chapter, it became clear that extracellular matrix deposited by mesenchymal stromal/stem cells during an in-vitro phase could allow to deliver the physiological cocktail of signaling molecules required for the regeneration of bone tissue. Subsequent devitalization and transplantation of the tissue offers the highly attractive opportunity to exploit the regenerative potency of the ECM, but within a cell-free, off-the-shelf material. Based on their design, these materials harbor not only all the cyto- and chemokines necessary for recruitment and differentiation of progenitor cells, but also for activation and regulation of the immune response, able to promote regeneration. This knowledge allowed developing an engineered, devitalized matrix, which proved to be a robust bone formation strategy ectopically and orthotopically, when ‘activated’ by co-transplanted SVF cells.

Finally, the fifth chapter demonstrates that combining an AV bundle and the engineered, avital matrix is sufficient to generate a germ of vascularization and bone, without the addition of a living cell compartment. Eventually, the potency of the AV bundle in promoting bony remodeling of the cartilage template was shown by a direct positive correlation of vascularization and bone formation. Together with a form-stable outer shell, which can be custom-shaped according to the patient’s needs, this prefabricated vascularized graft represents a real alternative bone graft surrogate.

This innovative concept investigated in my thesis opens interesting opportunities for clinical translation, because it allows to combine the safety and reliability of conventional surgical approaches, such as free tissue transfer, with innovative materials and tissue engineering technologies.

In fact, feasibility and safety of this approach was tested in a one-patient clinical case. A young patient with a complex maxillary defect, originating from the removal of an aggressive, malignant tumor, was not eligible for reconstruction of the defect by conventional means. To offer the patient a reasonable long term solution, the concept described above was clinically translated in a two-step approach, involving ectopic prefabrication of the graft, followed by orthotopic transfer of the tissue to the defect zone. In the first step, the exact size and shape of the defect were calculated from tomographic data. Through CAD-CAM techniques, an exactly matching, three-dimensional scaffolding material, made of devitalized cancellous bone, was generated. To provide a combined germ of vascularization and bone formation, an AV bundle was axially inserted in the material which was seeded with SVF cells, gained intraoperatively from the patient. The stromal and vascular progenitors contained in the freshly isolated SVF enhance the vascularization of the material through the AV-bundle, in turn improving its engraftment following orthotopic transfer, as well as tolerance to infection. At the same time progenitor cells of the SVF cells require a molecular trigger to differentiate into functional osteoblasts, which was achieved by supplying low amounts of rhBMP-2 together with the SVF cells [114,115]. Accurate, longitudinal imaging allowed to assess the development and maturity of the tissue. The AV bundle, created from two thoracodorsal vessels, proved to be an efficient vascularization method also in this clinical setting. The large-sized graft of nearly 28 cm3 was entirely vascularized within the first four weeks of ectopic implantation. At orthotopic transfer, the pedicle originating from the implemented AV bundle could be safely anastomosed to facial vessels by microsurgical means. The newly developing bone, assessed by CT and PET-CT scans to define structure and metabolism, showed increasing grades of maturity beginning from the 8^{th} to the 12^{th} week. With advancing metabolic activity within the bone graft, resorptive processes could also be observed.

Continuous imaging assessment made it possible to precisely surveil these processes and define the appropriate time point for graft transfer. Based on this, after 8 months of ectopic prefabrication, the bone graft could be harvested and transferred to the maxillary defect site.

This successful translation of the concept from the bench to the bedside provides interesting perspectives. The proof of principle that this innovative therapeutic strategy for large, complex bone defects of the maxillo-facial region is feasible and safe to perform, opens the possibility to treat a larger number of patients in a clinical trial. At the University Hospital of Basel, an estimated number of 10 to 15 patients a year would be eligible to be treated with this newly developed approach. Nevertheless, before aiming at the treatment of a larger cohort, the knowledge gained in the clinical case must be critically analyzed.

It is only a speculation that the osteoblasts involved in bone formation within the construct originate from the seeded SVF. Even though our preclinical animal model, using an osteoconductive material, demonstrated that SVF cells were required for bone formation, it is plausible that circulating progenitors are recruited to the graft in response to the BMP-2 and injury [116,117]. An indicator for prominent recruitment of bone-remodeling (osteoblasts and osteoclasts) cells to the graft is the marked resorption, observed in a larger extent than in our experimental animal models. The BMP-2, used as a molecular trigger for progenitor cells in the SVF to undergo bone formation, is known to induce resorption by attraction and activation of osteoclasts, especially when used in supraphysiological concentration [119]. These aspects urge to be investigated in an experimental animal model allowing for cell tracking and distinction of host and donor cells.

As described in the fifth chapter of my thesis, using an engineered matrix could provide the germ for bone formation avoiding the bottlenecks of freely diffusing BMP-2 and the

use of living cells. By presenting the biological cues required for bone formation in a physiological way in its ECM, both BMP-2 and living cells could become redundant. Mass-produced engineered and devitalized cartilaginous matrix, useable as an off-the-shelf material, could then be implemented together with an AV bundle to provide the inner germ of bone and vascularization. To use engineered matrices from hBMSC as a standardized and controlled therapeutic instrument, the challenges linked to the production thereof need to be tackled. The high inter- and intradonor variability of hBMSC requires appropriate controls and tests to define potency of the material. In this regard, generation and use of a cell line, with streamlined characteristics, could provide the solution [120].

As envisioned in the concept of my thesis, the AV bundle used in the clinical case provided a thorough vascularization of this large construct from an early time on, allowing revitalization of the avital material. This vital environment was permissive for bony remodeling with living osteoblasts and osteoclasts and yielded a functional germ of vascularization and bone. Finally, the highly complex logistics of this procedure, with harmonized surgical and tissue engineering processes, have proved to be feasible and would be applicable to a larger clinical trial. In planning additional cases, the processes may be further streamlined by knowing how to manage crucial points of the procedure.

To conclude, the concept described in my thesis opened the way to develop an innovative therapeutic strategy for large and complex bone defects, which was applied in a one-man clinical case. In turn, the lessons learned from this first clinical application pave the way for the treatment of a larger number of patients with the developed concept.

6. Curriculum Vitae

Personal Data

Name	Alexander Haumer
Address	Department of Biomedicine Hebelstrasse 20 CH-4031 Basel
Phone	+41 (0) 76 562 76 42; +41 (0) 61 265 38 98
E-Mail	alexander.haumer@usb.ch; haumer.alexander@gmail.com
Nationality	Italian, Austrian
Date of birth	08/08/1988

Education

June 2017	**GCP for Investigator, Swiss Medics accredited, Basel Switzerland**
April 2014	**Labortierkunde (LTK) Module 1 (FELASA B accreditation)**
12/2013	**Start of Ph.D. in Biomedicine, University of Basel (CH)** Working title: “Prefabrication of vascularized large bone grafts” Laboratory for Tissue Engineering (Prof. Ivan Martin), *Department of Biomedicine*, Basel, Switzerland Fellow of the European FP7 Marie Skłodowska-Curie Research Fellowship Programme (iTERM)
08/2008-08/2013	**M.D., Paracelsus Medical University, Salzburg (A)** M.D. thesis: “Injectable Multiblock P(PF-co-CL) Copolymer and Dual Drug Delivery for Treatment of Bone Defects” Laboratory for Tissue Engineering, *Mayo Clinic Rochester* (MN, USA)

11/2011	**United States Medical Licensing Examination (USMLE) Step 1**
2007-2008	**Faculty of Biology, Leopold-Franzens-Universität, Innsbruck (A)**
2007	**High School degree** Naturwissenschaftliches Realgymnasium Bozen/Bolzano, Italy

Professional Experience

09/2013-11/2013	**Internship, Weill Medical College of Cornell University , New York (NY, USA)** Plastic & Reconstructive Surgery, Prof. Henry Spinelli, Weill Medical College of Cornell University, New York (NY, USA)
06/2012 – 11/2012	**Research Fellowship, Mayo Clinic, Rochester (MN, USA)** Laboratory for tissue engineering and biomaterials (Prof. Michael J. Yaszemski), Mayo Clinic, Rochester (MN, USA)
11/2012-12/2012	**Clinical Rotation, Mayo Clinic, Rochester (MN, USA)** Department for Plastic & Reconstructive Surgery, Mayo Clinic, Rochester (MN, USA)

Teaching

09/2014-12/2014	**Tutor, Faculty of Biology** Biozentrum, University of Basel (CH)
08/2010-09/2013	**Tutor, Institute of Physiology and Pathophysiology** Paracelsus Medical University, Salzburg (A)
08/2011-09/2013	**Tutor, Institute of Pharmacology and Toxicology** Paracelsus Medical University, Salzburg (A)

Extracurricular Involvement & Memberships

Member of the board

Swiss national MD/PhD association (SMPA)

Member of the board of representatives

Swiss Representative, European MD/PhD association (EMPA)

Grant

"Reconstruction of a large maxillary defect using a custom-shaped, engineered and prevascularized bone substitute material: a first-in-man clinical case." Alexander Haumer; Project number PP-16-24; Propatient Forschungsstiftung, University Hospital Basel 2016

Oral Presentations

- "Reconstruction of a large maxillary defect by an engineered vascularized bone graft", Clinical Research Day University Hospital Basel Jan 2018
- "Engineering of Axially Vascularized Bone Grafts for the Treatment of Avascular Bone Necrosis"; 5th European MD/PhD conf.2016, Strasbourg (F); best presentation award
- "Tissue Engineering – from bench to bedside"; Paracelsus Medical University Salzburg (A), May 2016
- "Engineered Endochondral Ossification to Induce Osteogenesis and Vascularization in Bone Defects"; Clinical research meeting, University Hospital Basel 2014

Languages

- *German:* native speaker
- *Italian:* native speaker
- *English:* fluent operational proficiency
- *Spanish:* spoken and written skills for everyday purposes (DELE level B2)
- *French*: elementary proficiency

Publications

"*Delivery of cellular factors to regulate bone healing.*" **Haumer A**, Bourgine PE, Occhetta P, Born G, Tasso R, Martin I. Advanced Drug Delivery Reviews, 2018 Jan 21. pii: S0169-409X(18)30010-3. doi: 10.1016/j.addr.2018.01.010

"*Engineered, axially-vascularized osteogenic grafts from human adipose-derived cells to treat avascular necrosis of bone in a rat model*." Ismail T, Osinga R, Todorov A Jr, **Haumer A**, Tchang L Allafi N, Menzi N, Largo RD, Kaempfen A, Martin I, Schaefer DJ, Scherberich A Acta Biomater. 2017 Sep 8. pii: S1742-7061(17)30570-6. doi: 10.1016/j.actbio.2017.09.003

"*Ontogenic Identification and Analysis of Mesenchymal Stromal Cell Populations during Mouse Limb Bud and Long Bone Development"* Nusspaumer G & Jaiswal S, **Haumer A**, Barbero A, Ronen D, Lufkin T, Martin I and Zeller R; (Stem Cell Reports. 2017 Oct 10;9(4):1124-1138. doi: 10.1016/j.stemcr.2017.08.007)

"*From autologous flaps to engineered vascularized grafts for bone regeneration*" **Haumer A**, Ismail T, Lunger A, Osinga R, Scherberich A, Schaefer DJ, Martin I (book chapter in "*Tissue Engineering and Regeneration: Vascularization for Tissue Engineering and Regenerative Medicine*", Springer (May 2017)

"Fat-derived stromal vascular fraction cells enhance the bone forming capacity of devitalized engineered hypertrophic cartilage matrix." Todorov A & Kreutz M, **Haumer A**, Scotti C, Barbero A, Bourgine P, Scherberich A, Jaquiery C, Martin I; Stem Cells Transl Med. 2016 Jul 26. pii: sctm.2016-0006

"The medial femoral trochlea (MFT) flap with a monitor skin island – report of two cases." Tremp M, **Haumer A,** Wettstein R, Yi Xin Zhang, Honigmann P, Schaefer DJ, Kalbermatten D; Microsurgery. 2016 Aug 29. doi: 10.1002/micr.30093

"Contrast-Enhanced Microtomographic Characterisation of Vessels in Native Bone and Engineered Vascularised Grafts Using Ink-Gelatin Perfusion and Phosphotungstic Acid" Sutter S & Todorov A, Ismail T, **Haumer A**, Fulco I, Schulz G, Scherberich A, Kaempfen A, Martin I, and Schaefer DJ; Contrast Media and Molecular Imaging 2017 Apr 23

"Radiofrequency induced thermal therapy (RFITT): a retrospective analysis" **Haumer A,** Fissneider B, Haumer S (Proceedings of the 1st Meeting of the Multinational Chapter of the International Union of Angiology (IUA), Edizione Minerva Medica, 2016)

Prospective Plans

Residency in Plastic & Reconstructive surgery, USMLE steps 2 &3